MODELING DISPERSIONS IN INITIAL CONDITIONS FOR AIR-LAUNCHED ROCKETS AND THEIR EFFECT ON VEHICLE PERFORMANCE

by

Ingrid Mary Beerer

Bachelors of Science in Engineering Physics,
University of California, Berkeley (2011)

SUBMITTED TO THE DEPARTMENT OF AERONAUTICS AND ASTRONAUTICS
IN PARTIAL FULFILLMENT OF THE REQUIREMENTS FOR THE DEGREE OF

MASTER OF SCIENCE IN AERONAUTICS AND ASTRONAUTICS
AT THE
MASSACHUSETTS INSTITUTE OF TECHNOLOGY
SEPTEMBER 2013

Signature of Author .....
Ingrid Mary Beerer
Department of Aeronautics and Astronautics
August 22, 2013

Certified by .....
Dr. Phillip D. Hattis
Charles Stark Draper Laboratory
Thesis Supervisor

Certified by .....
Prof. Kerri Cahoy
Associate Professor of Aeronautics and Astronautics
Thesis Supervisor

Accepted by .....
Prof. Eytan H. Modiano
Professor of Aeronautics and Astronautics
Chair, Graduate Program Committee

Modeling Dispersions In Initial Conditions For Air-Launched Rockets And Their Effect On Vehicle Performance

by

Ingrid Mary Beerer

Submitted to the Department of Aeronautics and Astronautics on
August 22, 2013 in partial fulfillment of the Requirements for the degree of
Master of Science in Aeronautics and Astronautics

Abstract

Growing interest in air-launched rockets as a method for lofting satellites into orbit motivates the need to investigate the unique challenges that air launch presents. This thesis explores how uncertainties in an air-launched rocket's state at ignition can affect system performance and investigates a reference trajectory strategy to mitigate performance loss. First, representative vehicle configurations for a generic air-launch system are presented. Mass properties, propulsion characteristics, and vehicle aerodynamics are estimated for the generic rocket configuration. A six-degree-of-freedom (6-DOF) simulation models the vehicle's behavior during the uncontrolled drop phase prior to rocket ignition. The results of 1000 Monte Carlo runs with various initial conditions produce a statistical representation of the expected dispersions in vehicle state at ignition. A 6-DOF Simulink simulation of the rocket's first stage burn is used to quantify the vehicle's performance. The simulation is run for a variety of ignition states, reference trajectories, and constraints on the rocket's control system. The results indicate that for a highly responsive thrust vector control (TVC) system, the rocket experiences negligible performance losses due to dispersions in ignition conditions. However, for a rocket with a less responsive TVC system, dispersions will result in significant performance loss by the end of first stage burn. Finally, the thesis illustrates how selection of a reference trajectory that is optimized for a given dispersed ignition state can significantly reduce the system's performance loss due to dispersions.

Thesis Supervisor: Philip D. Hattis, Ph.D.
Title: Laboratory Technical Staff
Charles Stark Draper Laboratory, Inc.

Thesis Supervisor: Kerri Cahoy, Ph.D.
Title: Professor of Aeronautics and Astronautics

Acknowledgements

The author would like to thank her advisor, Dr. Phil Hattis, for his invaluable mentorship over the last year. She would also like to thank her advisor, Professor Kerri Cahoy, for her advice and support throughout her time at MIT. In addition, the author is very grateful for the wonderful mentorship she received while interning at Virgin Galactic, which motivated her interest in air-launched rockets and introduced her to the team at Draper. She would like to thank all her mentors at Draper and Virgin Galactic for giving her the opportunity to participate in this exciting project. Finally, she dedicates this thesis to the amazing group of women she met at MIT AeroAstro who quickly became her best friends.

Contents

List of Figures

List of Tables

Chapter 1. Introduction

1.1 Air-Launched Rockets to Orbit

In the early 2000s, the space community began a major shift toward developing smaller and cheaper satellites. Rapidly advancing small satellite technology enables small satellites (<500 kg) to accomplish mission objectives, which formerly required larger and more expensive platforms. With shrinking budgets, along with advances in electronics miniaturization, microsatellites (<100 kg) are increasingly used to accomplish both government and commercial space missions. Nanosatellites (<10 kg) and picosatellites (<1 kg) have become popular platforms for university education. Prime examples are CubeSats, 10-cm cube satellites developed by California Polytechnic University and Stanford University (Nugent et al. 2008). In addition, more countries are developing fledgling space programs on constrained budgets, boosting demand for small and low-cost satellites.

While small satellites are becoming increasingly popular, a major barrier to further advancement lies in the method for launching small satellites into orbit. Currently small satellites must piggyback on a large launch vehicle designed to loft a large primary payload to an orbit of the primary payload's choice. No affordable dedicated launch vehicle for small satellites currently exists. Therefore, small satellites must often settle for an orbit that is not ideal for their mission objectives. Obtaining a launch as a secondary

payload also places major schedule constraints on small satellite providers. The launch schedule is at the mercy of the primary payload and small payloads must be ready by the launch date or miss their opportunity. Finally, the limited availability of launch opportunities eliminates the possibility of launching small satellites on-demand in order to opportunistically observe unpredictable Earth science or space weather phenomena.

Historically, the most popular launch vehicles for satellites in the 1-50 kg range have been the Ukrainian Dnepr-1, Orbital Sciences' Minotaur, and the Indian PSLV (DePasquale et al. 2010). Launches on these vehicles are typically multi-manifested, lofting many small payloads at the same time. The smallest single payload launched on a dedicated launch vehicle was the 110 kg SCD 2, which was launched by Orbital Sciences' Pegasus® in 1998. However, prohibitively high launch costs have resulted in little demand for the Pegasus vehicle, whose future availability is uncertain (Leone 2012a). In the years 2000-2009, 41% of satellites in the 1-50 kg range were launched onboard the Dnepr-1. Yet the price of launching Dnepr-1 rockets, which are converted Soviet-era intercontinental ballistic missiles, have recently escalated (de Selding 2012). In 2012, Russian media reported it was likely the nation would discontinue launching Dnepr-1 (Messier 2012). Space Exploration Technologies' (SpaceX) Falcon 1, a small two-stage liquid rocket, may have been a popular choice for small satellite customers. However, SpaceX announced in 2012 that they have no future plans to launch Falcon 1 as the company focuses on the much larger Falcon 9 (O'neill 2011). The close of these programs would leave small satellite providers with even fewer launch vehicle options.

Greater demand for small satellite launches combined with diminishing launch vehicle options motivates the need for a new launch vehicle that provides dedicated and

responsive launches for small satellites. A dedicated rocket could significantly reduce launch costs and increase launch opportunities, allowing further growth in the small satellite market. Air-launched rockets to orbit, which are launched at altitude from a carrier aircraft, are an attractive option for a dedicated small satellite launcher. Traditionally, launch vehicles are launched from fixed ground locations within ranges, such as Vandenberg Air Force Base in California or Cape Canaveral in Florida. Unfortunately, maintenance of aging range infrastructure is escalating range costs. Stringent range safety rules necessitate laborious integration and verification processes, which may last months before a launch is approved. In addition, launches from a range may be delayed due to rain or high winds.

Air launch presents many advantages over traditional ground launch. First, air launch can eliminate the costs associated with maintaining a fixed range infrastructure. The launch point flexibility of air launch can reduce the probability of collateral damage in case of a failure, which would therefore simplify range safety regulations and allow satellites to be launched quickly and on-demand. An air launch system can also avoid areas with adverse weather conditions. Furthermore, the launch point flexibility of air launch allows for access to a wider selection of orbits. The carrier aircraft enables the rocket to achieve any launch azimuth without making expensive out-of-plane maneuvers.

Air launch provides improved performance over ground launch vehicles. By launching at an altitude above the dense atmosphere, air-launched rockets experience less performance loss due to drag. In addition, air-launched rockets are imparted with an initial velocity from the carrier aircraft, reducing the total Delta V required to reach orbit. Finally, air launch reduces the total mass of propellant needed to get to orbit because jet

engines on the carrier aircraft are more efficient at getting the launch vehicle to the launch altitude than rocket engines.

Whitehead (2006) illustrates that air-launching rockets in the 0.01 to 100 ton mass range at altitudes between 10 and 20 km significantly reduces the Delta V required to reach Low Earth Orbit (LEO) for both liquid and solid rockets. Similarly, Sarigul-Klijn, Noel, and Sarigul-Klijn (2004) consider the Delta V reductions that would result from air-launching Orbital Sciences' Minotaur launch vehicle (4-stage solid rocket; 36,200 kg) for various launch parameters. The results demonstrate that increasing the rocket's initial velocity at ignition has the greatest benefit to Delta V. However, existing carrier platforms capable of reaching supersonic speeds would only be able to launch relatively small launch vehicles (up to ~5,000 lbs.). Launching a larger vehicle at supersonic speeds requires a newly designed carrier platform. In addition, the results show that while increasing launch altitude reduces Delta V to orbit, there is little improvement over about 50,000 ft.

Figure 1.1—The Orbital Sciences' Pegasus launch vehicle dropped from its carrier aircraft. Image from *http://www.nustar.caltech.edu/about-nustar/launch-vehicle*

Acoustic reflection from the ground during launch can cause fuselage damage to rockets launched from the ground, often necessitating structural stiffening with an associated weight penalty. Air-launched rockets face less fuselage hazard by avoiding acoustic reflection from the ground and by launching at altitude where air density is lower. The lower atmospheric pressure at altitude also allows launch vehicles to have higher expansion area ratio nozzles, which improves specific impulse performance while minimizing vehicle weight and complexity (Sarigul-Klijn et al. 2008).

While air launch provides a wide array of advantages over ground launch, there are a few disadvantages. First, air launch requires a specially designed or modified carrier aircraft, which limits the overall size of the launch vehicle. Therefore, there is not much potential for growing air-launched rockets. Furthermore, all rockets that use cryogenic propellants suffer from boil off due to heating from solar radiation and air convection. Cryogenic tanks on ground launch vehicles can be replenished through umbilicals until launch. It would be difficult, and is therefore unlikely, for an air-launched vehicle to be replenished while mated to the carrier platform. Therefore, air-launched rockets that are carried outside the carrier aircraft will require larger tank volume margins to compensate for boil off. Finally, horizontal carriage and release induce lateral bending loads into the air-launched vehicle structure in the captive flight (takeoff and abort landing) and high angle of attack free flight, increasing structural mass particularly for pump-fed liquid systems.

Several different air launch concepts have been proposed. Launch vehicles could be carried above, below, or inside a carrier aircraft, towed behind an aircraft, or launched from a high altitude balloon. To date, only captive-on-the-bottom air-launched orbital

systems have been built. The X-15 and Scaled Composites' SpaceShipOne are examples of human piloted air-launched rockets that made suborbital flights. In 1990, Orbital Sciences' Pegasus launch vehicle became the first air-launched rocket to loft a satellite into orbit. As of June 2012, Pegasus has carried out 36 successful launches (Leone 2012a). Pegasus is a winged, three stage solid propellant rocket capable of launching about ~900 lb. to LEO (Noffz et al. 1991). The fully loaded launch vehicle weighs either 41,000 lb. (Pegasus) or 51,000 lbs. (Pegasus XL) depending on the configuration. The rocket is dropped at 40,000 ft. altitude from a converted airliner at Mach 0.8. Unfortunately, the Pegasus launch vehicle has proved to be an expensive choice for small satellite providers. In 2012, Pegasus XL launched the NASA NuStar satellite for a price of $36M, or $47,000 per pound of payload (Leone 2012a). Due to the prohibitively large launch cost and infrequent flight rate, Pegasus XL has seen little demand from small satellite customers. The 2012 launch of NuStar was the first for Pegasus XL in four years.

New air-launched rockets to orbit are currently under development. In 2012, Virgin Galactic announced their intention to build an orbital launch vehicle that will be air-launched from the WhiteKnightTwo jet aircraft, which was originally built to launch Virgin Galactic's suborbital tourism vehicle, SpaceShipTwo (Coppinger 2012). The launch vehicle, known as LauncherOne, is a two-stage liquid rocket designed to carry 100 to 225 kg payloads to LEO. This launch vehicle will therefore be able to serve the small satellite market by providing dedicated launches for small payloads. Another new commercial space venture, Stratolaunch, unveiled in 2011 its plan to build a much larger air-launched rocket capable of lofting 61,000 kg to LEO or 2,300 kg to geosynchronous orbit (Leone 2012b). This launch vehicle will provide the advantages of air launch, such

as the reduction of range costs, access to a wider selection of orbits, and high flight rate, to the mid-size payload market, including communications satellites.

1.2 Air Launch Trajectory Design and GN&C

Air-launched rockets present unique challenges for trajectory design and optimization. Contemporary launch vehicle guidance, navigation, and control (GN&C) systems use a preprogrammed reference trajectory and onboard measurements to control the thrust direction of the engine in order to steer the rocket along an optimized path to the desired orbit. However, unlike traditional ground launch, an air-launched rocket's initial altitude, velocity, and flight path angle are unfixed, which opens a wider parameter space for air launch trajectory optimization. The goal of trajectory optimization is to find the most efficient path to orbit.

On an ascent trajectory to LEO, a rocket suffers from losses due to atmospheric drag and gravity. Launching at altitude reduces, but does not eliminate drag losses. To spend the least amount of time flying through the atmosphere, and therefore minimize drag loss, a rocket would take a direct vertical trajectory to orbital altitude, followed by a circularization burn. However, this type of trajectory suffers from a maximum amount of gravity loss. On the other hand, if drag losses are ignored, the most efficient path to orbit is a horizontal launch into an elliptical orbit, followed by a circularization burn 180° from the launch point, which is essentially a Hohmann transfer. Whitehead (2006)

demonstrates that the optimal trajectory for an air-launched rocket to orbit lies somewhere between these two extremes. Exactly where the optimal trajectory for a specific air-launched rocket falls between the two extreme cases depends on the amount of drag the vehicle generates.

When launching from the ground, the initial position and velocity of the rocket is precisely known. An air-launched rocket, on the contrary, is dropped from a moving human-piloted aircraft and free-falls for a few seconds, experiencing perturbations along the way due to ambient environment effects before igniting its rocket engine. Therefore, the position, velocity, body attitude, and body rates at release and ignition are uncertain. Under current practice, the reference trajectory used to steer the vehicle during ascent, however, is derived assuming a specific initial body state, which may vary greatly from the actual initial state. The uncertainty in initial conditions, which is unique to air launch, presents a challenge for trajectory design and optimization.

Uncertainties in the initial state at ignition are either imparted by the carrier aircraft at release or produced by the variable environment during the uncontrolled drop phase. Initial position errors at ignition are nearly entirely due to the carrier aircraft position at release. The position error can consist of three components: along-track error, lateral error, and altitude error. Sikharulidze, Karpov, and Ivanov (2005) present a method to compensate for initial along-track (or downrange) and launch time errors for an air-launched rocket. To achieve direct insertion into a rendezvous point in orbit, where all orbital elements are specified, downrange and launch time errors can be compensated by adjusting the thrust values of the two upper stages. Sikharulidze, Karpov, and Ivanov (2005) ignore errors in lateral position and altitude.

In the case where the desired orbit is circular with specified altitude and inclination, and all other orbital elements are free parameters, the downrange and launch time errors need not be considered. However, errors in velocity, attitude, and body rates at ignition due to uncertainties in the release and drop phase dynamics may be significant. Flight data from past air launch programs illustrate the magnitude of these uncertainties. In the early 2000s Air Launch, LLC began development of an air-launched rocket, which would be carried internally within a C-17 aircraft. While the rocket was never built, Air Launch performed drop tests of inert test articles from a C-17. The test article experienced significant yaw dispersions during drop (up to 18 degrees), which was attributed to unpredicted asymmetries in the vehicle aerodynamics (Sarigul-Klijn et al. 2006).

Flight data from Orbital Sciences' Pegasus shows that the rocket undergoes significant vertical and lateral forcing during the first ~2 seconds of the drop phase. The forcing is the result of the hook release mechanism, which takes a finite amount of time (~0.02 s) to fully lose contact with the vehicle (Johnson, Bies, and McManus 1994). The higher performance Pegasus XL launch vehicle failed on its maiden flight, terminating after about 3 minutes of flight. The failure was attributed to an underestimation of the vehicle's aerodynamic complexity and the inability of the GN&C autopilot system to account for off-nominal sideslip angles (Hall, Holland, and Blevins 2011). The Pegasus XL failure demonstrates how uncertainties in the vehicle state in the early seconds of flight can significantly affect system performance.

1.3 Thesis Objectives & Overview

The lessons learned from Pegasus and other air launch programs illustrate that uncertainties in the rocket state at ignition can be large and have detrimental effects if not properly mitigated. With growing interest in air launch as a means to loft satellites to LEO, handling dispersions in ignition conditions requires further investigation. This thesis seeks to answer three questions:

1. For a representative air-launched rocket configuration, what are the ranges of expected dispersions in vehicle velocity, attitude, and body rates at ignition?
2. How much performance loss, in terms of payload mass to orbit, is incurred due to off-nominal ignition conditions when the rocket guidance follows a reference trajectory optimized for nominal ignition conditions?
3. Finally, can a method be developed to mitigate this performance loss by allowing the guidance system to select a trajectory better suited for the actual ignition condition?

The thesis is organized into six chapters, the first being this Introduction. Chapter 2 presents the design of representative configurations of an air-launched rocket. The Delta V required to launch a payload into LEO from an air-launched rocket is estimated. Assuming a two-stage liquid propellant vehicle and a certain desired payload mass, the Rocket Equation is used to derive the optimal mass and propellant-to-weight ratio of each stage. Finally, the dimensions and mass properties of the configuration are estimated.

Chapter 3 develops an aerodynamic model of the rocket designed in Chapter 2. The US Air Force Missile DATCOM software is used to calculate the aerodynamic coefficients, which are functions of Mach number, angle of attack, and sideslip angle. Chapter 4 describes the construction of a six degree-of-freedom (6-DOF) MATLAB® simulation to model the rocket's behavior during the uncontrolled drop phase between release and ignition. The results from 1000 Monte Carlo runs of the simulation with a range of vehicle release and local wind conditions produce a statistical description of the expected uncertainties in vehicle velocity, attitude, and body rates at ignition.

Chapter 5 presents a Simulink® model of a Guidance, Navigation, and Control (GN&C) system, which uses Thrust Vector Control (TVC) to steer the rocket. The GN&C model is used in a 6-DOF simulation of the powered portion of the rocket flight between ignition and first stage burnout. An optimized reference trajectory for the first stage is derived for nominal ignition conditions using a combination of the Powered Explicit Guidance (PEG) algorithm and the Program to Optimize Simulated Trajectories (POST). The vehicle's guidance system uses this reference trajectory to steer the gimbaled rocket engine. The simulation models the first stage burn for both nominal and various off-nominal ignition conditions in order to quantify the performance loss incurred due to dispersions. Furthermore, Chapter 6 investigates a method to mitigate these performance losses by allowing the guidance system to select a better-suited reference trajectory for the actual vehicle state at ignition.

Chapter 2: Vehicle Configuration

2.1 Vehicle Mass & Geometry

The first step is to generate a vehicle configuration for a generic rocket that may be used in an air launch system. Most rockets have two to four stages (Isakowitz 2004). While increasing the number of stages increases performance, it also increases complexity and therefore the cost of the launch vehicle (Francis 1999). As a dedicated small satellite launcher will likely be designed to minimize cost and complexity a two-stage to orbit vehicle configuration is selected. Furthermore, the ultimate goal of this study is to quantify vehicle performance losses that are incurred due to dispersions early in the first stage flight. Since only the first stage performance is of interest there is no reason to consider a third or fourth stage. The two-stage configuration requires that the second stage be liquid propellant (or hybrid), because the second stage must be able to relight in order to perform a final circularization burn. Liquid propellant is also selected for the first stage for simplicity and because liquid rockets can achieve a higher specific impulse than solids.

The launch vehicle mass at liftoff needed to loft a payload to orbit depends on the mass of payload and the Delta V required to reach the desired orbit. The total Delta V

required to reach an orbit is given by Equation (2.1) (Sarigul-Klijn, Noel, and Sarigul-Klijn 2004).

$$\Delta V = V_{orbit} + \Delta V_{drag} + \Delta V_{gravity} + \Delta V_{steering} + \Delta V_{atmosphere\ pressure} - V_{Earth\ rotation} - V_{carrier\ aircraft} \quad (2.1)$$

The desired orbital velocity of a payload in a circular orbit is given by V_{orbit} and can be found by Equation (2.2).

$$V_{orbit}{}^2 = \frac{GM_{\oplus}}{(R_{\oplus} + h_{orbit})} \quad (2.2)$$

Where G is the gravitational constant, $M_{\oplus}$is the mass of the Earth, $R_{\oplus}$ is the radius of the Earth, and h_{orbit} is the altitude of the desired circular orbit. For a 200 km orbit, the orbital velocity is 7,786 m/s. Both ground and air-launched vehicles can benefit from the rotational velocity of the Earth, $V_{Earth\ rotation}$. Launching from the equator in the due East direction imparts the rocket with a maximum velocity of 463 m/s. For any other location on the Earth, the velocity imparted to the rocket by the Earth's rotation is given by Equation (2.3) below (Sarigul-Klijn, Noel, and Sarigul-Klijn 2004).

$$V_{Earth\ rotation} = \left(463\frac{m}{s}\right)\cos\phi\sin\beta \quad (2.3)$$

Where ϕ is the launch latitude and β is the launch azimuth, the angle measured clockwise from due north to the rocket's plane of motion. Air-launched rockets enjoy the additional benefit of the carrier aircraft's velocity, $V_{carrier\ aircraft}$, which further reduces the total ΔV to orbit.

Drag losses are caused by aerodynamic forces, which retard the vehicle's motion during flight through the atmosphere. Planform drag loss is proportional to the vehicle's cross-sectional area. (Parasitic drag effects are expected to be very small compared to

planform drag and are therefore ignored.) For medium sized launch vehicles, such as the Atlas or Delta, drag losses are typically on the order of 40 to 160 m/s (Sarigul-Klijn, Noel, and Sarigul-Klijn 2004). The rocket also loses energy due to gravity, typically on the order of 1500 m/s, because the rocket must fight the Earth's gravitational force to reach orbital altitude. To minimize gravity loss, the rocket needs to pitch over to the local horizontal as early as possible in its trajectory. Air-launched vehicles typically have lower gravity losses compared to ground launch because air-launched rockets are able to pitch to a horizontal position more quickly.

Steering losses, $\Delta V_{steering}$, further increase the total ΔV to orbit. In order to steer the launch vehicle, some of the rocket's thrust must be applied perpendicular to the rocket's body axis. Therefore, the thrust vector and velocity vector are not always aligned. Air-launched rockets that are released from a carrier aircraft flying horizontally, with a flight path angle ~ 0°, will typically suffer from greater steering losses compared to ground launch because the air-launched rocket must fly a pull up maneuver at high angle of attack. Finally, rocket engines have best performance in vacuum. Therefore, during atmospheric flight, the rocket suffers losses due to decreased engine performance. A key advantage of air launch is that launching at altitude reduces the ambient atmospheric pressure, reducing atmospheric pressure losses.

The total ΔV required to reach LEO from the Earth's surface ranges from about 8,000 to 10,000 m/s (Whitehead 2006). Air launching a mid-size rocket at subsonic velocities from an altitude of 50,000 ft. reduces ΔV to orbit by about 400 to 600 m/s (Sarigul-Klijn, Noel, and Sarigul-Klijn 2004). An intermediate ΔV of 9,000 – 500 = 8,500 m/s is used in the calculations below. The vehicle configurations presented here are two-

stage to orbit liquid rockets. The optimal ratio of Stage-1/Stage-2 mass is selected to maximize payload mass to orbit. Delta V is related to vehicle mass by the Rocket Equation (2.4):

$$\Delta V = v_e \ln \frac{m_0}{m_f} \tag{2.4}$$

Where v_e is the rocket's exhaust velocity, m_0 is the initial mass, and m_f is the final mass. The exhaust velocity is related to the specific impulse, I_{sp}, of the rocket by Equation (2.5).

$$v_e = I_{sp} \cdot g \tag{2.5}$$

Where g is the local acceleration due to gravity. The I_{sp} here is assumed to be equal to that of the Falcon 1 first stage, 310 s (Falcon 1 User's Guide 2008).

For a two-stage launch vehicle, the Delta V is given by

$$\Delta V = v_e \ln \frac{m_0}{m_0 - \delta m_{s1}} + v_e \ln \frac{m_0 - m_{s1}}{m_0 - m_{s1} - \delta m_{s2}} \tag{2.6}$$

Where m_{s1} and m_{s2} are the masses of Stage 1 and Stage 2, respectively. The Propellant Mass Fraction (δ or PMF) is the ratio of propellant mass to total (wet + dry) mass of each stage. Equation (2.6) assumes that δ and v_e are the same for both stages. The stages are assumed to have a propellant mass fraction of 0.90. This value is similar to that for other small to mid-sized two-stage liquid rockets as shown in Table 2.1. The sum of the Stage 1 and 2 masses is equal to m_{stack}. The total mass of the vehicle, m_0, is equal to the sum of m_{stack} and the payload mass, m_{pld}.

$$m_0 = m_{stack} + m_{pld} \tag{2.7a}$$

$$m_{stack} = m_{s1} + m_{s2} \tag{2.7b}$$

Table 2.1—Properties of Existing Two-Stage Liquid Launch Vehicles

Vehicle	Mass (klbm.)	Propellant	Stage 1 weight/ stack weight	PMF Stage 1	PMF Stage 2
Falcon 1	61	LOX/kerosene	0.83	0.94	0.91
Dnepr-1*	461	N2O4/UDMH	0.77	0.92	0.89
Titan II	340	N2O4/Aerozine-50	0.80	0.97	0.91

Sources: Falcon 1 User's Guide (2008); Dnepr-1 Users Guide (2001); Isakowitz et al. (2004)
* Dnepr-1 has an additional 9 klbm. third stage for precision orbit insertion

Two rocket configurations, which will be referred to as the "Air Launch Light" and "Air Launch Heavy", are considered in this study. Air Launch Light and Air Launch Heavy have a stack mass (m_{stack}) of 20,000 and 40,000 lbs., respectively. For a given value of m_{stack} the payload mass to orbit depends on the ratio of Stage-1/Stage-2 mass. Substituting $m_{s1} = f m_{stack}$ and $m_{s2} = (1-f) m_{stack}$ results in Equation (2.8).

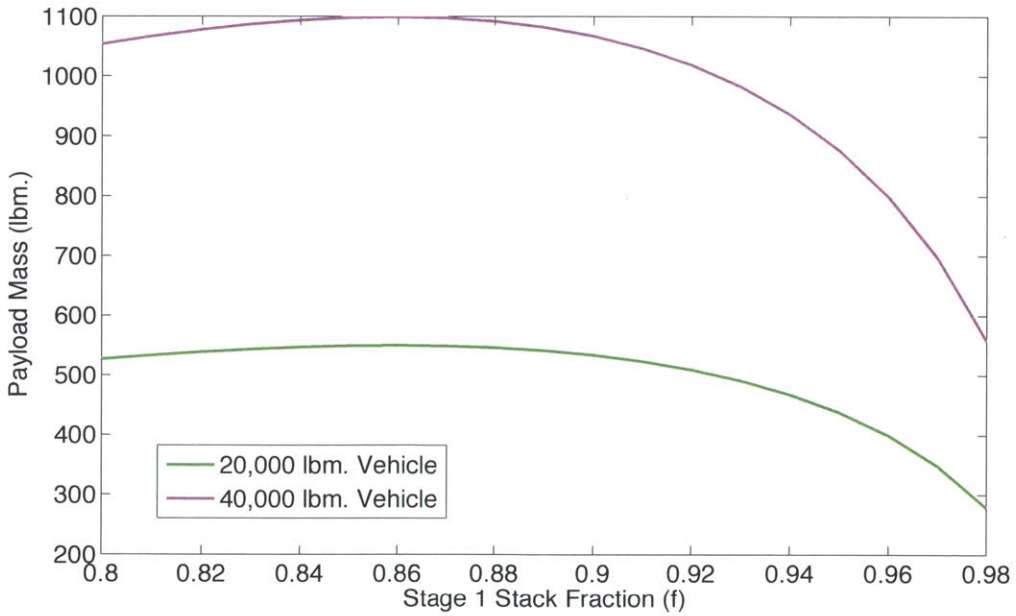

Figure 2.1—Payload mass to LEO for vehicles with 20,000 lb. and 40,000 lb. stack weight as a function of m_{s1}: m_{stack} ratios

$$\Delta V = v_e \ln \frac{m_0}{m_0 - \delta f m_{stack}} + v_e \ln \frac{m_0 - f m_{stack}}{m_0 - f m_{stack} - (1-f)\delta m_{stack}} \tag{2.8}$$

For fixed values of ΔV, v_e, δ, and m_{stack}, the parameter f is varied in order to find the peak value of m_0, thereby optimizing the payload mass. Figure 2.1 shows the payload mass to orbit over a range of f values for Air Launch Light (*green*) and Air Launch Heavy (*magenta*). For Air Launch Light, the optimal payload mass to orbit is about 550 lbs., corresponding to a vehicle where Stage 1 makes up 86% of the stack weight. Similarly, the optimal Stage 1 stack fraction for Air Launch Heavy is 86% resulting in a 1,100 lb. payload.

The next step is to determine the approximate vehicle geometry. The Falcon 1 launch vehicle, a two-stage 61,000 lb. liquid rocket, is used as a scale model. It should be noted that an air-launched rocket requires more structural mass than a ground launched rocket in order to support higher bending loads. While the Falcon 1 vehicle is therefore not a perfect scale model, it provides a reasonable estimate. Given an approximate 58 ft. length and 5 ft. diameter, the average density of the Falcon 1 is about 42.5 lb./ft^3 or 680 kg/m^3. Assuming this average density for the air launch rocket, the approximate volumes of Stage 1 and Stage 2 are calculated for both the 20,550 lbm. and 41,100 lbm. vehicles. Lengths and diameters are chosen to yield the desired volume for each cylindrical stage. Tables 2.2 and 2.3 list the stage masses and dimensions for both vehicle configurations.

Table 2.2—Air Launch Light Mass and Dimensions

Stage	Dry Mass (kg)	Propellant Mass (kg)	Length (m)	Diameter (m)
1	780	7,020	7.2	1.5
2	127	1,143	3.0	0.9
Payload + Fairing	250	-	1.0	0.9

Table 2.3—Air Launch Heavy Mass and Dimensions

Stage	Dry Mass (kg)	Propellant Mass (kg)	Length (m)	Diameter (m)
1	1,560	14,040	9.25	1.8
2	254	2286	3.75	1.1
Payload + Fairing	500	-	1.5	1.1

A nose cone, which houses the payload, is mounted above Stage 2. Nose cone shapes are designed to minimize atmospheric drag. There are many different rocket nose cone shapes, such as conical, spherically blunted, ogive, elliptical, and parabolic (Chin 1961). For simplicity, a parabolic nose cone is used in this study for both vehicle configurations. A parabolic shape is also used to design the rocket engine nozzle. Finally, a conical inter-stage section connects the first and second stages. Cross sections and three-dimensional views of the rocket shapes are shown in Figures 2.2—2.3.

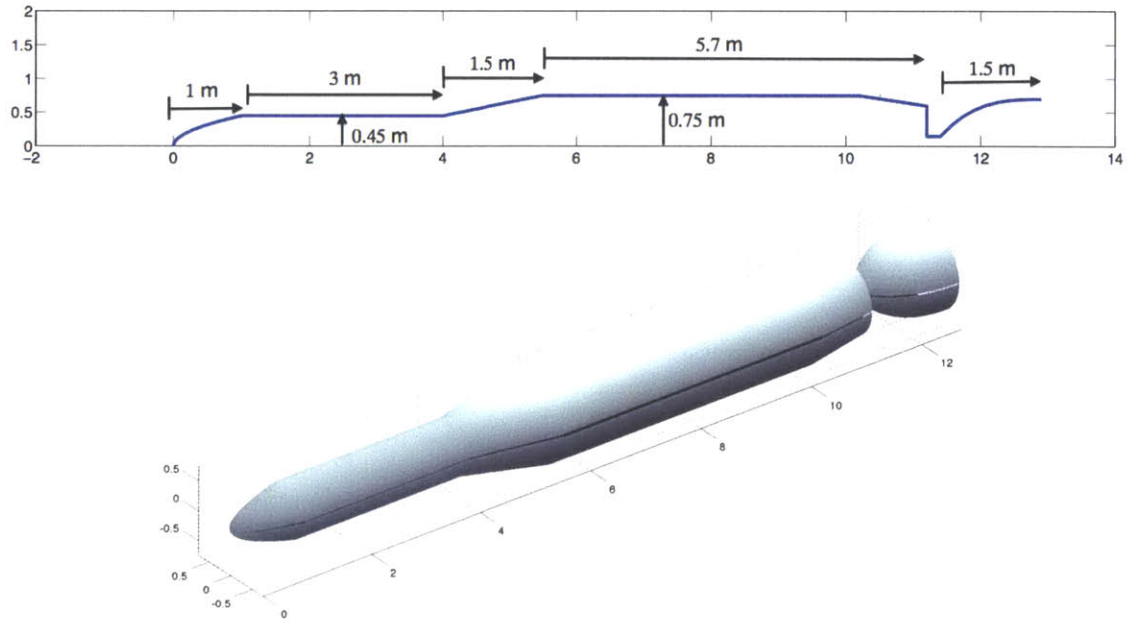

Figure 2.2—Air Launch Light outer mold line (*top*) and three-dimensional view (*bottom*)

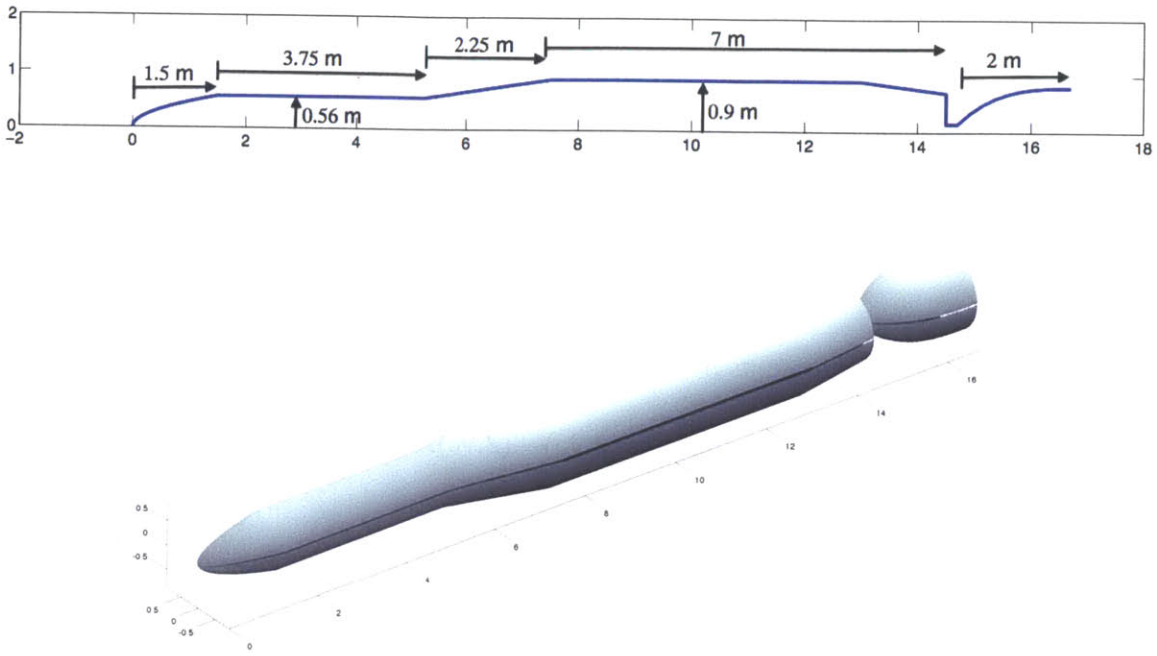

Figure 2.3—Air Launch Heavy outer mold line (*top*) and three-dimensional view (*bottom*)

2.2 Moments of Inertia

In order to solve the 6DOF equations of motion describing the vehicle dynamics during the uncontrolled drop, it is necessary to calculate the inertia tensor about the rocket's center of mass. The inertia tensor is calculated using body-fixed axes with the origin at the vehicle center of mass and x-axis running along the vehicle's longitudinal axis. For simplicity, the rocket is assumed to have uniform density. The center of mass is therefore equal to the center of volume of the vehicle. The point from the nose tip running along the x-axis where half of the rocket's volume lies forward and half aft is

found by adding up thin slices of volume. The center of mass point becomes the origin of the coordinate system in order to calculate the inertia tensor about the center of mass.

The inertia tensor is given by:

$$I = \begin{bmatrix} I_{xx} & -I_{xy} & -I_{xz} \\ -I_{yx} & I_{yy} & -I_{yz} \\ -I_{zx} & -I_{zy} & I_{zz} \end{bmatrix} \tag{2.8}$$

I_{xx}, I_{yy}, and I_{zz} are the moments of inertia with respect to the x-, y-, and z-axes, respectively, and are given by Equations (2.9a)—(2.9c).

$$I_{xx} = \int_m (y^2 + z^2) dm \tag{2.9a}$$

$$I_{yy} = \int_m (x^2 + z^2) dm \tag{2.9b}$$

$$I_{zz} = \int_m (x^2 + y^2) dm \tag{2.9c}$$

The moments of inertia are a measure of how far mass is distributed away from a given axis. For example, I_{xx} is calculated by summing the square of the distance to the x-axis for each infinitesimal point mass. The remaining terms in the inertia matrix are called the products of inertia and are given Equations (2.10a)—(2.10c):

$$I_{xy} = I_{xy} = \int_m xy \, dm \tag{2.10a}$$

$$I_{xz} = I_{zx} = \int_m xz \, dm \tag{2.10b}$$

$$I_{yz} = I_{zy} = \int_m yz \, dm \tag{2.10c}$$

The vehicle configurations considered here are axisymmetric. When one of the primary axes (x, y, or z) lines up with the axis of symmetry of an axisymmetric body, as

is true for these rocket configurations, the products of inertia are all zero. Another implication of this symmetry is that the moments of inertia in the plane perpendicular to the axis of symmetry (the $y-z$ plane in this case) are equal. Thus, we expect $I_{yy} = I_{zz}$.

In order to derive the moments of inertia, we evaluate equations (2.9a)—(2.9c) by substituting $dm = \rho dxdydz$.

$$I_{xx} = \int_m (y^2 + z^2)dm = \int_V (y^2 + z^2)\,\rho dxdydz \tag{2.11a}$$

$$I_{yy} = I_{zz} = \int_m (x^2 + z^2)dm = \int_V (x^2 + z^2)\,\rho dxdydz \tag{2.11b}$$

Since the body is axisymmetric, it is convenient to convert equations (2.11) into cylindrical coordinates. The axis of symmetry is the x-axis and therefore remains unchanged. We transform the y and z coordinates with the expressions $y = r\cos\theta$ and $z = r\sin\theta$. The expression $dxdydz$ becomes $rdrd\theta dx$.

$$I_{xx} = \int_V (r^2\cos^2\theta + r^2\sin^2\theta)\,\rho\, rdrd\theta dx \tag{2.12a}$$

$$I_{yy} = I_{zz} = \int_V (x^2 + r^2\sin^2\theta)\,\rho\, rdrd\theta dx \tag{2.12b}$$

These integrations are performed taking advantage of the vehicles' symmetry, whereby the radius is a function of x only, $R = f(x)$. The vehicle is divided into very thin slices, or cross-sections, along the x-axis, and a sum is taken over each slice. The derivation for this sum is shown below for I_{yy} and I_{zz}.

$$I_{yy} = I_{zz} = \int_0^L \int_0^{R(x)} \int_0^{2\pi} (x^2 + r^2\sin^2\theta)\,\rho\, r\, d\theta dr dx$$

$$I_{yy} = I_{zz} = \rho \int_0^{2\pi} \int_0^{L} \int_0^{R(x)} x^2 r \, d\theta dr dx + \rho \int_0^{2\pi} \int_0^{L} \int_0^{R(x)} r^3 \sin^2\theta \, d\theta dr dx$$

$$I_{yy} = I_{zz} = 2\pi\rho \int_0^{L} \int_0^{R(x)} x^2 r \, dr dx + \rho\pi \int_0^{L} \int_0^{R(x)} r^3 \, dr dx$$

$$I_{yy} = I_{zz} = 2\pi\rho \int_0^{L} x^2 \frac{R(x)^2}{2} dx + \rho\pi \int_0^{L} \frac{R(x)^4}{4} dx$$

$$I_{yy} = I_{zz} = 2\pi\rho \sum_{x_i} {x_i}^2 \frac{R(x_i)^2}{2} \Delta x + \rho\pi \sum_{x_i} \frac{R(x_i)^4}{4} \Delta x \tag{2.13}$$

Where the vehicle of length L has been broken into N slices along the x-axis, such that $x_0 = 0$, $x_N = L$, and $\Delta x = L/N$. I_{yy} and I_{zz} are calculated for both vehicle configurations using Equation (2.13) assuming a uniform density and N=10,000.

The I_{xx} term determines how much resistance the vehicle has to roll motion. In this case, the fact that much of the vehicle's interior mass is liquid must be considered. In the absence of friction between the liquid and cylindrical walls, the liquid would experience no roll motion and hence would not contribute to the I_{xx} moment of inertia. Therefore, the mass of the liquid, which is assumed to reside in the inner 90% of the volume, is not included in the calculation of I_{xx}. The moment of inertia is therefore that of a hollow cylinder and is calculated below.

$$I_{xx} = \int_V r^3(\cos^2\theta + \sin^2\theta)\, \rho \, dr d\theta dx$$

$$I_{xx} = \int_0^{L} \int_{R_1(x)}^{R_2(x)} \int_0^{2\pi} r^3 \rho \, d\theta dr dx$$

$$I_{xx} = 2\pi\rho \int_0^L \frac{R_2(x)^4 - R_1(x)^4}{4} dx$$

$$I_{xx} = 2\pi\rho \sum_{x_i} \frac{R_2(x)^4 - R_1(x)^4}{4} \Delta x \tag{2.14}$$

Where $R_2(x)$ is the outer radius and $R_1(x)$ is the inner radius, which here is 93% of $R_2(x)$, such that the volume of the hollow portion is 90% of the total vehicle volume. Equation (2.14) is solved for both vehicle configurations and the results are recorded in Tables 2.4 and 2.5.

Table 2.4— Air Launch Light Mass Properties

Parameter	**Value**	**Units**
Total Mass at Launch	9,321	kg
CG (measured from nose)	7.60	m
I_{zz}	89,440	kg-m^2
I_{yy}	89,440	kg-m^2
I_{xx}	401	kg-m^2

Table 2.5—Air Launch Heavy Mass Properties

Parameter	**Value**	**Units**
Total Mass at Launch	18,643	kg
CG (measured from nose)	9.77	m
I_{zz}	104,950	kg-m^2
I_{yy}	104,950	kg-m^2
I_{xx}	565	kg-m^2

2.3 Propulsion System Characteristics

Finally, the characteristics of the vehicles' propulsion systems must be determined. As illustrated in Table 2.6, most liquid ground-launched rockets have liftoff thrust to weight ratios (*T/W*) of 1.2 to 1.5. A higher *T/W* ratio reduces steering and gravity losses but tends to increase loss from atmospheric drag. Since air-launched vehicles suffer from less drag loss, the optimal thrust to weight ratio is likely higher than for ground-launch (Sarigul-Klijn, Noel, and Sarigul-Klijn 2004). Therefore a *T/W* ratio of 1.75 at ignition is selected for the air launch vehicles considered here. This implies that the first stage engine imparts a thrust equal to 1.75 times the vehicle gross weight at ignition. In the following chapters, vehicle performance losses due to dispersed ignition conditions will be quantified. It is assumed that any performance loss that results from dispersions early in the rocket's flight will be evident by the end of the first stage burn. Therefore, only the first stage burn will be modeled and it is sufficient to define the first stage propulsion characteristics alone.

The next step is to determine the specific impulse and mass flow rate during the first stage burn. It is assumed the rockets' first stage engines have the same specific impulse (I_{sp}) as the Falcon 1 launch vehicle's first stage. Given these values, the mass flow rate is calculated using Equation (2.15).

$$\dot{m} = \frac{T}{I_{sp} g} \tag{2.15}$$

Where $\dot{m}$ is the mass flow rate in kg/s and T is the first stage thrust in Newtons. The propulsion system characteristics for both vehicle configurations are summarized in Tables 2.7 and 2.8.

Table 2.6—Propulsion System Characteristics for Existing Two-stage Liquid Rockets

Vehicle	Weight (klb.)	Propellant	*T/W*	*Stage 1* I_{sp} (s)
Falcon 1	53	LOX/kerosene	1.36	310
Soyuz U	683	LOX/kerosene T-1	1.33	245*
Titan II	340	N_2O_4/Aerozine-50	1.4	296

Sources: Falcon 1 User's Guide, 2008; Isakowitz et al., 2004.

* The strap-on boosters are considered the first stage, although these boosters and the "second stage" core engine light simultaneously at liftoff. The second stage core (LOX/kerosene) has an Isp of 264s.

Table 2.7—Air Launch Light Propulsion System Characteristics

Weight	*T/W*	*T*	I_{sp}	$\dot{m}$
91,410 N (20,550 lbf.)	1.75	160,000 N (35,960 lb.)	310 s	52.6 kg/s

Table 2.8—Air Launch Heavy Propulsion System Characteristics

Weight	*T/W*	*T*	I_{sp}	$\dot{m}$
182,820 N (41,100 lbf.)	1.75	320,000 N (71,930 lb.)	310 s	105 kg/s

Chapter 3: Aerodynamics

Chapter 3 presents aerodynamic models for both vehicle configurations. First, the relevant coordinate frames used in this study are presented. In addition, methods for transforming between these coordinate frames are explained. Section 3.2 describes how aerodynamic coefficients are used to represent the aerodynamic forces and moments acting on a vehicle during flight. Finally, Section 3.3 discusses how U.S. Air Force Missile DATCOM software is used to derive the aerodynamic coefficients and presents the resulting aerodynamic models.

3.1 Coordinate Frames

A three-dimensional rectangular coordinate system is described by three mutually orthogonal lines that intersect at an origin. A vector can therefore be represented by three components, corresponding to the vector's distance from each of the three perpendicular lines. Coordinate frames that are commonly used to represent flight vehicles (missiles, aircraft, launch vehicle, etc.) include:

1. *Inertial Frame:* A frame fixed in space in which Newton's laws of motion hold. The *Earth-Centered Inertial (ECI)* frame is an inertial frame with origin at Earth's center. (Although not truly inertial because the frame translates with the Earth about the Sun, the ECI frame can be considered approximately inertial for most aircraft flight envelopes.)
2. *Earth-centered, Earth Fixed (ECEF)*: A frame with origin at Earth's center and that rotates in inertial space with the Earth. Hence, its axes are fixed with respect to the Earth's surface.
3. *Body Frame*: A frame with origin at a reference center of mass on the vehicle and whose axes are fixed to the vehicle, and therefore rotate along with the rigid body.
4. *Wind Frame:* A frame attached to the vehicle with the origin at the center of mass and the x-axis along the direction of on-coming wind.

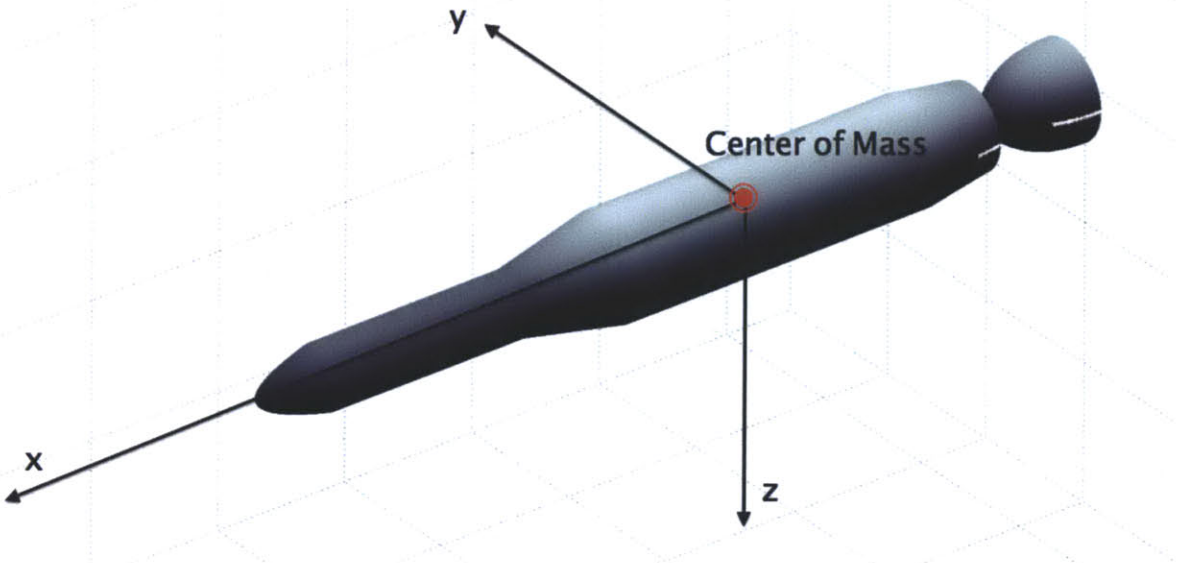

Figure 3.1—The Body Coordinate Frame

In the 6-DOF dynamics simulation presented here, multiple coordinate frames are used, each of which obey the right hand rule. It is important to understand how to represent vectors in each coordinate system and how to transform from one frame to another. The body-fixed coordinate frame is illustrated in Figure 3.1. It is a right-handed coordinate system with origin at the vehicle's center of mass. The x-axis lies along the longitudinal, or roll, axis of the vehicle and is positive toward the nose. The y-axis, or pitch axis, is positive along the right wing. Finally, the z-axis, or yaw axis, is positive downward.

The Euler angles, yaw (ψ), pitch (θ), and roll (ϕ), are often used to relate body-fixed and Earth-fixed coordinate frames. Figure 3.2 illustrates how the Euler angles define the vehicle attitude relative to the Earth-fixed frame. To transform a vector in Earth-fixed coordinates to Body coordinates a rotation matrix is applied for each of the

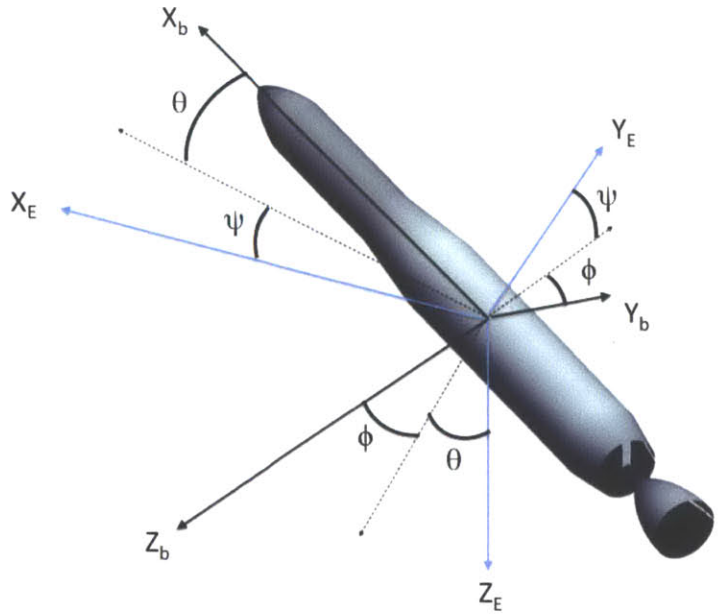

Figure 3.2—The Euler Angles describe the vehicle body attitude relative to an Earth-fixed or Inertial reference frame.

Euler angles. The rotations must be performed in the order: *yaw*, *pitch*, then *roll*:

$$T_{E\to B} = \begin{bmatrix} 1 & 0 & 0 \\ 0 & \cos\phi & \sin\phi \\ 0 & -\sin\phi & \cos\phi \end{bmatrix} \begin{bmatrix} \cos\theta & 0 & -\sin\theta \\ 0 & 1 & 0 \\ \sin\theta & 0 & \cos\theta \end{bmatrix} \begin{bmatrix} \cos\psi & \sin\psi & 0 \\ -\sin\psi & \cos\psi & 0 \\ 0 & 0 & 1 \end{bmatrix}$$

$$T_{E\to B} \tag{3.1}$$

$$= \begin{bmatrix} \cos\theta\ \cos\psi & \cos\theta\ \sin\psi & -\sin\theta \\ \sin\phi\sin\theta\cos\psi - \cos\phi\sin\psi & \sin\phi\sin\theta\sin\psi + \cos\theta\cos\psi & \sin\phi\cos\theta \\ \cos\phi\sin\theta\cos\psi + \sin\phi\sin\psi & \cos\phi\sin\theta\sin\psi - \sin\phi\cos\psi & \cos\phi\cos\theta \end{bmatrix}$$

The wind axes are dictated by the direction of the oncoming wind relative to the vehicle. The x-axis lies along the direction of the oncoming wind. The wind vector is equal to the negative of the air-relative velocity vector of the vehicle's center of mass. The wind and body frames are related by the angle of attack, α, and the sideslip angle, β, as illustrated in Figure 3.3. These quantities are given by the Equations (3.2a)—(3.2c).

$$\alpha = \tan^{-1}\left(\frac{w}{u}\right) \tag{3.2a}$$

$$\beta = \tan^{-1}\left(\frac{v}{V_0}\right) \tag{3.2b}$$

$$V_0 = \sqrt{u^2 + v^2 + w^2} \tag{3.2c}$$

Where u, v, and w, are the components of the velocity vector of the reference center of mass along the x-, y-, and z- body axes, respectively. The angle of attack, α, is sometimes referred to as the *body-axis* angle of attack to differentiate it from the *total* angle of attack, α_T. The total angle of attack is given by Equation (3.3) and the difference between α and α_T is illustrated in Figure 3.3.

$$\alpha_T = \tan^{-1}(\sqrt{v^2 + w^2}/u) \tag{3.3}$$

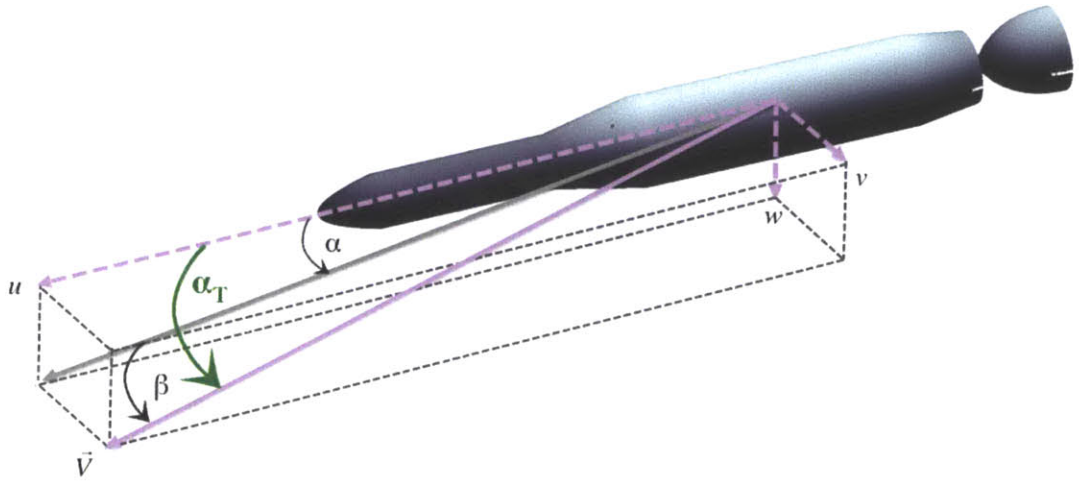

Figure 3.3 —The body and wind coordinate frames are related by angle of attack, α, the sideslip angle, β, and the *total* angle of attack, α_T.

In order to transform a vector in body-frame coordinates to wind-frame coordinates, apply two rotation matrices: one about the sideslip angle (β) and one about the angle of attack, (α):

$$T_{B\to W} = \begin{bmatrix} \cos\alpha & 0 & \sin\alpha \\ 0 & 1 & 0 \\ -\sin\alpha & 0 & \cos\alpha \end{bmatrix} \begin{bmatrix} \cos\beta & \sin\beta & 0 \\ -\sin\beta & \cos\beta & 0 \\ 0 & 0 & 1 \end{bmatrix}$$

$$T_{B\to W} = \begin{bmatrix} \cos\alpha\cos\beta & \sin\beta & \cos\alpha\cos\beta \\ -\cos\alpha\sin\beta & \cos\beta & -\sin\alpha\sin\beta \\ -\sin\alpha & 0 & \cos\alpha \end{bmatrix} \tag{3.4}$$

Finally, Figure 3.4 illustrates how the angle of attack, pitch, and flight path angle are related. The flight path angle (γ), is the angle between the vehicle's velocity vector and the Earth-fixed $x-y$ plane, which is horizontal to the Earth's surface.

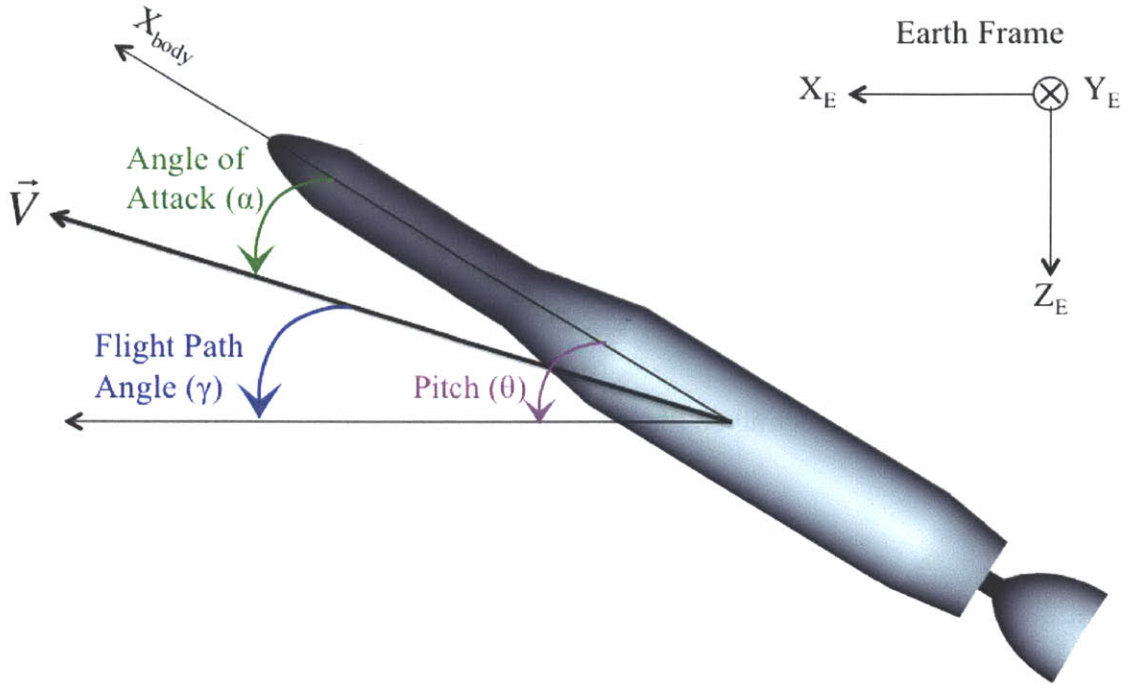

Figure 3.4—Angle of attack, pitch, and flight path angle.

3.2 Aerodynamic Coefficients

During the uncontrolled drop phase, the only forces acting on the rocket are the gravitational force from Earth and aerodynamic forces imparted by the atmosphere. The magnitude and direction of the gravitational force depends only on the position of the vehicle and is derived in Section 4.1. Deriving the aerodynamic forces is more complicated because they depend on the vehicle geometry, attitude, and air-relative velocity. The aerodynamic forces and moments acting on a vehicle are commonly expressed in terms of dimensionless coefficients listed in Table 3.1.

Table 3.1—Aerodynamic Coefficients

Coefficient	*Definition*	*Frame*
C_N	Normal Force Coefficient	Body
C_A	Axial Force Coefficient	Body
C_Y	Side Force Coefficient	Body
C_L	Lift Coefficient	Wind
C_D	Drag Coefficient	Wind
C_M	Pitching Moment Coefficient	Body
C_n	Yawing Moment Coefficient	Body
C_l	Rolling Moment Coefficient	Body

The forces and moments acting on the vehicle are obtained from Equations (3.5a)—(3.5i).

$$F_x = qSC_A \tag{3.5a}$$

$$F_y = qSC_Y \tag{3.5b}$$

$$F_z = qSC_N \tag{3.5c}$$

$$F_{DRAG} = qSC_D \tag{3.5d}$$

$$F_{LIFT} = qSC_L \tag{3.5e}$$

$$\bar{L} = qSbC_l \tag{3.5f}$$

$$M = qS\bar{c}C_M \tag{3.5g}$$

$$N = qSbC_n \tag{3.5h}$$

$$q = \frac{1}{2}\rho V^2 \tag{3.5i}$$

Where S is the wing reference area, b is the reference wing span, $\bar{c}$ is the wing mean geometric chord, q is the free-stream dynamic pressure, ρ is the local air density and V is the air speed. The atmospheric pressure field exerts forces over the entire vehicle in various directions. However, the total sum of the vectorial forces can be equivalently represented by three forces acting along each of the body axes. Forces F_x, F_y, and F_z

represent forces in the body frame, as illustrated in Figure 3.1. Thus, F_x acts along the vehicle's longitudinal axis and is positive toward the nose. F_y is positive along the direction of the right wing, and F_z is positive downward. The lift and drag forces, on the contrary, act along the wind-frame axes. The drag force (F_{DRAG}) acts in the direction opposite to the vehicle's air-relative velocity vector. The drag force is therefore a retarding force, opposing the vehicle's forward motion. The lift force acts perpendicular to the drag force as illustrated in Figure 3.5.

The moments ($\bar{L}, N, M$) represent moments about each of the three body axes. The sense of each moment is determined by the right hand rule and is illustrated in Figure 3.6. $\bar{L}$, the rolling moment, is the moment about the body x-axis and is defined to be positive in the clockwise direction. M, the pitching moment, is the moment about the body y-axis.

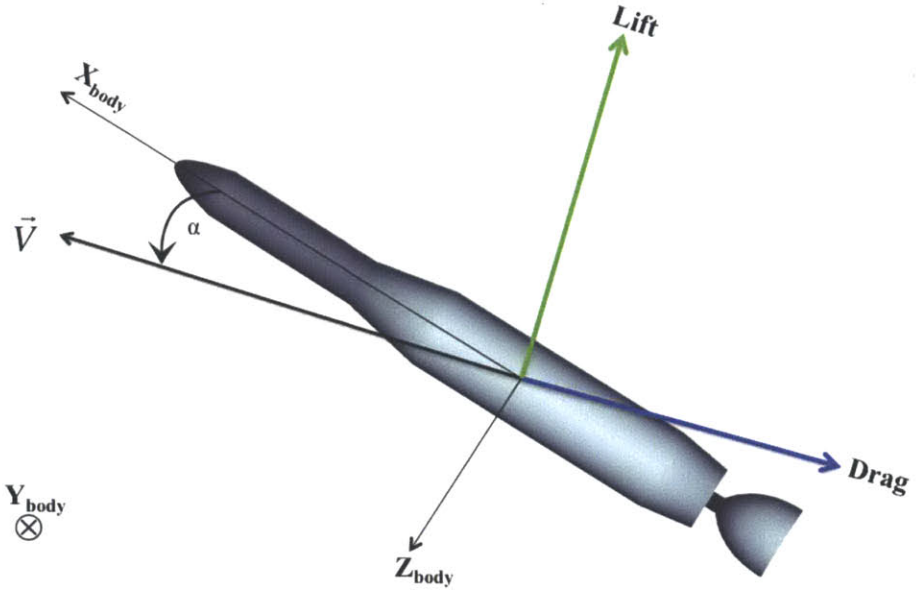

Figure 3.5—The drag force (F_{DRAG}) acts opposite to the vehicle's air-relative velocity vector, while the lift force (F_{LIFT}) acts perpendicular to the drag force.

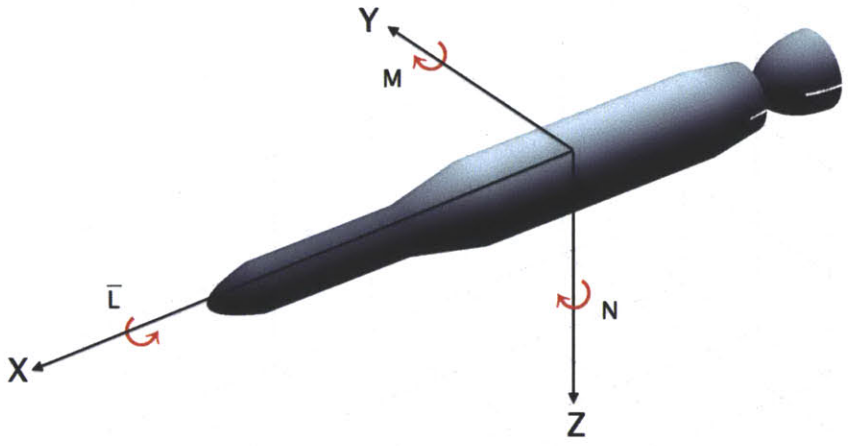

Figure 3.6—The senses of the moments $(\bar{L}, N, M)$ about each of the three body axes are determined by the right hand rule.

It is positive when the nose of the vehicle moves upward toward the negative body z-axis. N, the yawing moment, is positive in a clockwise direction about the body z-axis, when the nose of the vehicle moves toward the right wing.

3.3 Missile DATCOM

In this work, the body frame aerodynamic coefficients (C_N, C_A, C_Y, C_M, C_l, C_n) are used to calculate the aerodynamic forces and moments acting on the vehicle. Aerodynamic coefficients depend on the geometry of the vehicle and can be derived experimentally with wind tunnel tests or by computer simulation. Here, the coefficients are obtained from USAF Missile DATCOM. This software is an industry standard

aerodynamic prediction tool used to quickly construct aerodynamic models for a variety of missile configurations. Originally developed in 1985 by the US Army Aviation and Missile Research, Development and Engineering Center (AMRDEC) and the Air Vehicles Directorate of the Air Force Research Laboratory (AFRL/RB), the code has been enhanced over the past 25 years. The March 2011 FORTRAN 90 Version of Missile DATCOM is used in this work. DATCOM is run in batch mode with at least one user-defined input file and generates several output files containing aerodynamic data requested by the user.

Missile DATCOM can model the aerodynamics for axisymmetric or elliptical bodies, where the longitudinal axis is the axis of symmetry. The vehicle geometry and flight conditions are defined in a text file named "for005.dat." Input values are defined using FORTRAN namelists. The software can be run with a variety of optional features. The user chooses to implement these options by setting "name cards" in the for005.dat file.

Aerodynamic control surfaces are sometimes used for launch vehicle attitude control. However, aerosurfaces come with an added weight and cost penalty. Since cost would be of the utmost importance to the designer of a dedicated small satellite launch vehicle, the vehicles in this study are chosen to have no aerosurfaces. This choice also greatly simplifies prediction of the aerodynamic coefficients by Missile DATCOM. The body geometry is defined using "Option 2" for axisymmetric bodies, whereby the radius is defined as a function of x-coordinate along the axis of symmetry measured from the nose. The AXIBOD namelist is defined using two arrays, X and R. Each value of X_i corresponds to a longitudinal position where the radius is R_i.

Aerodynamic coefficients are a function of Mach number, angle of attack, and sideslip angle. The user sets the namelist MACH equal to an array containing each Mach number at which aerodynamic data are desired. The user has the choice to either fix the sideslip angle (β) and vary the body-axis angle of attack (α), or fix the roll angle (ϕ), and vary the total angle of attack (α_T). Here, the first option is selected. The sideslip β is set to a single value, and the namelist ALPHA is set to an array of values of α. Therefore, for a given value of β, Missile DATCOM outputs the aerodynamic coefficients for each (MACH, ALPHA) pair requested by the user. The exit diameter is set to zero (DEXIT=0) to ensure that the full base drag is included in the axial force calculation. The input and output quantities are defined in English units (ft., in., etc.) by setting "DIM FT." The default values for the reference lengths and areas ($\bar{c} = b = 5$ ft and $S = 19.634$ ft^2) are used.

Missile DATCOM uses a body-fixed coordinate system that differs from the body coordinate system defined earlier in this chapter. The Missile DATCOM coordinate system is illustrated in Figure 3.7. This type of coordinate frame is sometimes called the

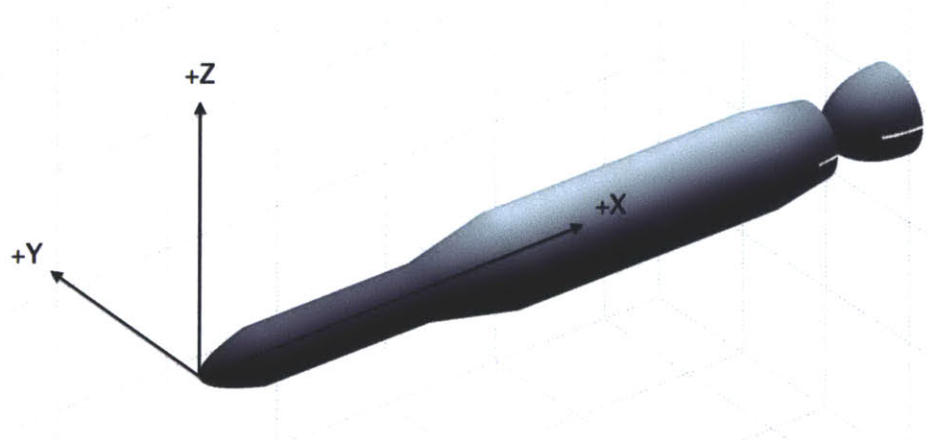

Figure 3.7—Missile DATCOM coordinate system.

"structural frame" and is frequently used during vehicle assembly. The x-axis lies along the longitudinal direction of the vehicle, but is defined positive aft of the nose. The positive z-axis points up and the y-axis completes the right-handed system, with positive y pointing to the right of the vehicle. The axial and normal force coefficients from Missile DATCOM are therefore defined positive in the opposite direction of the traditional body axes, as illustrated in Figure 3.8. The forces in the traditional body frame (as defined in Section 3.2) are obtained using Equation (3.6).

$$\begin{bmatrix} F_x \\ F_y \\ F_z \end{bmatrix} = qS \begin{bmatrix} -C_A \\ C_Y \\ -C_N \end{bmatrix} \tag{3.6}$$

Where C_A and C_N are the coefficients produced by Missile DATCOM. The origin of the coordinate system used in Missile DATCOM lies along the axis of symmetry, the x-axis. The location of the origin on the x-axis is defined by the user by setting the parameter, X0, which corresponds to the x-coordinate of the nose tip. Here, X0=0 which

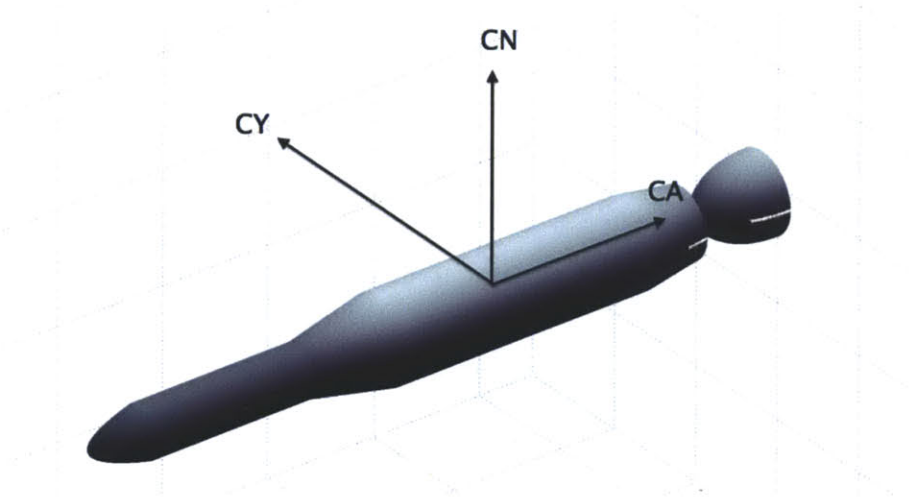

Figure 3.8—Body force coefficients given by Missile DATCOM

sets the origin at the nose tip. Therefore, the moment coefficients represent moments about the nose, which will later be transformed to moments about the center of mass.

Figure 3.9 illustrates the positive orientations of the moment coefficients as defined by Missile DATCOM. The pitching moment coefficient orientation is defined by the right hand rule convention about the positive y-axis. The rolling moment and yawing moment coefficients are defined in the negative right hand rule convention relative to Missile DATCOM's positive x- and z-axes. However, note that the senses of C_n and C_l are therefore consistent with the right hand rule convention for the traditional body-fixed frame defined in Section 3.2.

The magnitude and direction of the body force coefficients do not depend on the placement of X0. However, the magnitude and direction of the moment coefficients depend on the origin location. For example consider the aerodynamic normal force, which causes a pitching moment about the y-axis. The normal force acts at a location on the vehicle known as the center of pressure, a distance X_{cp} from the nose along the x-axis, as illustrated in Figure 3.10. The pitching moment is then given by Equation (3.7).

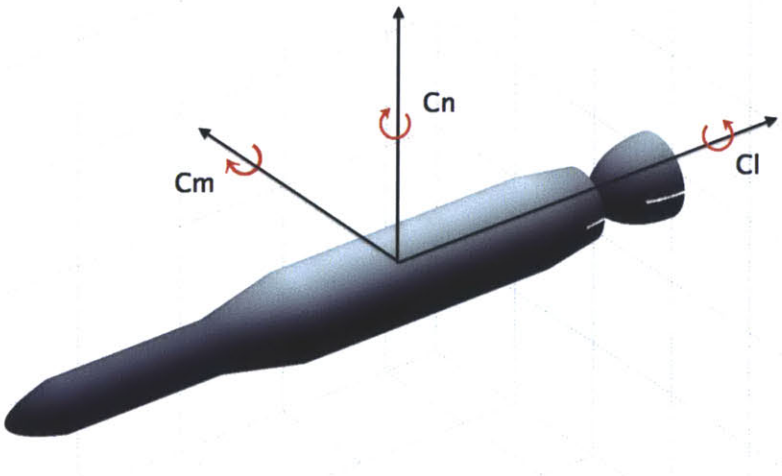

Figure 3.9—Moment Coefficients as defined by Missile DATCOM

$$M = F_z(X_{cp} - X0) \tag{3.7}$$

The center of pressure location varies with Mach number, angle of attack, and sideslip. Missile DATCOM calculates X_{cp} for each (Mach, alpha, beta) set and records it in terms of multiples of the reference length, x_{cp}.

$$\frac{X_{cp}}{\bar{c}} = x_{cp} \tag{3.8}$$

Substituting Equations (3.5), (3.8), and X0=0 into Equation (3.7) results in the following Equation.

$$qS\bar{c}C_M = qSC_N\, x_{cp}\bar{c}$$

$$C_M = C_N\, x_{cp} \tag{3.9}$$

The 6DOF equations of motion, which will be discussed in Chapter 4, require the moments about the center of mass. A torque on the vehicle exists when the center of pressure is offset from the vehicle center of gravity, as illustrated in Figure 3.10. The pitching moment about the center of mass is calculated using Equation (3.10):

$$M = F_z(X_{cp} - CG) \tag{3.10}$$

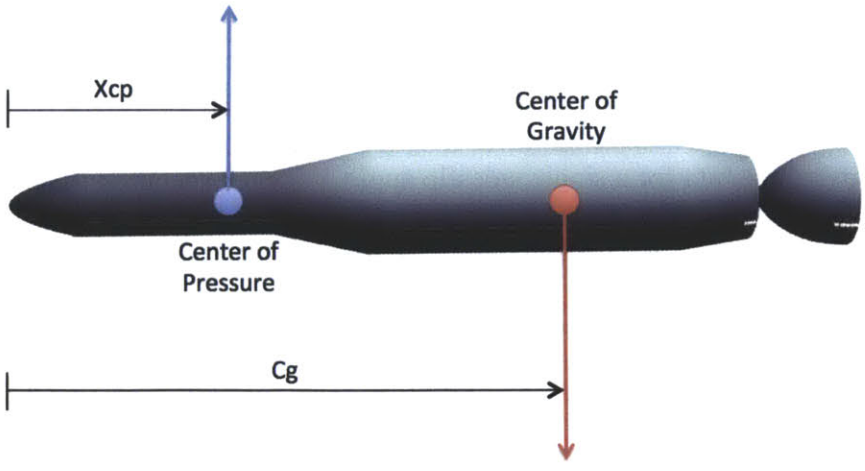

Figure 3.10—The normal and gravitational forces may cause vehicle torques.

Where X_{cp} and CG are both measured from the nose. Note that when $(X_{cp} - CG) < 0$, (which is generally the case) a negative normal force results in a positive pitching moment about the center of mass. Similarly, the yawing moment is given by Equation (3.11).

$$N = -F_y(X_{cp} - CG) \tag{3.11}$$

In this case, a positive side force produces a positive moment about the z-axis. Note that the pitching and yawing moments can be arrived at with knowledge of the normal force, axial force, and center of pressure location. Therefore, it is not necessary to independently keep track of the C_M and C_n coefficients.

3.4 Missile DATCOM Results

All the aerodynamic data needed for this analysis is contained in the output file named "for006.dat." A sample output file is provided in Appendix A. The output file first displays the user input information provided in for005.dat. Each for006.dat output file contains aerodynamic data for a single sideslip angle. For each specified Mach number the output file contains a table of aerodynamic coefficients and center of pressure location at each angle of attack listed in the input file. The output file provides each of the aerodynamic coefficients in Table 3.1 in addition to various coefficient partial derivatives.

The 6DOF dynamic simulation requires each of the three body-axis force coefficients from Table 3.6 and the center of pressure location, X_{cp}. The software was run for both vehicle configurations for Mach numbers 0.48, 0.5, and 0.52. For each Mach number, aerodynamic coefficients are calculated at angles of attack from 0 to 180° in 5° increments, and for sideslip angles from -80° to 80° in 10° increments. For the drop phase 6-DOF dynamic simulation, during which the Mach number is always close to 0.5, the aerodynamic coefficients are determined at each increment by 3-D interpolation over these data. Figures 3.11 – 3.14 present C_N, C_A, C_Y, and X_{cp} as a function of angle of attack for various fixed values of sideslip (at Mach 0.5) for Air Launch Light.

Chapter 5 describes the construction of a 6DOF simulation of the first stage burn, during which the rocket experiences velocities up to about Mach 10. In order to derive the aerodynamic coefficients necessary for this simulation, Missile DATCOM was run at Mach 0.5, 0.6, 0.7, 0.8, 0.9, 1.0, 1.2, 1.4, 1.6, 1.8, 2, 2.5, 3, 4, 5, 6, 7, 8, and 9. The values of C_N, C_A, and X_{cp} are shown as a function of angle of attack for various Mach numbers (and fixed $\beta = 0°$) for Air Launch Light in Figures 3.15, 3.16, and 3.18, respectively. The side force coefficient C_Y is shown as a function of sideslip angle for various Mach numbers (and fixed $\alpha = 20°$) in Figure 3.17. Note that the magnitude of the aerodynamic forces is greatest near Mach 1. Furthermore, for rocket ascent trajectories the magnitude of the aerodynamic forces quickly falls off with altitude because aerodynamic forces are a function of atmospheric density. Therefore, at the highest Mach numbers, by which time the rocket has ascended above most of the atmosphere, aerodynamic effects are minimal.

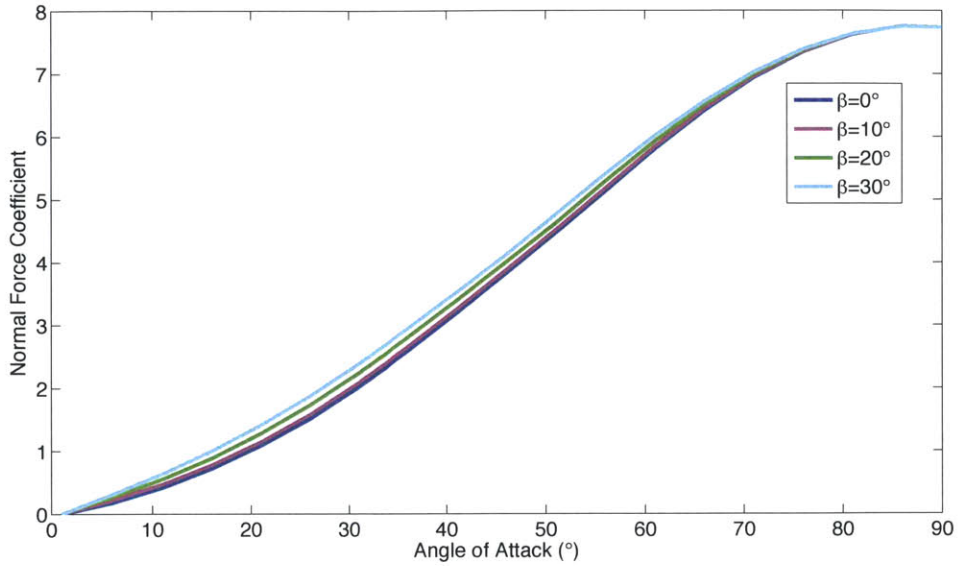

Figure 3.11—Normal Force Coefficient as a function of angle of attack for various sideslip angles and fixed Mach 0.5

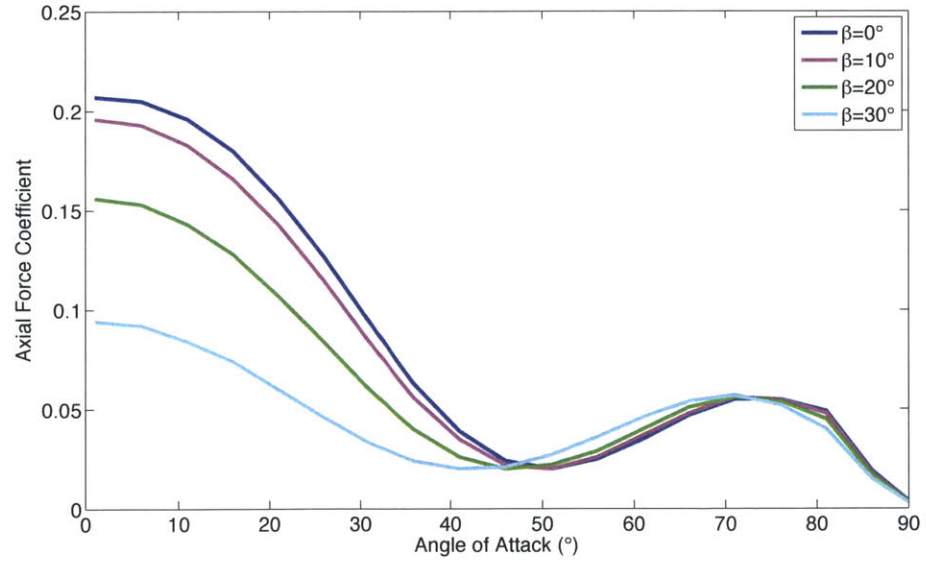

Figure 3.12—Axial Force Coefficient as a function of angle of attack for various sideslip angles and fixed Mach 0.5

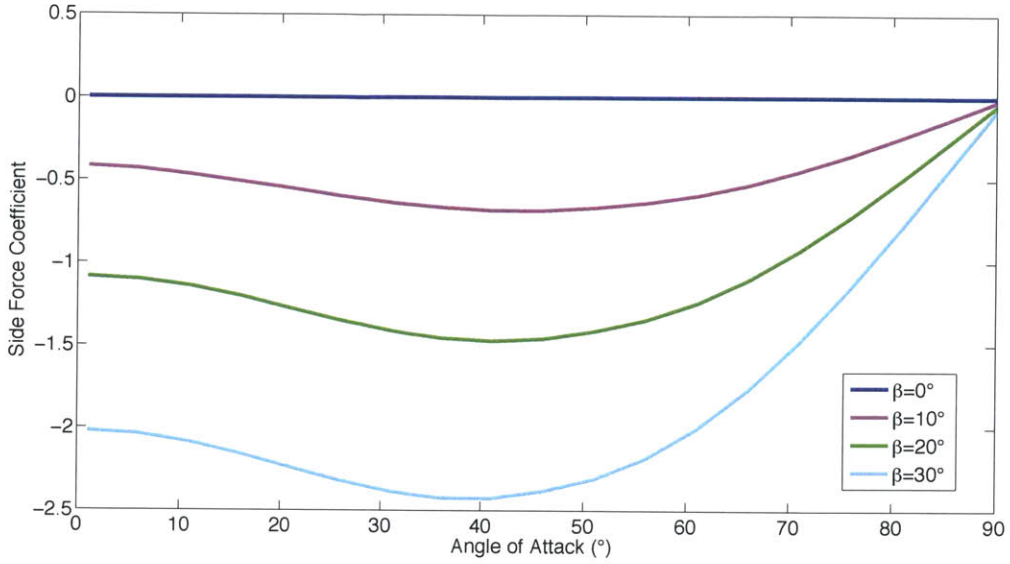

Figure 3.13—Side Force Coefficient as a function of angle of attack for various sideslip angles and fixed Mach 0.5

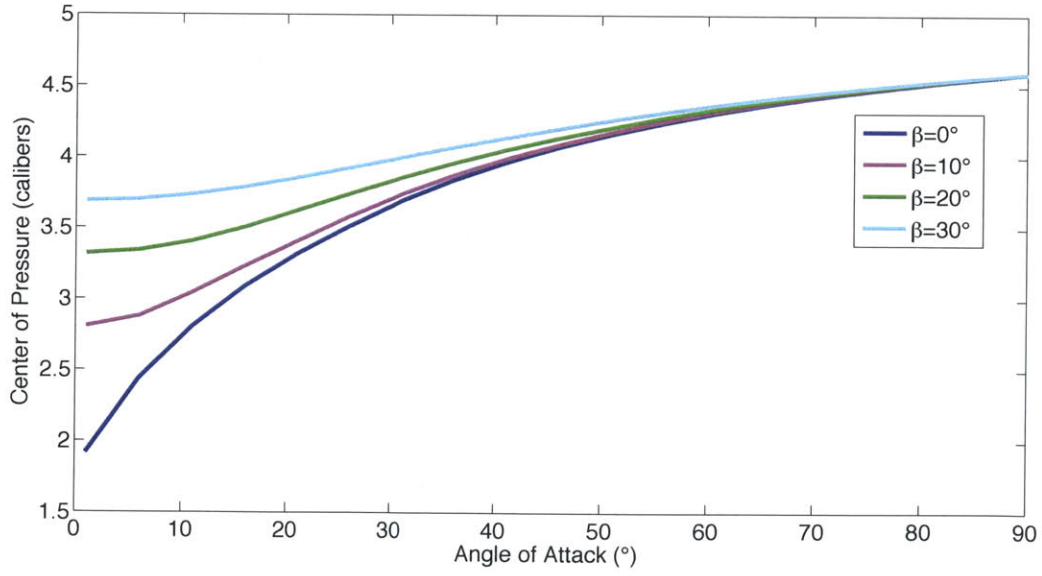

Figure 3.14—Center of Pressure Location (measured in calibers from the nose) as a function of angle of attack for various sideslip angles and fixed Mach 0.5

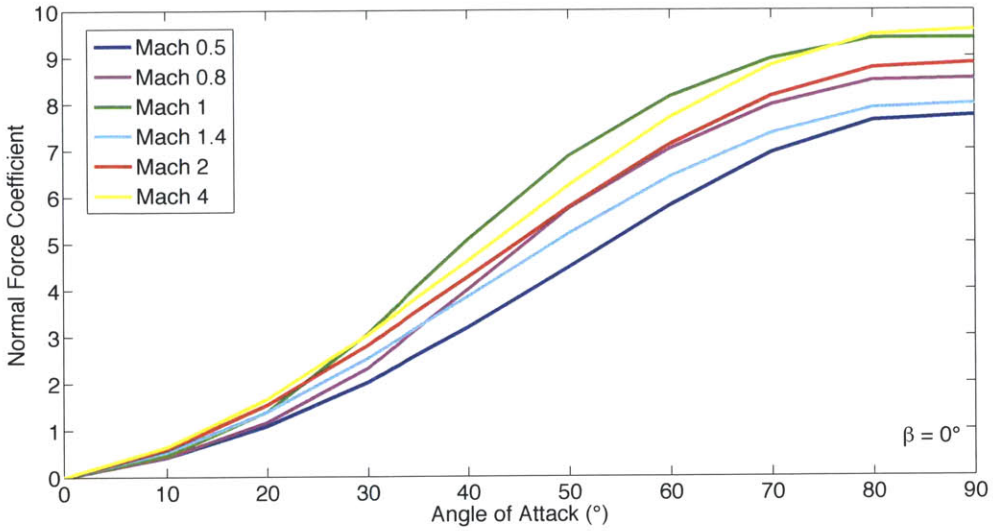

Figure 3.15—Normal Force Coefficient as a function of angle of attack for various Mach numbers and fixed $\beta = 0°$.

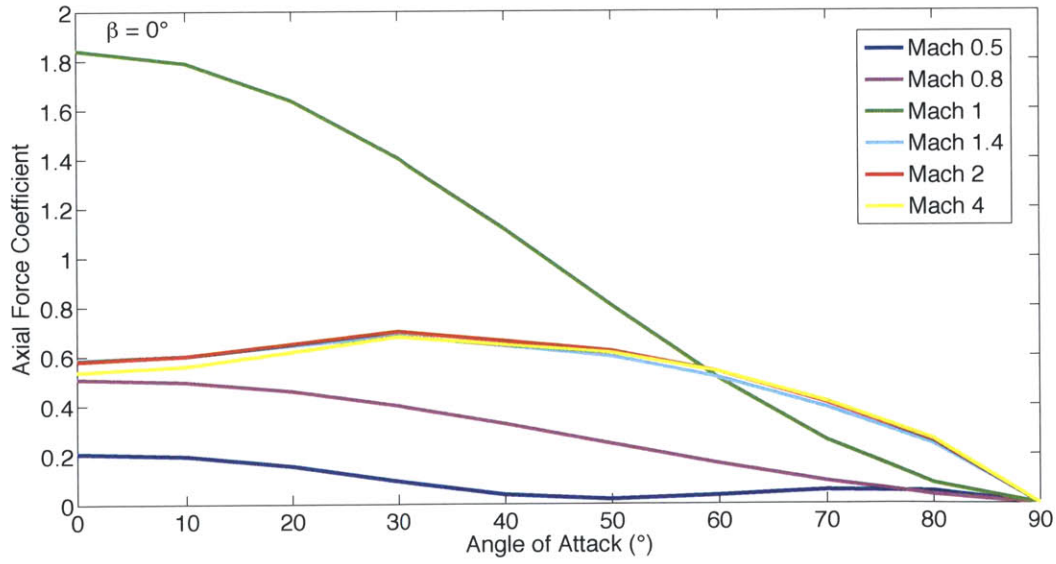

Figure 3.16—Axial Force Coefficient as a function of angle of attack for various Mach numbers and fixed $\beta = 0°$.

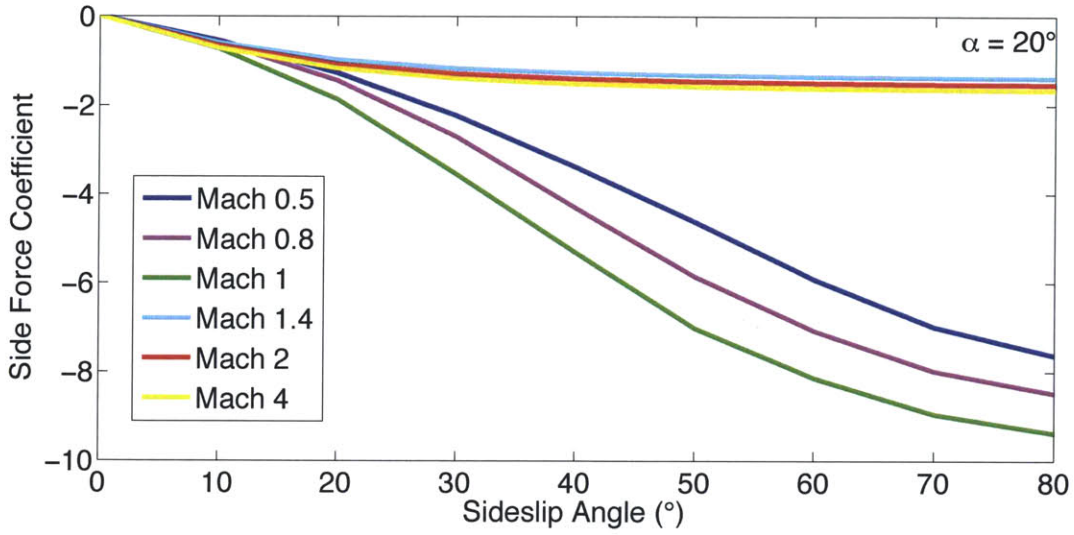

Figure 3.17—Side Force Coefficient as a function of sideslip angle for various Mach numbers and fixed $\alpha = 20°$.

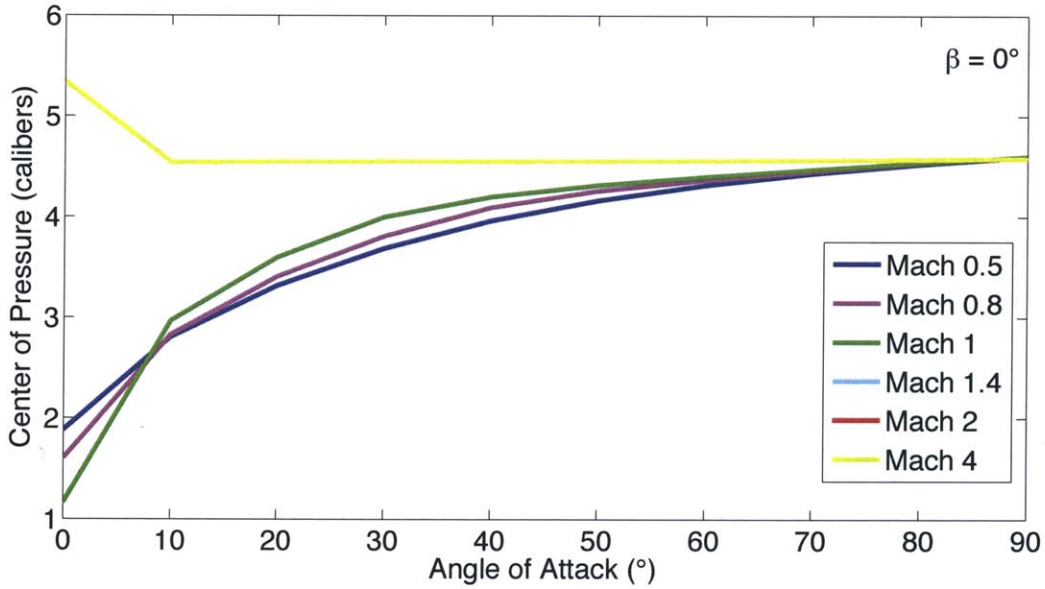

Figure 3.18—Center of Pressure location (measured in calibers from the nose) as a function of angle of attack for various Mach numbers and fixed $\beta = 0°$.

Chapter 4: Six Degree-of-Freedom Simulation

4.1 Equations of Motion

With the aerodynamic coefficients and vehicle mass properties in hand, the full six degree-of-freedom (6DOF) equations of motion can be solved. Chapter 4 investigates the rocket's behavior during the few seconds between release from the carrier aircraft and ignition. During this phase of flight the only forces acting on the vehicle are the Earth's gravitational force and the aerodynamic forces. Five simplifying assumptions are adopted for the drop phase 6-DOF simulation:

1. The vehicle is assumed to be a *rigid body*, which implies that the vehicle's size and shape do not change over time.
2. The vehicle is assumed to experience *no roll motion*. Logan et al. (2006) investigate the aerodynamics of a generic air-launched rocket (similar in shape to the vehicles considered in this study) at low Mach number and high angle of attack. The results showed that the rocket experienced negligible rolling moment for speeds of Mach 0.4 to 0.5. (The drop phase analysis presented in this study assumes the rocket is dropped at Mach 0.5.)
3. The Earth is assumed to be spherical and rotating at a constant angular velocity.
4. It is assumed that the atmosphere (in the absence of winds) rotates with the Earth.

Wind speeds are therefore defined with respect to the Earth's surface.

5. During the 4-second drop phase simulation, the Earth-fixed coordinate frame is considered an inertial coordinate frame.

4.1.1 Translational Motion

Here the equations describing the translational motion of the vehicle's center of mass are derived in body-fixed coordinates. The motion of the vehicle's center of mass is given by Equation (4.1), Newton's second law.

$$\sum \vec{F} = m\vec{a} = m\frac{d\vec{V}}{dt} \tag{4.1}$$

Where $\vec{a}$ and $\vec{V}$ are the acceleration and velocity of the center of mass, respectively. The velocity of the center of mass in the body frame is given Equation (4.2).

$$\vec{V} = u\hat{\imath} + v\hat{\jmath} + w\hat{k} \tag{4.2}$$

Where $\hat{\imath}$, $\hat{\jmath}$, and $\hat{k}$ are the unit vectors along the x-, y-, and z-axes in the body frame, respectively. The body-fixed coordinate system is attached to the rigid vehicle and rotates relative to the inertial coordinate frame. Therefore, the unit vectors, $\hat{\imath}$, $\hat{\jmath}$, and $\hat{k}$, also change with time. The angular velocity at which the body frame rotates relative to the inertial frame is given by Equation (4.3).

$$\vec{\omega} = \omega_x\hat{\imath} + \omega_y\hat{\jmath} + \omega_z\hat{k} = p\hat{\imath} + q\hat{\jmath} + r\hat{k} \tag{4.3}$$

Where p, q, and r are the roll, pitch, and yaw rates, respectively. According to the *Theorem of Coriolis*, the total time derivative of the velocity of the center of mass is given by Equation (4.4).

$$\left(\frac{d\vec{V}}{dt}\right)_{inertial} = \left(\frac{d\vec{V}}{dt}\right)_{body} + \vec{\omega}\times\vec{V} \tag{4.4}$$

Substituting this expression into Equation (4.1) results in Equation (4.5).

$$F = m\left(\frac{d\vec{V}}{dt}\right)_{body} + m(\vec{\omega}\times\vec{V}) \tag{4.5}$$

Where the cross product is evaluated:

$$\vec{\omega}\times\vec{V} = \begin{pmatrix} \hat{\imath} & \hat{\jmath} & \hat{k} \\ p & q & r \\ u & v & w \end{pmatrix} = (wq - vR)\hat{\imath} + (ur - wp)\hat{\jmath} + (vp - uq)\hat{k} \tag{4.6}$$

Newton's Second Law can then be expressed by Equations (4.7a)—(4.7c).

$$\sum \vec{F}_x = m\left(\frac{du}{dt} + wq - vR\right)\hat{\imath} \tag{4.7a}$$

$$\sum \vec{F}_y = m\left(\frac{dv}{dt} + ur - wp\right)\hat{\jmath} \tag{4.7b}$$

$$\sum \vec{F}_z = m\left(\frac{dw}{dt} + vp - uq\right)\hat{k} \tag{4.7c}$$

The total force acting on the vehicle during the uncontrolled drop is the sum of the aerodynamic forces from atmospheric pressure and the Earth's gravitational force.

$$\sum \vec{F}_x = F_{Aero,x} + F_{g,x} \tag{4.8a}$$

$$\sum \vec{F}_y = F_{Aero,y} + F_{g,y} \tag{4.8b}$$

$$\sum \vec{F}_z = F_{Aero,z} + F_{g,z} \tag{4.8c}$$

The aerodynamic forces acting along each of the body-axes are readily obtained from the body-frame aerodynamic coefficients by Equations (4.9a)—(4.9c).

$$F_{Aero,x} = qSC_A \tag{4.9a}$$

$$F_{Aero,y} = qSC_Y \tag{4.9b}$$

$$F_{Aero,z} = qSC_N \tag{4.9c}$$

The gravitational force is given in Earth-fixed coordinates by Equation (4.10).

$$F_g = mg\widehat{z_E} \tag{4.10}$$

Where g is the local acceleration due to Earth's gravity (9.81 m/s^2) and $\widehat{z_E}$ is the unit vector pointing from the vehicle center of mass in the direction of Earth's center of mass. The gravitational force vector is transformed into body coordinates using the rotation matrix in Equation (3.1). The resulting vector, Equation (4.11b), is written in terms of the Euler angles.

$$F_{g,B} = T_{E\to B}\begin{bmatrix}0\\0\\g\end{bmatrix} \tag{4.11a}$$

$$F_{g,B} = \begin{bmatrix}-g\sin\theta\\ g\ \sin\phi\cos\theta\\ g\ \cos\phi\cos\theta\end{bmatrix} \tag{4.11b}$$

Equations (4.9a)—(4.9c) and (4.11b) are substituted into Equations (4.7a)—(4.7c). The time-rate of change of the body velocities are then solved for, resulting in Equations (4.12a)—(4.12c).

$$\dot{u} = \frac{F_{Aero,x}}{m} - g\sin\theta + rv - qw \tag{4.12a}$$

$$\dot{v} = \frac{F_{Aero,y}}{m} + g\sin\phi\cos\theta - ru + pw \tag{4.12b}$$

$$\dot{w} = \frac{F_{Aero,z}}{m} + g\cos\phi\cos\theta + qu - pv \tag{4.12c}$$

4.1.2 Rotational Motion

Section 4.1.2 considers the rotation of a rigid body about its center of mass. Rotational dynamics can be derived from Equation (4.13).

$$\overrightarrow{T_B} = \left(\frac{d\overrightarrow{H_B}}{dt}\right)_{inertial} \tag{4.13}$$

Where $\overrightarrow{T_B}$ and $\overrightarrow{H_B}$ are the net torque acting on the vehicle and the vehicle's angular momentum vector in body-frame coordinates, respectively. The angular momentum of an infinitesimal point mass, δm, located at position $\vec{r}$ relative to the center of mass is given by Equation (4.14).

$$\delta\overrightarrow{H_B} = [\vec{r}\times(\omega_B\times\vec{r})]\delta m \tag{4.14}$$

Substituting $\vec{r} = x\hat{\imath} + y\hat{\jmath} + z\hat{k}$ and $\overrightarrow{\omega_B} = p\hat{\imath} + q\hat{\jmath} + r\hat{k}$ and performing the integration over all point masses yields:

$$\overrightarrow{H_B} = \begin{bmatrix} p\int(y^2+z^2)\,dm - q\int(xy)dm - r\int(xz)dm \\ q\int(x^2+z^2)\,dm - r\int(yz)dm - p\int(yx)dm \\ r\int(x^2+y^2)\,dm - p\int(zx)dm - q\int(zy)dm \end{bmatrix} \tag{4.15}$$

Equation (4.15) can be equivalently expressed in terms of the inertia tensor, I:

$$\overrightarrow{H_B} = I\begin{bmatrix} p \\ q \\ r \end{bmatrix} = I\overrightarrow{\omega_B} \tag{4.16}$$

Once again using the Theorem of Coriolis, the total time derivative of the inertial angular momentum is broken into the time derivative of angular momentum in the body frame and the angular momentum of the body-frame relative to the inertial frame.

$$\overrightarrow{T_B} = \left(\frac{d\overrightarrow{H_B}}{dt}\right)_{inertial} = \left(\frac{d\overrightarrow{H_B}}{dt}\right)_{body} + \overrightarrow{\omega_B} \times \overrightarrow{H_B} \tag{4.17}$$

Substituting Equation (4.16) into (4.17) produces:

$$\overrightarrow{T_B} = I\frac{d\overrightarrow{\omega_B}}{dt} + \overrightarrow{\omega_B} \times (I\overrightarrow{\omega_B}) \tag{4.18}$$

Next, performing the matrix multiplication and cross products yields Equation (4.19).

$$T_B = \begin{bmatrix} \dot{p}I_{xx} + qr(I_{zz} - I_{yy}) + (pq + \dot{r})I_{xz} \\ \dot{q}I_{yy} + rp(I_{xx} - I_{zz}) + (p^2 - r^2)I_{xz} \\ \dot{r}I_{zz} + pq(I_{yy} - I_{xx}) + (qr - \dot{p})I_{xz} \end{bmatrix} = \begin{bmatrix} \bar{L} \\ M \\ N \end{bmatrix} \tag{4.19}$$

Where $\bar{L}$, M, and N are the components of torque about the x, y, and z body axis, respectively.

The Earth's gravitational force acts through the vehicle's center of mass, which is the origin of the body-frame coordinate system. Therefore, the gravitational force produces no torque on the vehicle. The aerodynamic normal and side forces, however, act through the center of pressure, which is typically offset from the vehicle's center of mass. Therefore the torques, M and N, are obtained from the aerodynamic moment coefficients:

$$M = qS\bar{c}C_M \tag{4.20a}$$

$$N = qSbC_n \tag{4.20b}$$

The values of C_M and C_n are calculated at each simulation time-step by interpolating over Mach number, angle of attack, and sideslip angle. The vehicle is assumed to experience negligible roll motion. Therefore, $\bar{L} = 0$. Finally, solving for the time derivatives of the body rates yields (4.21a)—(4.21c).

$$\dot{p} = \frac{L}{I_{xx}} + \frac{qr(I_{yy} - I_{zz})}{I_{xx}} \tag{4.21a}$$

$$\dot{q} = \frac{M}{I_{yy}} + \frac{pr(I_{zz} - I_{xx})}{I_{yy}} \tag{4.21b}$$

$$\dot{r} = \frac{N}{I_{zz}} + \frac{pq(I_{xx} - I_{yy})}{I_{zz}} \tag{4.21c}$$

4.1.3 Complete 6-DOF Equations of Motion

Equations (4.12a)—(4.12c) and (4.21a)—(4.21c) represent the full six-degree-of-freedom equations of motion for a rigid body. The six equations contain six unknowns: *p*, *q*, *r*, *u*, *v*, and *w*. These variables represent quantities in body-fixed coordinates. However, it is of interest to obtain results, such as the vehicle's final position, velocity, and attitude, in inertial coordinates. The body rates (p, q, r) are used to compute the time derivatives of the Euler angles (ϕ, θ, ψ) as follows:

$$\dot{\phi} = p + \sin\phi \tan\theta\, q + \cos\phi \tan\theta\, r \tag{4.22a}$$

$$\dot{\theta} = q \cos\phi - r \sin\phi \tag{4.22b}$$

$$\dot{\psi} = q \sin\phi \sec\theta + r \cos\phi \sec\theta \tag{4.22c}$$

The transformation matrix, $T_{E\to B}$, is then applied to transform the body frame velocity *(u, v, w)* into Earth-fixed coordinates:

$$\begin{bmatrix} \dot{x_E} \\ \dot{y_E} \\ \dot{z_E} \end{bmatrix} = T_{E\to B} \begin{bmatrix} u \\ v \\ w \end{bmatrix} \tag{4.23a}$$

$$\dot{x_E} = (\cos\theta \cos\psi)u + (-\cos\phi \sin\psi + \sin\phi \sin\theta \cos\psi)v + (\sin\phi \sin\psi + \cos\phi \sin\theta \cos\psi)w \tag{4.23b}$$

$$\dot{y}_E = (\cos\theta \sin\psi)u + (\cos\phi \cos\psi + \sin\phi \sin\theta \sin\psi)v \quad (4.23c)$$
$$+ (-\sin\phi \cos\psi + \cos\phi \sin\theta \sin\psi)w$$

$$\dot{z}_E = (-\sin\theta)u + (\sin\phi \cos\theta)v + (\cos\phi \cos\theta)w \quad (4.23d)$$

Finally, the Euler angles and position vector in the Earth-fixed frame are solved for by Equations (4.24a)—(4.24f).

$$\phi = \phi_0 + \int_0^t \left(\frac{d\phi}{dt}\right) dt \quad (4.24a)$$

$$\theta = \theta_0 + \int_0^t \left(\frac{d\theta}{dt}\right) dt \quad (4.24b)$$

$$\psi = \psi_0 + \int_0^t \left(\frac{d\psi}{dt}\right) dt \quad (4.24c)$$

$$x_E = x_{E,0} + \int_0^t \left(\frac{dx_E}{dt}\right) dt \quad (4.24d)$$

$$y_E = y_{E,0} + \int_0^t \left(\frac{dy_E}{dt}\right) dt \quad (4.24e)$$

$$z_E = z_{E,0} + \int_0^t \left(\frac{dz_E}{dt}\right) dt \quad (4.24f)$$

The equations of motion derived above are implemented in a 6-DOF simulation in MATLAB. The simulation integrates the 12 simultaneous differential equations listed in Table 4.1. Integration is performed using the MATLAB function, *ode45*, which implements a fourth-order Runge-Kutta numerical integration technique. The inputs to *ode45* include a function handle to a user-defined function, a vector representing the initial conditions, and the desired size and number of integration time-steps. The function handle points to a user-defined MATLAB function, which contains the system of differential equations. This function defines the "right-hand side" of the equations in

Table 4.1. The initial conditions include the inertial velocity ($\dot{x_E}, \dot{y_E}, \dot{z_E}$), the Euler Angles ($\phi$, θ, ψ), and their time derivatives ($\dot{\phi}$, $\dot{\theta}$, $\dot{\psi}$). The initial position is defined at (0,0,0). The *ode45* function outputs a time series of the values of the following variables at each desired time-step: $(x_E, y_E, z_E, \phi, \theta, \psi, u, v, w, p, q, r)$.

Table 4.1 — The 6-DOF Equations of Motion Implemented in MATLAB

$$\begin{bmatrix} \dot{x_E} \\ \dot{y_E} \\ \dot{z_E} \end{bmatrix} = T_{B\to E} \begin{bmatrix} u \\ v \\ w \end{bmatrix} \qquad where\ T_{E\to B} = f(\theta, \phi, \psi)$$

$$\dot{\phi} = p + \sin\phi \tan\theta\, q + \cos\phi \tan\theta\, r$$

$$\dot{\theta} = q\cos\phi - r\sin\phi$$

$$\dot{\psi} = q\sin\phi \sec\theta + r\cos\phi \sec\theta$$

$$\dot{u} = \frac{F_{Aero,x}}{m} - g\sin\theta + rv - qw \qquad where\ F_{Aero,x} = f(u, v, w)$$

$$\dot{v} = \frac{F_{Aero,y}}{m} + g\sin\phi\cos\theta - ru + pw \qquad where\ F_{Aero,y} = f(u, v, w)$$

$$\dot{w} = \frac{F_{Aero,z}}{m} + g\cos\phi\cos\theta + qu - pv \qquad where\ F_{Aero,z} = f(u, v, w)$$

$$\dot{p} = \frac{L}{I_{xx}} + \frac{qr(I_{yy} - I_{zz})}{I_{xx}}$$

$$\dot{q} = \frac{M}{I_{yy}} + \frac{pr(I_{zz} - I_{xx})}{I_{yy}}$$

$$\dot{r} = \frac{N}{I_{zz}} + \frac{pq(I_{xx} - I_{yy})}{I_{zz}}$$

4.2 Nominal Drop Dynamics

This section defines the "nominal" drop phase dynamics, which will serve as a point of comparison for subsequent "dispersed" drop scenarios. The air-launched rocket is assumed to drop from a carrier aircraft flying horizontally. Sarigul-Klijn, Noel, and Sarigul-Klijn (2004) illustrate that while air-launched rocket performance improves at higher launch altitudes, there is little improvement over about 50,000 ft. (15.24 km). Therefore, 15.24 km is selected as the nominal drop altitude. Orbital Sciences' Pegasus and Scaled Composite's SpaceShipOne are launched at speeds of Mach 0.8 and Mach 0.5, respectively (Rovner 1991; Linehan 2008). Here, an initial velocity at release of Mach 0.5 is assumed. The initial angle of attack at drop is assumed to be a small positive value, 4°, which helps the rocket pitch up in order to begin its ascent trajectory. The initial flight path angle is zero, and the pitch angle is therefore also 4°. For the

Table 4.2 — Nominal Initial (Release) Conditions

Parameter	***Value***	***Units***
Altitude	15.24	km
Mach Number	0.5	-
Flight Path Angle	0	°
Alpha	4	°
Beta	0	°
Pitch	4	°
Yaw	0	°/s
Pitch Rate	0	°/s
Yaw Rate	0	°/s
Side Wind Speed	0	m/s

Table 4.3 — Values of Constant Parameters

Parameter	***Value***	***Units***
Gravitational Constant	6.674×10^{-11}	$m^2 kg^{-1} s^{-2}$
Earth Mass	5.972×10^{24}	kg
Earth Radius	6,371	km
Atmospheric Density	0.1864	$kg\ m^{-3}$
Speed of Sound	295.1	m/s

nominal case, the initial yaw and sideslip angles are set to 0°. In addition, it is assumed that the body rates are each 0°/s at release. Finally, lateral wind speeds are assumed to be 0 m/s. These nominal initial (release) conditions are summarized in Table 4.2. Table 4.3 lists values of relevant constants used in the simulation, including the Earth's mass and radius. The atmospheric density and speed of sound listed here are the values at 15.24 km above sea level according to the 1976 US Standard Atmosphere Model.

The duration of the drop phase is chosen to be 4-seconds, close to the ~5-second drop for Pegasus (Rovner 1991). The full 6DOF equations of motions are solved at each 0.001-second time step during the total 4-second drop. Figure 4.1 shows the angle of attack, pitch, sideslip, yaw, pitch rate, and yaw rate as a function of time for Air Launch Light. Table 4.4 summarizes the final vehicle state at the end of the 4-second drop, when the rocket ignites its engine. By the end of the drop, the vehicle has pitched up to 39.1° above the horizontal. The angle of attack, 53°, is even greater than the pitch angle because the vehicle has picked up a velocity in the downward direction (toward the Earth), resulting in a negative flight path angle. At the end of the drop phase, the vehicle also has a significant positive pitch rate, 27.0 °/s. Under nominal release conditions, there is zero initial sideslip angle and zero lateral winds. Therefore, the sideslip angle, yaw, and

yaw rate are each zero at ignition. The final velocity and position are given in inertial coordinates. The given (x,y,z) position is relative to the release point, which is set at (0,0,0). Finally, the vehicle's path in the inertial x-z plane is shown in Figure 4.2, with the vehicle's initial and final pitch orientation superimposed.

Table 4.5 and Figures 4.3—4.4 display Air Launch Heavy's behavior during the 4 s drop phase. Similar to Air Launch Light, this vehicle has a large pitch (48°) and large pitch rate (34°/s) at ignition. The pitch and pitch rate are larger compared to lighter version due to differences in the vehicles' aerodynamics and mass properties. Both vehicles have zero sideslip, yaw, and yaw rate at ignition. Note that the final inertial position and velocity of the two vehicles is nearly identical.

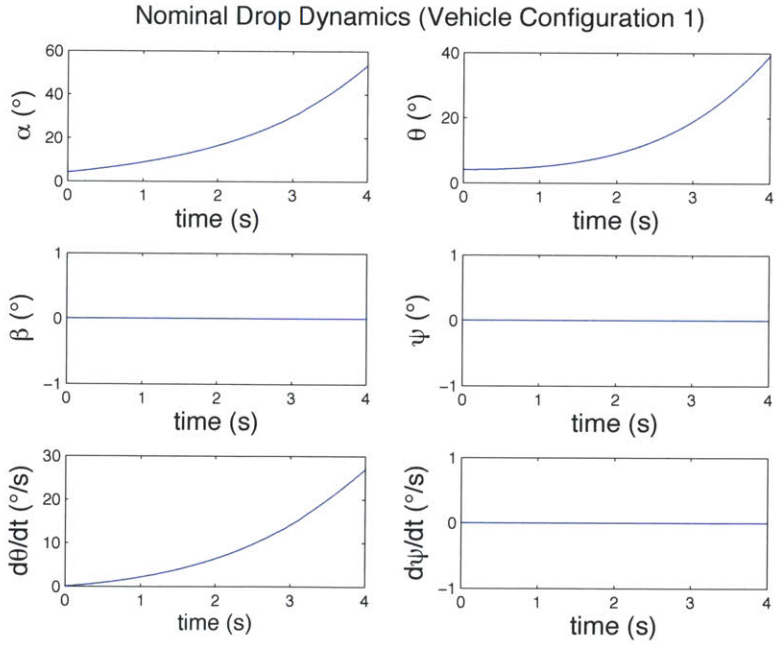

Figure 4.1 — Results from the 6-DOF simulation for Air Launch Light with nominal drop conditions.

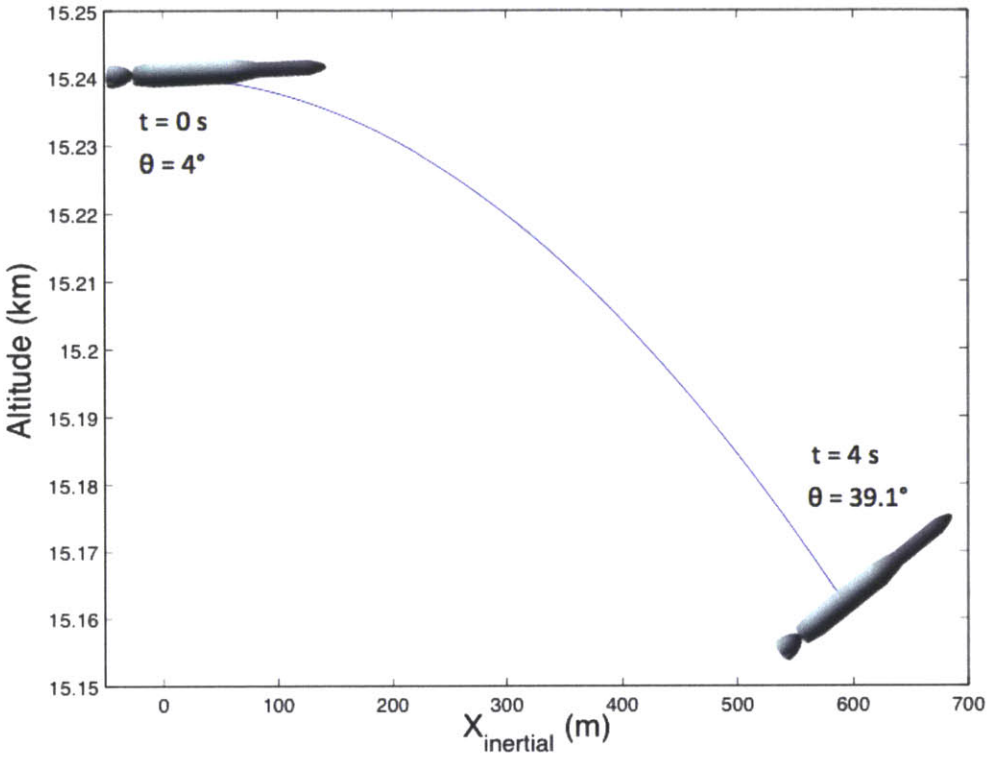

Figure 4.2 — Path followed by Air Launch Light in inertial coordinates during drop

Table 4.4 — Nominal Ignition Conditions for Air Launch Light

Parameter	***Value at Ignition***	***Units***
θ	39.1	°
ψ	0	°
α	53.3	°
β	0	°
$\dot{\theta}$	27.0	°/s
$\dot{\psi}$	0	°/s
$x_{Inertial}$	588.9	m
$y_{Inertial}$	0	m
$z_{Inertial}$	76.3	m
$v_{x,Inertial}$	146.4	m/s
$v_{y,Inertial}$	0	m/s
$v_{z,Inertial}$	37.2	m/s

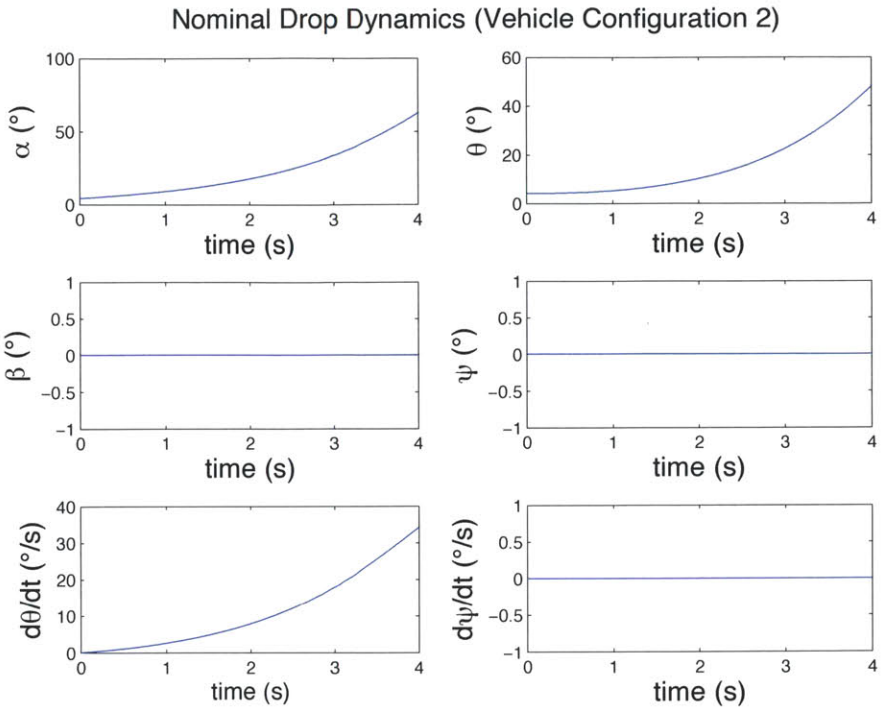

Figure 4.3 — Results from the 6DOF simulation for Air Launch Heavy with nominal drop conditions.

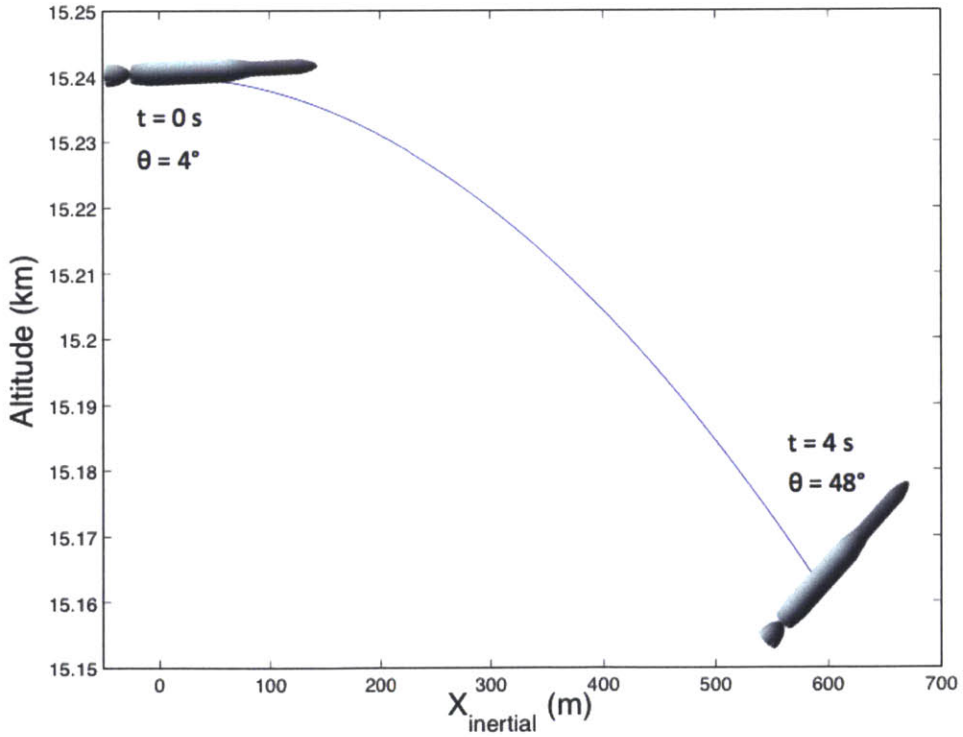

Figure 4.4 — Path followed by Air Launch Heavy in inertial coordinates during drop

Table 4.5 — Ignition Conditions for Air Launch Heavy

Parameter	*Value at Ignition*	*Units*
θ	48.0	°
ψ	0	°
α	62.3	°
β	0	°
$\dot{\theta}$	34.2	°/s
$\dot{\psi}$	0	°/s
$x_{Inertial}$	589.1	m
$y_{Inertial}$	0	m
$z_{Inertial}$	76.8	m
$v_{x,Inertial}$	146.4	m/s
$v_{y,Inertial}$	0	m/s
$v_{z,Inertial}$	37.5	m/s

4.3 Carrier Aircraft and Environmental Uncertainties

The previous section modeled the expected rocket behavior during the drop phase assuming nominal release conditions. However, releasing a rocket from a human-piloted carrier aircraft into an unpredictable atmospheric environment will certainly result in deviations from these "nominal" drop conditions. It is of interest therefore to first estimate the expected uncertainties in the carrier aircraft state at drop and lateral wind speeds and then determine how these dispersions will affect the rocket's final state at ignition.

The carrier aircraft may cause the rocket to be released at off-nominal initial velocity, angle of attack, attitude, and body rates. Furthermore, the vehicle aerodynamic coefficients are estimates and are therefore not precisely known. It is necessary to consider uncertainties in the aerodynamic model, such as the location center of pressure.

Historical atmospheric data from Earth-GRAM 2010 is used to determine a reasonable estimate for the mean and standard deviation of lateral wind speeds. Earth-GRAM 2010 is a global atmosphere model providing density, temperature, pressure, winds, and atmospheric chemical composition as a function of latitude and longitude from sea level to orbital altitudes. Earth-GRAM 2010 also provides historical atmospheric data from launch ranges. Figures 4.5 and 4.6 illustrate the seasonal variations in wind speeds at an altitude of 15.25 km above the Vandenberg Air Force Base from the year 2006 (Justus and Leslie 2008). The plots show the mean and standard deviations for each calendar month. Note that the highest wind speeds occur in the winter months.

Rockets are typically launched from Vandenberg AFB toward the south, southwest, or southeast in order to avoid flying over populated land. A rocket launched from Vandenberg in a southerly direction will be subject to lateral Eastward winds. Figures 4.5 and 4.6 demonstrate that wind speeds tend to be much higher in the Eastward direction compared to the Northward direction. The data in Figure 4.5 illustrates that typical Eastward winds in the winter are about 20 m/s with a standard deviation of about 10 m/s. Therefore it is reasonable to expect eastward wind speeds between 0 and 40 m/s.

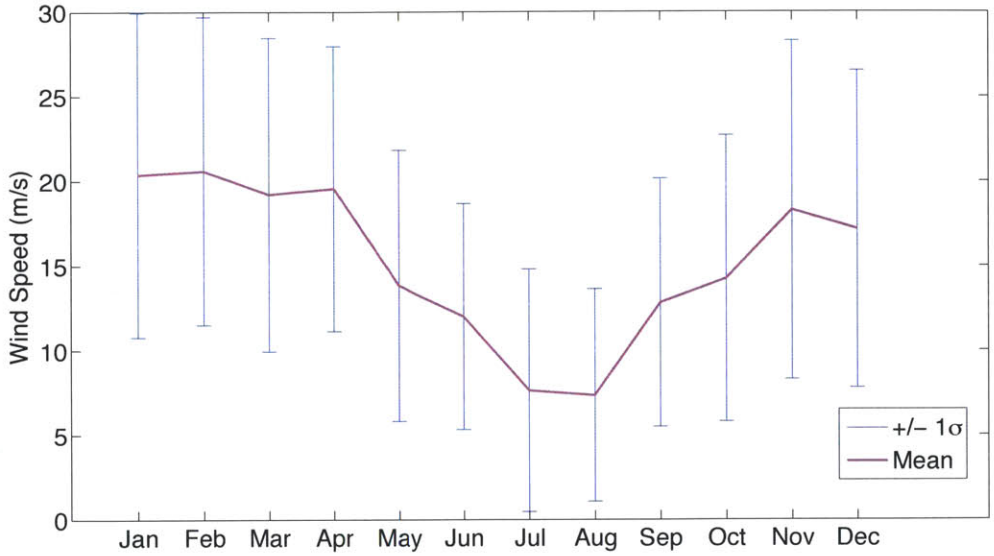

Figure 4.5 — Mean and standard deviations of Eastward wind speeds at 15.25 km above Vandenberg AFB

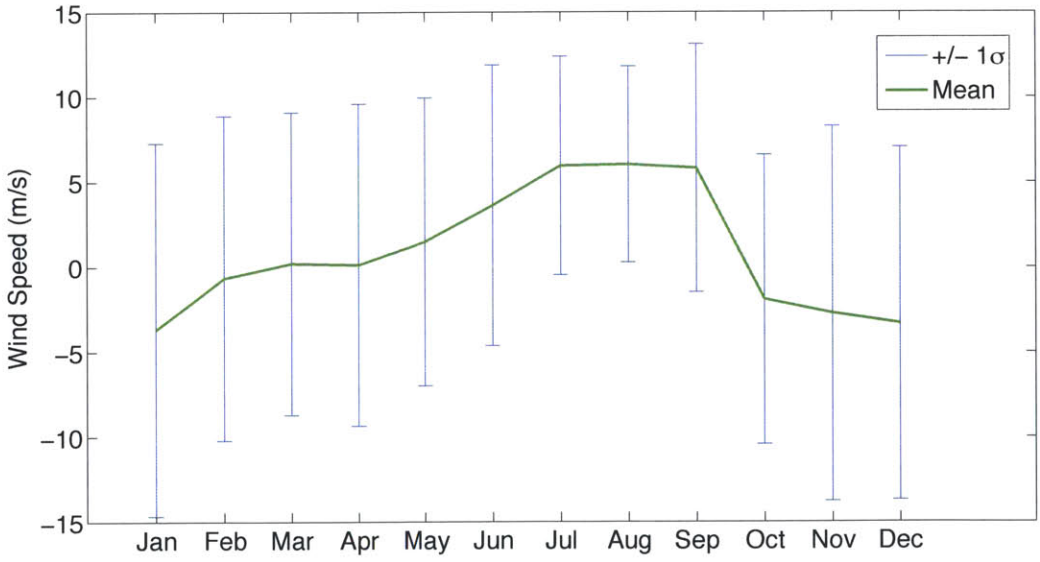

Figure 4.6 — Mean and standard deviations of Northward wind speeds at 15.25 km above Vandenberg AFB

4.4 Effects of a Single Dispersed Variable

The goal of this chapter is to evaluate how carrier aircraft release conditions, aerodynamic model errors, and unpredictable lateral winds affect the rocket's state at ignition. This section investigates one dispersed parameter at a time in order to identify which parameters generate the greatest dispersions in the vehicle's ignition condition. The 6-DOF drop phase simulation is run with all but one parameter set equal to the "nominal" values listed in Table 4.2. The single dispersed variable is set to a value either above or below its nominal value, as shown in the first columns of Tables 4.6 and 4.7. Off-nominal values of Mach number, θ, ψ, $\dot{\theta}$, $\dot{\psi}$, center of pressure location, and lateral wind speeds are investigated. The initial flight path angle is assumed to be 0°. Therefore the initial pitch angle is equal to the angle of attack. Also note that the nominal center of pressure (XCP) location is a function of Mach number, angle of attack, and sideslip. In order to model uncertainty in the XCP location, a constant +/- 0.5 m offset is added to the nominal XCP value.

The effects of each single dispersed parameter on the rocket's attitude and body rates at ignition are listed in Tables 4.6 and 4.7. Note that the pitch rate ($\dot{\theta}$) at release has the greatest effect on the rocket's pitch, pith rate, and angle of attack at ignition. An off-nominal pitch rate of 3°/s and –3°/s at release (with all other parameters nominal) produce a final pitch of about 63° and 13°, respectively. Since the rocket's engine is approximately aligned with the body's longitudinal axis, such a large dispersion in initial pitch means that the initial thrust vector at ignition is very uncertain. The results in Tables 4.6 and 4.7 also show that a small yaw or yaw rate at release can cause a significant yaw

and yaw rate at ignition. Finally, Tables 4.6 and 4.7 illustrate that normal wind speeds of 10—40 m/s cause very significant motion in the yaw plane.

Table 4.6— Effects of Single Dispersed Parameter on Air Launch Light Ignition State

	$\theta_{ignition}$ (°)	$\dot{\theta}_{ignition}$ (°/s)	$\alpha_{ignition}$ (°)	$\psi_{ignition}$ (°)	$\dot{\psi}_{ignition}$ (°/s)	$\beta_{ignition}$ (°)
Nominal Case	39.1	27.0	53.3	0	0	0
Mach 0.55	46.9	33.5	59.8	0	0	0
Mach 0.45	32.4	21.5	48.4	0	0	0
$\theta = 7$ °	53.4	33.0	67.5	0	0	0
$\theta = 1$ °	24.1	19.5	38.6	0	0	0
$\psi = 2$ °	38.9	26.6	53.5	12.5	9.0	-11.7
$\psi = -2$ °	38.9	26.6	53.5	-12.5	-9.0	11.7
$\dot{\theta} = 3$ °/s	62.7	37.0	76.8	0	0	0
$\dot{\theta} = -3$ °/s	13.2	12.9	27.8	0	0	0
$\dot{\psi} = 2$ °/s	38.5	25.9	53.6	20.0	14.7	-18.2
$\dot{\psi} = -2$ °/s	38.5	25.9	53.6	-20.0	-14.7	18.2
XCP+0.5 m	48.0	36.4	62.3	0	0	0
XCP-0.5 m	31.3	19.4	45.6	0	0	0
Side wind = 10 m/s	38.5	25.7	53.5	19.5	16.4	-17.7
Side wind = 20 m/s	36.9	22.8	54.0	35.3	28.3	-29.0
Side wind = 30 m/s	34.6	19.4	55.5	49.5	36.4	-36.1
Side wind = 40 m/s	32.4	16.7	58.8	60.6	40.6	-40.0

Table 4.7 — Effects of Single Dispersed Parameter on Air Launch Heavy Ignition State

	$\theta_{ignition}$ (°)	$\dot{\theta}_{ignition}$ (°/s)	$\alpha_{ignition}$ (°)	$\psi_{ignition}$ (°)	$\dot{\psi}_{ignition}$ (°/s)	$\beta_{ignition}$ (°)
Nominal Case	**48.0**	**34.2**	**62.3**	**0**	**0**	**0**
Mach 0.55	58.3	42.4	71.2	0	0	0
Mach 0.45	39.4	27.1	55.4	0	0	0
$\theta = 7$ °	64.7	40.9	79.0	0	0	0
$\theta = 1$ °	30.1	25.1	44.7	0	0	0
$\psi = 2$ °	47.7	33.3	62.7	16.7	15.1	-15.5
$\psi = -2$ °	47.7	33.3	62.7	-16.7	-15.1	15.5
$\dot{\theta} = 3$ °/s	73.4	44.2	87.7	0	0	0
$\dot{\theta} = -3$ °/s	19.2	18.2	33.9	0	0	0
$\dot{\psi} = 2$ °/s	47.1	32.2	62.8	24.3	22.1	-21.7
$\dot{\psi} = -2$ °/s	47.1	32.2	62.8	-24.3	-22.1	21.7
XCP+0.5 m	56.7	43.6	71.0	0	0	0
XCP-0.5 m	40.3	26.3	54.7	0	0	0
Side wind = 10 m/s	46.8	31.3	62.7	26.8	26.7	-23.5
Side wind = 20 m/s	43.7	25.6	64.2	47.1	42.0	-35.2
Side wind = 30 m/s	40.0	20.1	69.7	64.0	49.2	-41.0
Side wind = 40 m/s	36.6	14.6	82.5	76.3	50.6	-43.2

4.5 Monte Carlo Simulation

Section 4.4 investigated the effects of a single dispersed variable. However, in reality, many carrier aircraft and environmental variables will be dispersed at the same time. It is therefore important to model random dispersions in all uncertain parameters simultaneously in order to fully describe the rocket's range of possible ignition states. The 6DOF drop phase simulation is run 1000 times with different sets of release conditions and lateral wind speeds. Each variable is randomly selected from a Gaussian distribution of values. Table 4.8 lists each dispersed variable, its mean value, and its 3σ values. In the absence of more specific distribution models, Gaussian distributions are used because they are expected to yield qualitatively representative results. The resulting histograms of vehicle state variables at ignition (Figures 4.8 and 4.9) resemble Gaussian distributions, which provide justification for using a Gaussian model for the distribution of drop variables.

Table 4.8 —Expected Deviations in Drop Parameters

Parameter	***Units***	***Mean***	3σ
Air-relative Mach Number	-	0.5	+/- 0.05
Pitch (θ)	°	4	+/- 3
Yaw (ψ)	°	0	+/- 2
Pitch Rate ($\dot{\theta}$)	°/s	0	+/- 3
Yaw Rate ($\dot{\psi}$)	°/s	0	+/- 2
Center of Pressure (from nose)	m	XCP*	+/- 0.5
Side Wind	m/s	0	+/- 10

*The location of the center of pressure for each vehicle configuration depends on Mach number, angle of attack, and sideslip

Figure 4.7 shows Air Launch Light's angle of attack (α), pitch (θ), pitch rate ($\dot{\theta}$), sideslip (β), yaw (ψ), and yaw rate ($\dot{\psi}$) as a function of time for each 1000 runs superimposed. Figure 4.7 illustrates the range of ignition conditions that are possible given the expected dispersions summarized in Table 4.8. Figure 4.8 presents histograms of the values of α, θ, $\dot{\theta}$, β, ψ, and $\dot{\psi}$ at ignition for all 1000 runs. Each histogram resembles a Gaussian distribution. Finally, the mean and standard deviation for each of these six distributions are summarized in Table 4.9. Also listed in Table 4.9 are the mean and standard deviations of the velocity of the rocket's center of mass at ignition along each of the three inertial axes. First note that the mean values of each of these nine parameters are very close to those for the "nominal" case, as shown in Table 4.4. The standard deviations of α, θ, β, and ψ at ignition are all on the order of 10°. Perhaps more significant, the standard deviations of $\dot{\theta}$ and $\dot{\psi}$ are on the order of 10°/s.

Figure 4.9 shows α, θ, $\dot{\theta}$, β, ψ, and $\dot{\psi}$ as a function of time during the drop phase for Air Launch Heavy and Figure 4.10 displays the associated histograms of these variables at ignition. The means and standard deviations are listed in Table 4.10. Once again, the mean values in Table 4.10 are very similar to the results from the nominal drop case as shown in Table 4.5. Furthermore, Air Launch Heavy shows similarly large deviations about the mean for each state variable at ignition.

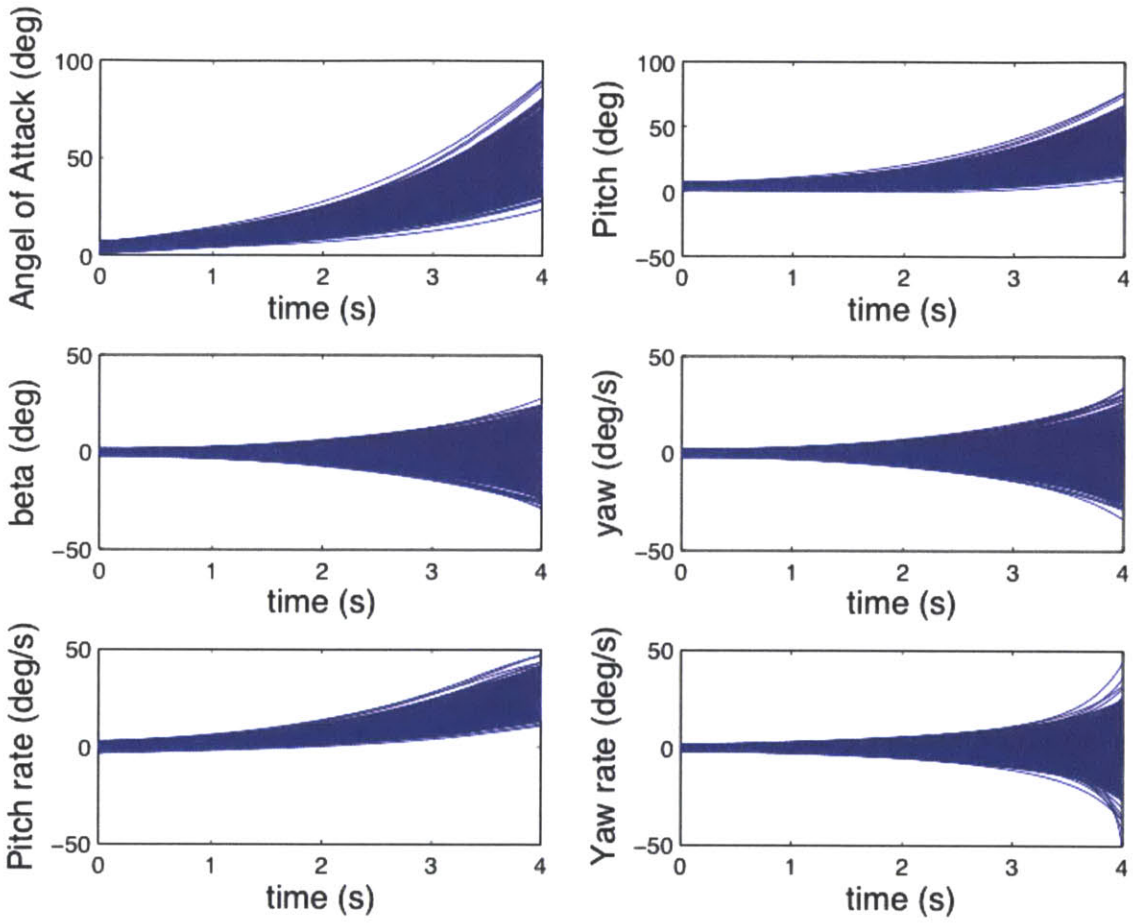

Figure 4.7 — Air Launch Light body attitude and rates over time for all 1000 Monte Carlo runs

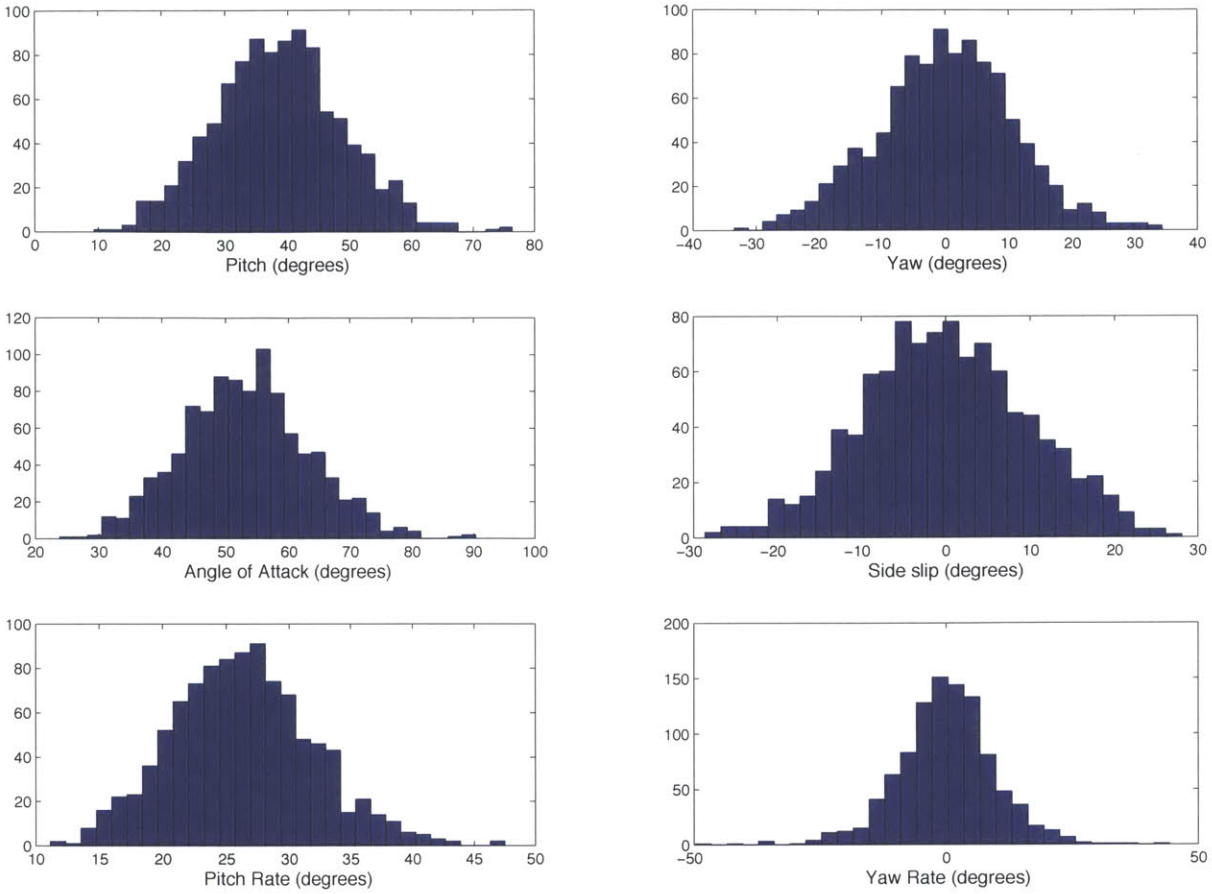

Figure 4.8 — Histograms of α, θ, $\dot{\theta}$, β, ψ, and $\dot{\psi}$ at ignition for all 1000 Monte Carlo runs (Air Launch Light)

Table 4.9 — Ignition State Variable Dispersions for Air Launch Light

Parameter	*Units*	*Mean*	*Standard Deviation*
$\theta_{ignition}$	°	38.8	10.2
$\dot{\theta}_{ignition}$	°/s	26.4	5.60
$\alpha_{ignition}$	°	53.3	10.0
$\psi_{ignition}$	°	0.02	10.7
$\dot{\psi}_{ignition}$	°/s	-0.04	9.59
$\beta_{ignition}$	°	-0.02	9.85
Vx	m/s	146.0	4.89
Vy	m/s	0.00	0.281
Vz	m/s	37.2	0.454

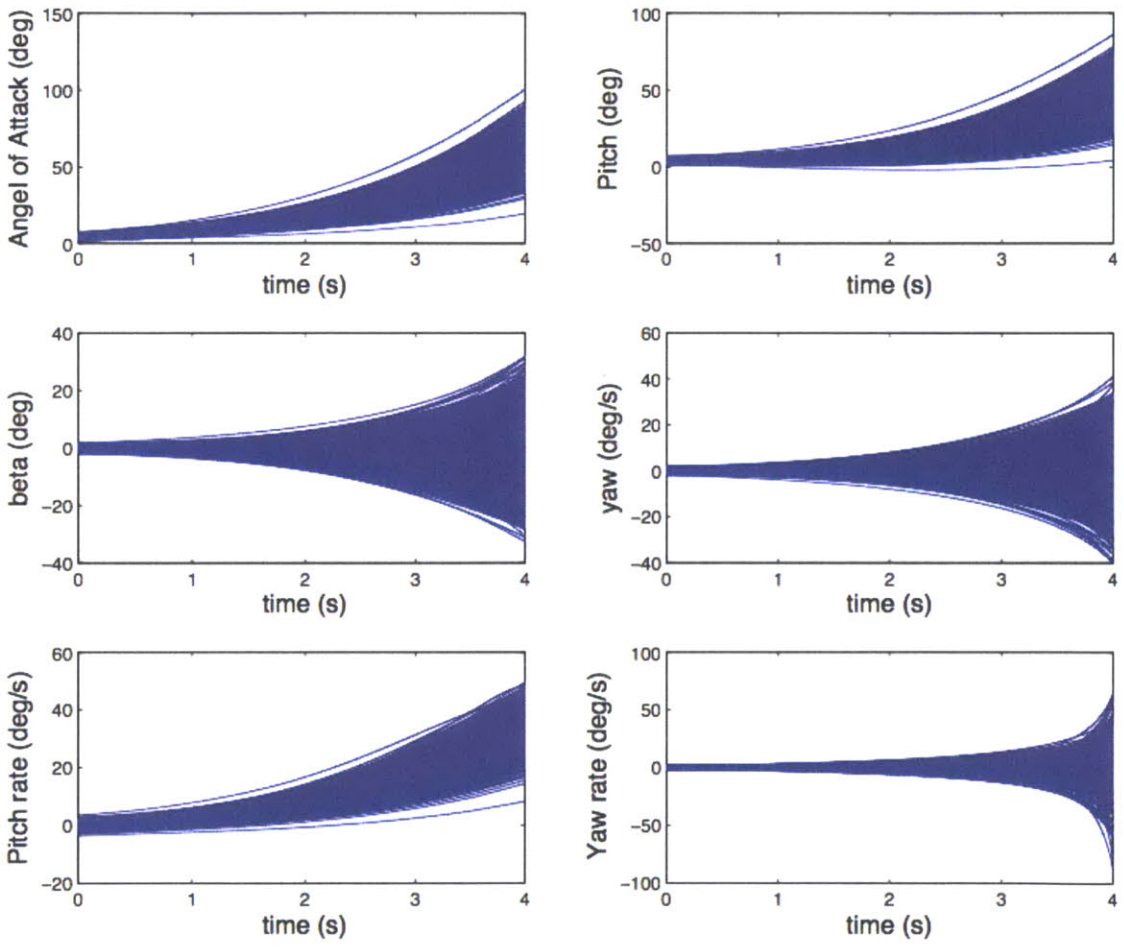

Figure 4.9 — Air Launch Heavy body attitude and rate variables over time for all 1000 Monte Carlo runs

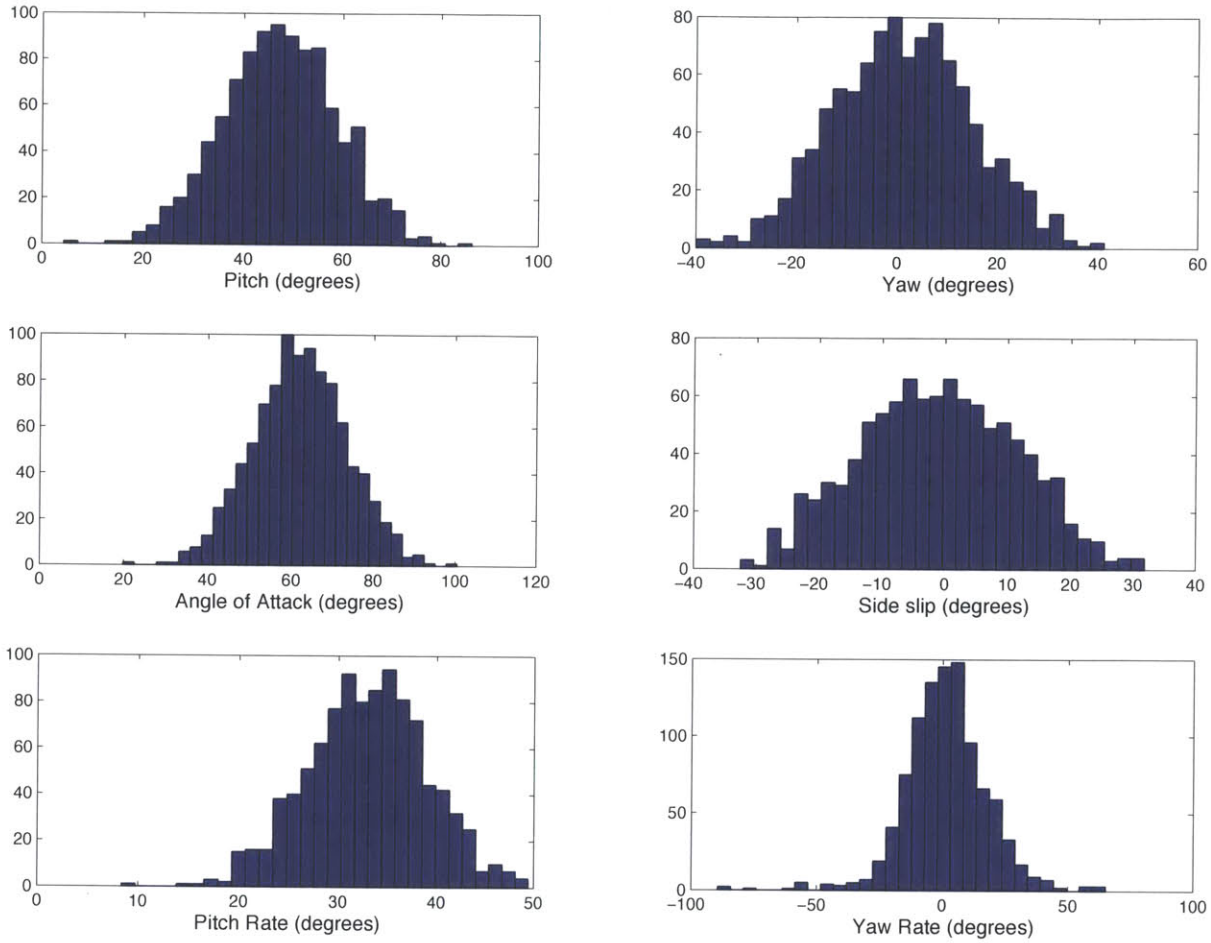

Figure 4.10 — Histograms of α, θ, $\dot{\theta}$, β, ψ, and $\dot{\psi}$ at ignition for all 1000 Monte Carlo runs (Air Launch Heavy)

Table 4.10 — Ignition State Variable Dispersions for Air Launch Heavy

Parameter	***Units***	***Mean***	***Standard Deviation***
$\theta_{ignition}$	°	47.4	11.4
$\dot{\theta}_{ignition}$	°/s	33.0	6.01
$\alpha_{ignition}$	°	62.2	11.3
$\psi_{ignition}$	°	1.16	13.8
$\dot{\psi}_{ignition}$	°/s	1.34	16.5
$\beta_{ignition}$	°	-1.05	12.4
V_x	m/s	146.3	4.82
V_y	m/s	0.01	0.19
V_z	m/s	37.5	0.35

Chapter 5: Guidance, Navigation, and Control

The previous chapter considered the behavior of an air-launched rocket during the uncontrolled drop phase prior to engine ignition. By simulating the drop phase dynamics for a range of drop conditions, a statistical representation of the expected vehicle state at ignition was attained. Given these expected dispersions in ignition conditions, the next step is to investigate how the dispersions affect the vehicle's performance during the first stage burn. Chapter 5 describes the construction of a 6DOF model in Simulink® of the rocket dynamics during the first stage of the rocket's ascent. This simulation will be used to evaluate the vehicle's performance given a variety of ignition conditions and reference trajectories. The simulation includes a model of the Guidance, Navigation, and Control (GN&C) system, which ensures that the rocket follows the desired ascent trajectory. The GN&C subsystems and the method used to generate optimized reference trajectories are presented in this chapter.

5.1 GN&C Overview

Once the rocket engine ignites, the vehicle's motion is monitored and controlled by an onboard GN&C system, which steers the rocket onto the desired ascent trajectory. The rocket is maneuvered in pitch and yaw by thrust vector control (TVC). The rocket's thrust direction is altered by rotating the gimbaled engine away from the longitudinal axis as illustrated in Figure 5.1. The engine rotation produces a net torque on the vehicle, which is used to control the rocket's attitude. Typically a separate attitude control system is used to control the vehicle's roll motion, which is not considered here.

A block diagram of the rocket's GN&C system is shown in Figure 5.2. The system consists of four parts: the plant (vehicle), the controller, the TVC actuator, and the vehicle state measurements. The controller consists of an inner and outer loop. The inputs to the outer, or guidance, loop are the desired thrust direction from the reference trajectory and onboard sensory data. The guidance law uses these inputs to produce an angular rate command for the inner loop. The inner, or TVC, loop takes the rate

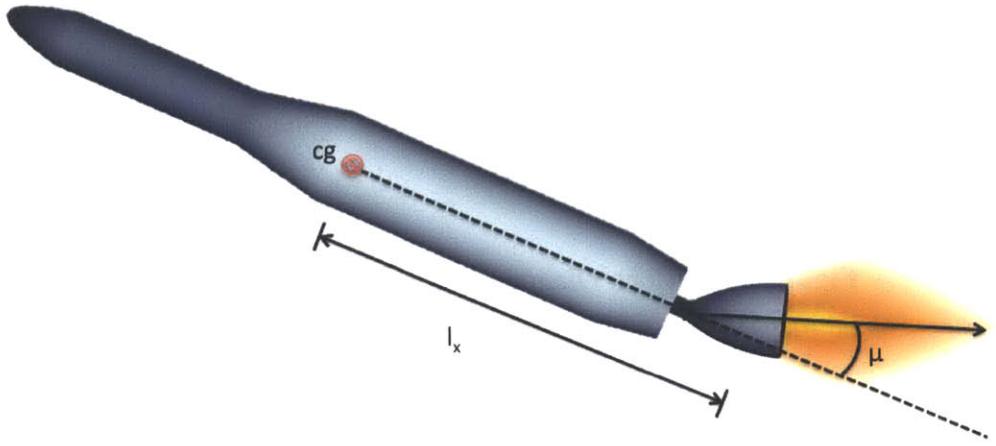

Figure 5.1 – Gimbaled Rocket Engine

commands from guidance and provides an engine position command for the TVC actuator. The guidance loop typically runs at a lower sampling rate than the TVC loop. In the Simulink model constructed here, the guidance and TVC loops run at 10 and 50 Hz, respectively. The Simulink model of the vehicle dynamics and GN&C system is shown in Figure 5.3. The four subsystems (the controller, TVC actuator, the plant, and the vehicle state measurements) will be described in the following sections.

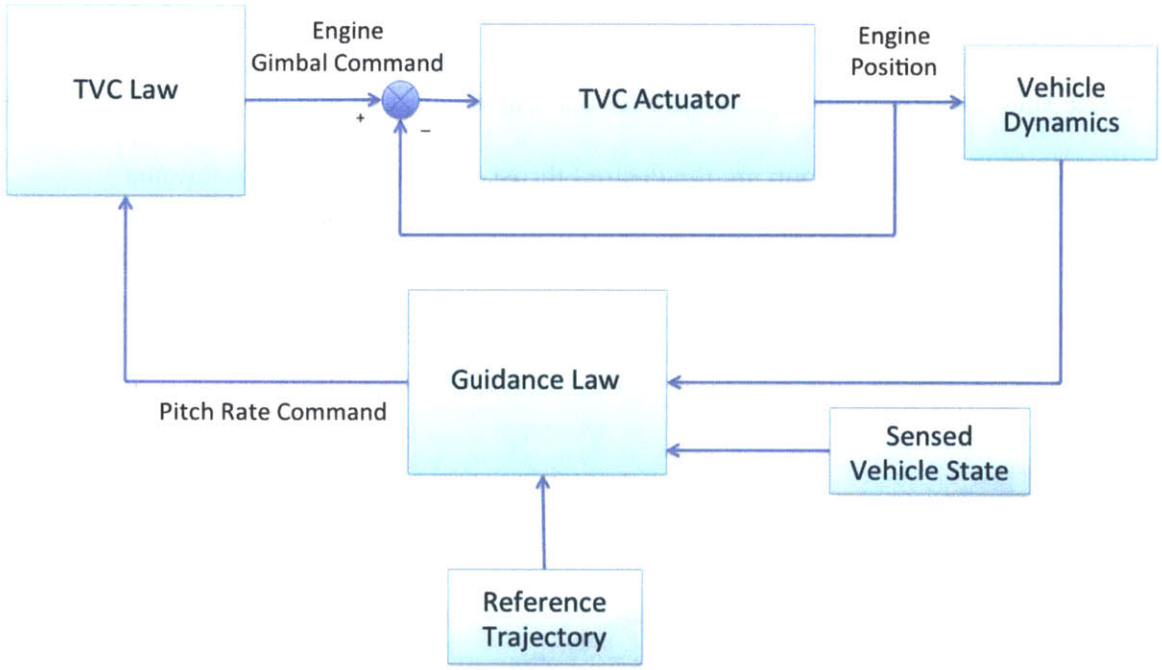

Figure 5.2 – Block Diagram of rocket GN&C system

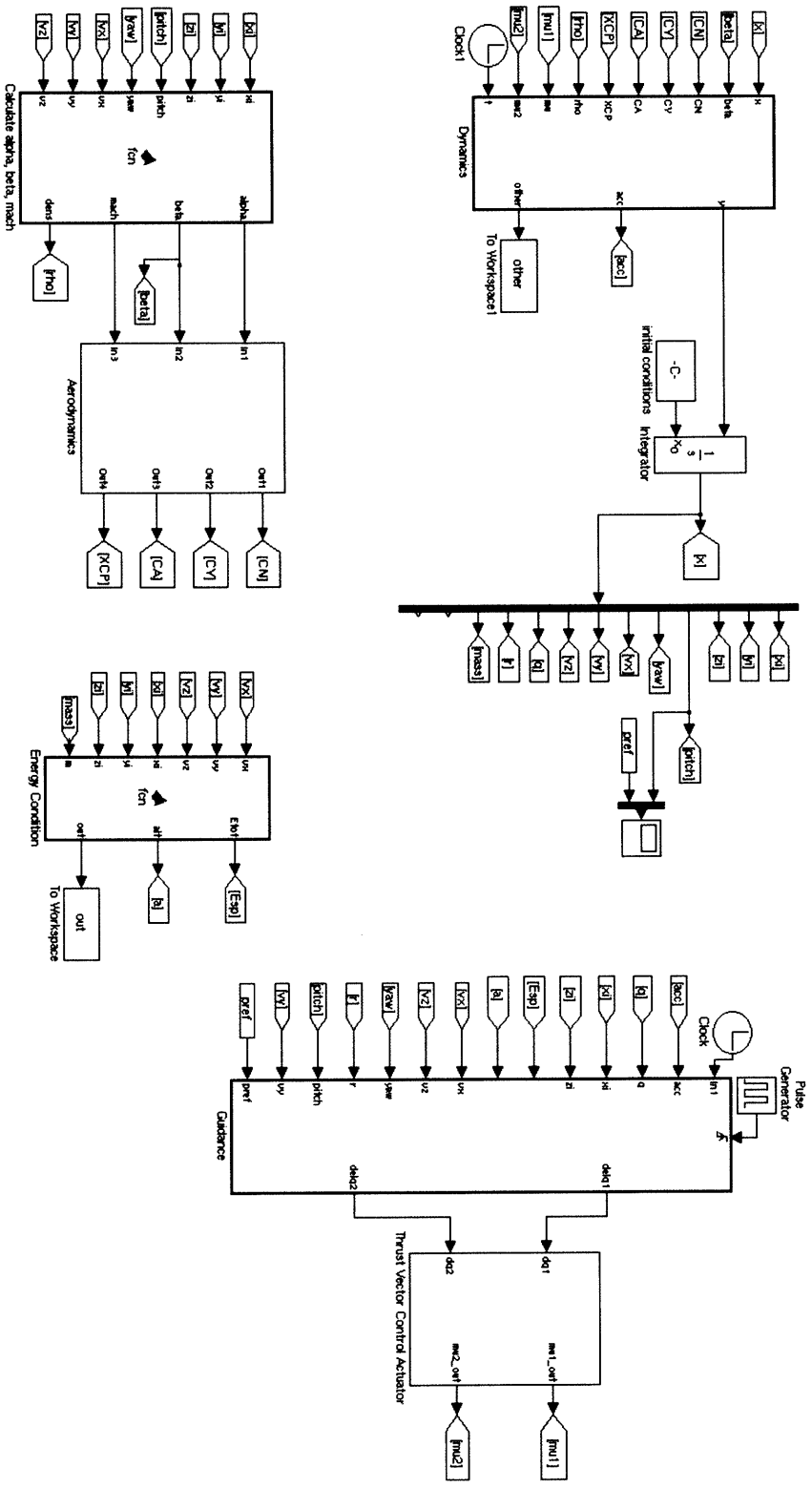

Figure 5.3 – Simulink Model of the rocket system with guidance and control in the loop

5.2 Guidance

The guidance loop uses a pre-programmed reference trajectory and onboard sensor measurements to provide the inner TVC loop with an angular rate command. During an actual rocket flight, the vehicle state is obtained from onboard rate gyros and/or inertial measurement units (IMUs). These instruments do not provide perfect knowledge of the vehicle state. Errors may arise from instrument quantization or when an IMU is mounted away from the vehicle's center of gravity. However, in this simulation, the vehicle is assumed to have perfect knowledge of the vehicle state. Guidance receives state information directly from the vehicle dynamics block.

A pre-programmed reference trajectory is loaded onto the vehicle from the mission planner prior to release from the carrier aircraft. The reference trajectory contains a time series of the desired position, velocity, and body attitude throughout the vehicle's ascent. The guidance law used in this Simulink model commands the vehicle to follow the reference trajectory's pitch profile. The pitch rate command is generated at each time step from Equation (5.1).

$$\Delta q = q_{ref} + K_P(\theta_{ref} - \theta) - q \tag{5.1}$$

In the above equation, θ_{ref} and q_{ref} are the reference trajectory's pitch orientation and pitch rate, respectively, θ and q are the sensed pitch orientation and pitch rate, respectively, and Δq is the output pitch rate command. K_P is a proportional gain applied to the pitch orientation error term, $(\theta_{ref} - \theta)$. A launch vehicle's controller gains may be constant or may change to better suit different flight conditions over the course of the

ascent. This process of tuning gains for different flight regimes is known as gain scheduling (McNamara 2011). In this simulation the ascent trajectory is broken into four phases and the value of K_P changes between phases. The gain values for each phase were manually tuned to produce desirable overshoot and settling time.

5.3 Reference Trajectories and Optimization

During the endoatmospheric portion of a rocket's flight, the reference trajectory is typically a pre-determined attitude profile as a function of time or velocity (Pinson, Schmitt and Hanson 2008). The reference ascent trajectories used in the subsequent analysis were generated using the Program to Optimize Simulated Trajectories (POST). This tool was developed jointly by Lockheed Martin and NASA Langley Research Center and is widely used to optimize both atmospheric and orbital trajectories. To run POST, the user defines a set of dependent variables, such as the desired end condition and any other constraints. The dependent variables used in this simulation are the final altitude, velocity, and flight path angle. The user also selects the performance function to optimize, which in this case is the final vehicle mass at the end of the first stage burn. The reason for selecting this performance function will be explained in Section 6.1. POST takes into account the vehicle's initial position, velocity, and body attitude at ignition. It

also accounts for the vehicle's aerodynamics from user-defined aerodynamic coefficient tables. The trajectory is broken into phases specified by the user. POST optimizes the performance function subject to the dependent variable constraints by determining values for the independent or control variables during each phase. Here, the first stage trajectory is broken into eight phases and the control variables are the pitch and pitch rate.

POST requires the user to provide an initial "guess" for the control variables. An initial guess for the pitch and pitch rate was obtained from the Powered Explicit Guidance (PEG) algorithm. PEG, which was initially developed for the Space Shuttle, finds the optimal solution to the ascent problem using a linear tangent steering law based on the tangent of the thrust angle. The PEG algorithm is implemented in MATLAB. The initial position, velocity, and pitch are input into the program. The end conditions (altitude, velocity, flight path angle) are also defined by the user. Unlike POST, PEG does not contain an atmosphere model and therefore does not take into account aerodynamic forces. The PEG algorithm produces a reference pitch profile, which is used as the initial guess for POST. POST then finds an optimized pitch profile accounting for both gravitational and aerodynamic losses. Trajectories are generated for the nominal ignition state and various off-nominal ignition conditions. A sample Input file for the POST program is presented in Appendix B.

5.4 Thrust Vector Control

The inner control loop consists of the TVC law and the TVC actuator. The Simulink model of the TVC loop is shown in Figure 5.4. The input to the TVC law is the angular rate command from guidance. The TVC law, which is modeled here as a PID controller, converts the rate command into a desired gimbal angle command for the TVC actuator. The PID controller transfer function takes the form of Equation 5.2.

$$\frac{K_I}{s} + K_P + K_D s \tag{5.2}$$

Where K_I, K_P, and K_D are constant gains. The gains were manually tuned to yield a desirable bandwidth and gain margin. The difference between the desired and sensed engine deflection angle is sent to the TVC actuator. Flight vehicles typically use electromechanical, electro-hydraulic, or pneumatic actuators to gimbal the engine. The actuator modeled in this simulation is electromechanical. It is modeled as a lead-lag compensator followed by an integrator. The transfer function for the lead-lag compensator is given by Equation (5.3).

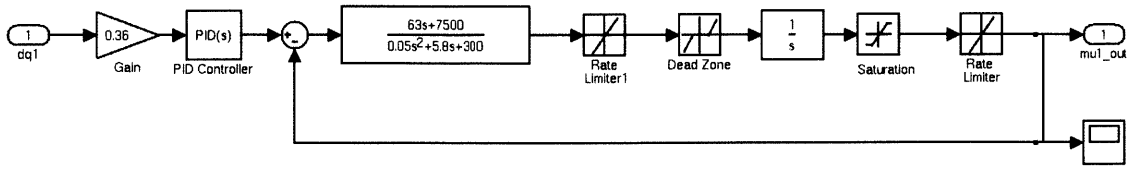

Figure 5.4 – Simulink Model of the Thrust Vector Control System

$$\frac{(s - z)}{(s - p_1)(s - p_2)} \tag{5.3}$$

Where z, p1 and p2 are the zero and poles of the transfer function, respectively.

Electromechanical TVC actuators are nonlinear systems and the nonlinearities are included in the Simulink model. Electromechanical actuators suffer from static friction, or stiction, which prevents the actuator from reacting to changes in command below a certain threshold. This effect is modeled in Simulink using a dead-zone block, which prevents the TVC from making very small changes in the engine deflection angle. Furthermore, there are limits on the angular rate and acceleration at which the actuator can operate. A fast actuator allows for better control of the vehicle and therefore lowers steering performance losses. However, a TVC capable of high angular rates and accelerations requires larger motors, increased power consumption, and larger batteries, which drives up the total cost and weight of the rocket. Limits on the TVC actuators onboard the Space Shuttle are shown in Table 5.1.

Constraints are placed on the TVC angular rate and acceleration in the model using Simulink rate limiter blocks. The first of these blocks places a limit on the rate of change of the angular velocity signal (the acceleration) and the second limits the rate of

Table 5.1—TVC Actuator Limits onboard the Space Shuttle

Engine with TVC Actuator	Type	Maximum Angle	Maximum Rate
Shuttle Solid Rocket Boosters (SRBs)	hydraulic	±5.27° (pitch) ±5.27° (yaw)	6 °/s
Shuttle Main Engine	hydraulic	±10° (pitch) ±8° (yaw)	20°/s
Shuttle Orbital Maneuvering System (OMS)	electromechanical	±5.89° (pitch) ±6.44° (yaw)	3°/s

Sources: Penchuk & Croopnick (1983); Kranzusch (2007)

change of the angular position (the rate). The maximum gimbal angle is limited using a Simulink saturation block. In Chapter 6, the rocket will be modeled separately using different TVC actuator limits. This enables an investigation of the performance sensitivity to dispersions given different constraints on the TVC actuator. A faster actuator allows for greater vehicle control. It is therefore expected that a rocket equipped with a fast actuator can quickly correct for dispersions in ignition conditions. However, rockets with slower TVC systems, which are unable to quickly correct for off-nominal conditions, may suffer greater losses from dispersions.

As an example, the difference in vehicle response given a fast or slow actuator is demonstrated below. Figure 5.5 shows the engine gimbal angle response during the first 20 seconds of flight for a rocket equipped with a fast TVC actuator (maximum angle of ±6°, angular velocity of ±17°/s, and angular acceleration of ±180°/s^2). The resulting vehicle pitch profile closely tracks the reference pitch as shown in Figure 5.7. Next, consider a rocket equipped with a TVC actuator whose angular acceleration is highly constrained. The second actuator has the same limits on gimbal angle and angular velocity as above (±6°; ±17°/s) but a maximum angular acceleration of ±5.7°/s^2. Figures 5.6 and 5.8 present the vehicle's gimbal angle and pitch response with this sluggish TVC actuator. The figures demonstrate that the vehicle is much slower to respond to changes in command, which results in wide deviations from the reference trajectory.

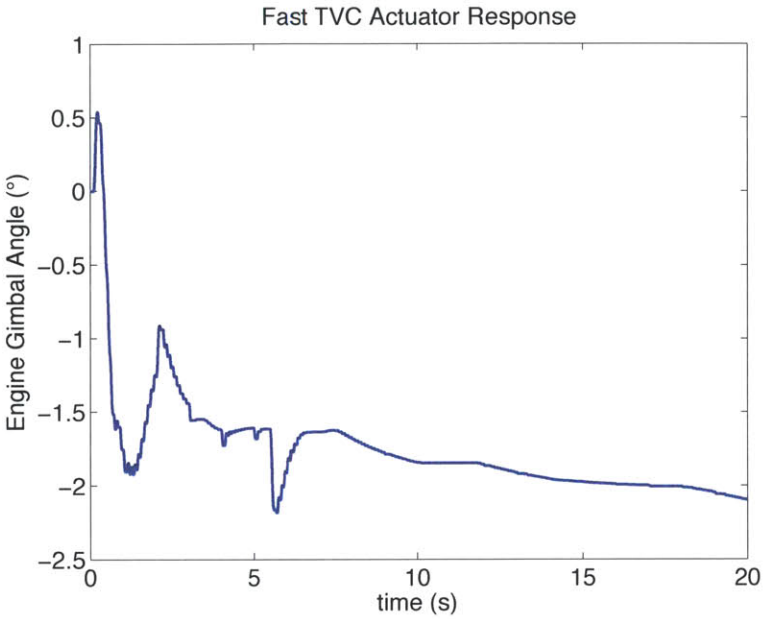

Figure 5.5 – Engine gimbal angle response for a fast TVC actuator

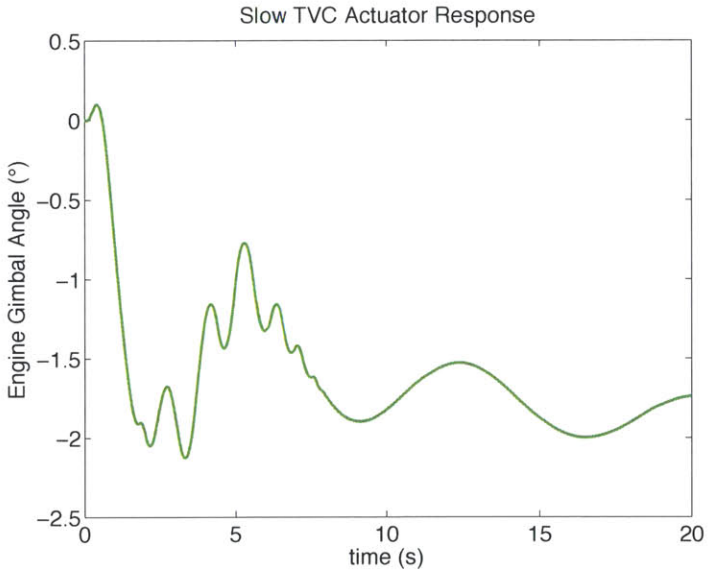

Figure 5.6 – Engine gimbal angle response for slow TVC actuator

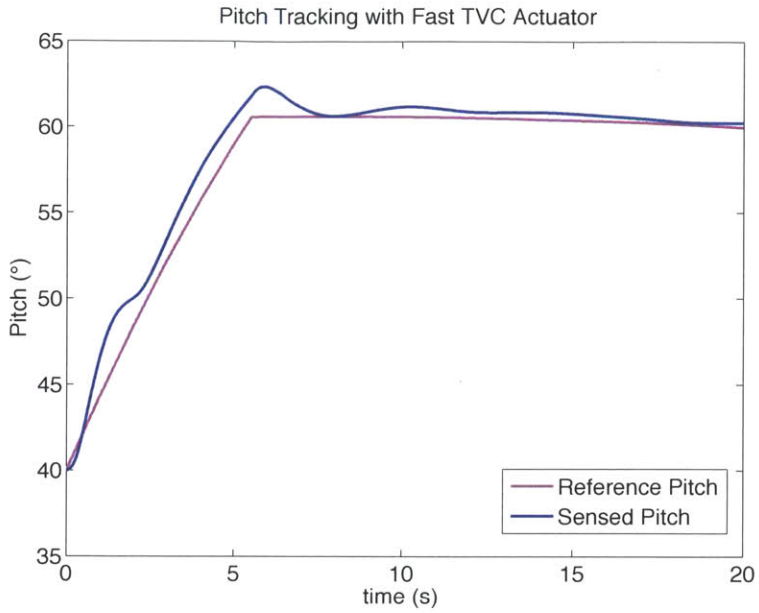

Figure 5.7 – Pitch angle for a rocket equipped with a fast TVC actuator

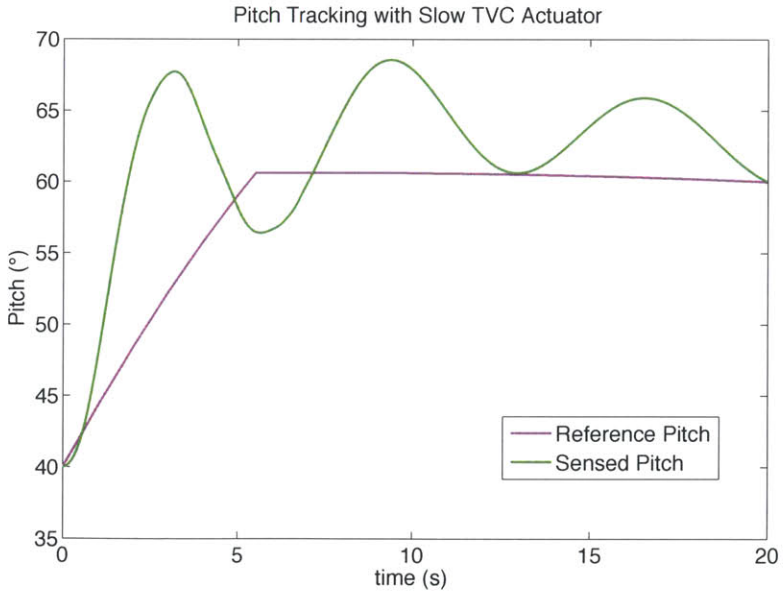

Figure 5.8 – Pitch angle for a rocket equipped with a slow TVC actuator

5.5 Vehicle Dynamics

The final subsystem is the vehicle dynamics block, which is commonly known as the "plant". The inputs to the plant include the engine gimbal angle, the aerodynamic forces, and the current vehicle state. The dynamics block then integrates the equations of motion to determine the vehicle state at the next time step. The equations of motion contained in the dynamics block are the same as those derived in Chapter 4. The only difference is the addition of the engine thrust, which affects the rocket's translational and rotational motion.

The translational equations of motion (4.12)—(4.12c) become:

$$\dot{u} = \frac{T\cos\mu_1\cos\mu_2}{m} + \frac{F_{Aero,x}}{m} - g\sin\theta + rv - qw \tag{5.4a}$$

$$\dot{v} = \frac{T\cos\mu_1\sin\mu_2}{m} + \frac{F_{Aero,y}}{m} + g\sin\phi\cos\theta - ru + pw \tag{5.4b}$$

$$\dot{w} = \frac{T\sin\mu_1\cos\mu_2}{m} + \frac{F_{Aero,z}}{m} + g\cos\phi\cos\theta + qu - pv \tag{5.4c}$$

Where T is the magnitude of the engine's thrust and μ_1 and μ_2 are the engine gimbal angles in the pitch and yaw plane, respectively.

It is assumed that the vehicle's roll motion is controlled by a separate attitude control system, which will not be considered here. Therefore, for this study the vehicle is assumed to experience no roll motion. Taking advantage of this assumption, Equations (4.22a)—(4.22c) can be simplified by substituting $\phi = 0°$.

$$\dot{\phi} = p + \tan\theta\, r \tag{5.5a}$$

$$\dot{\theta} = q \tag{5.5b}$$

$$\dot{\psi} = r\sec\theta \tag{5.5c}$$

Next, since $\dot{\phi} = 0$ the body rate p is found by $p = -\tan\theta\, r$. The body rates q and r are calculated at each time step by integrating Equations (5.6a)—(5.6b)

$$\dot{q} = \frac{M}{I_{yy}} + \frac{pr(I_{zz} - I_{xx})}{I_{yy}} \tag{5.6a}$$

$$\dot{r} = \frac{N}{I_{zz}} + \frac{pq(I_{xx} - I_{yy})}{I_{zz}} \tag{5.6b}$$

Where the moments are now the sum of the torques due to the aerodynamic forces and rocket thrust. The rotational equations of motion are therefore:

$$\dot{q} = \frac{F_N l_1 + T l_2 \sin\mu_1 \cos\mu_2}{I_{yy}} + \frac{pr(I_{zz} - I_{xx})}{I_{yy}} \tag{5.6a}$$

$$\dot{r} = \frac{F_Y l_1 + T l_2 \cos\mu_1 \sin\mu_2}{I_{zz}} + \frac{pq(I_{xx} - I_{yy})}{I_{zz}} \tag{5.6b}$$

Where $l_1$and l_2 are the moment arms for the aerodynamic and thrust forces, respectively.

Finally, during the first stage burn of the ascent trajectory, the rocket will attain air-relative velocities upwards of Mach 10. It is therefore necessary to generate aerodynamic coefficient data for the rocket under high Mach numbers. Missile DATCOM was once again used to generate aerodynamic models for both rocket configurations for angles of attack ranging from 0 to 180°, sideslip angles between -80° and 80°, and Mach numbers between 0.5 and 12. The aerodynamic data was then loaded into Simulink 3D lookup tables as shown in Figure 5.9. The lookup tables use 3D interpolation to determine the aerodynamic coefficients as a function of angle of attack, sideslip, and Mach number at each time step of the simulation.

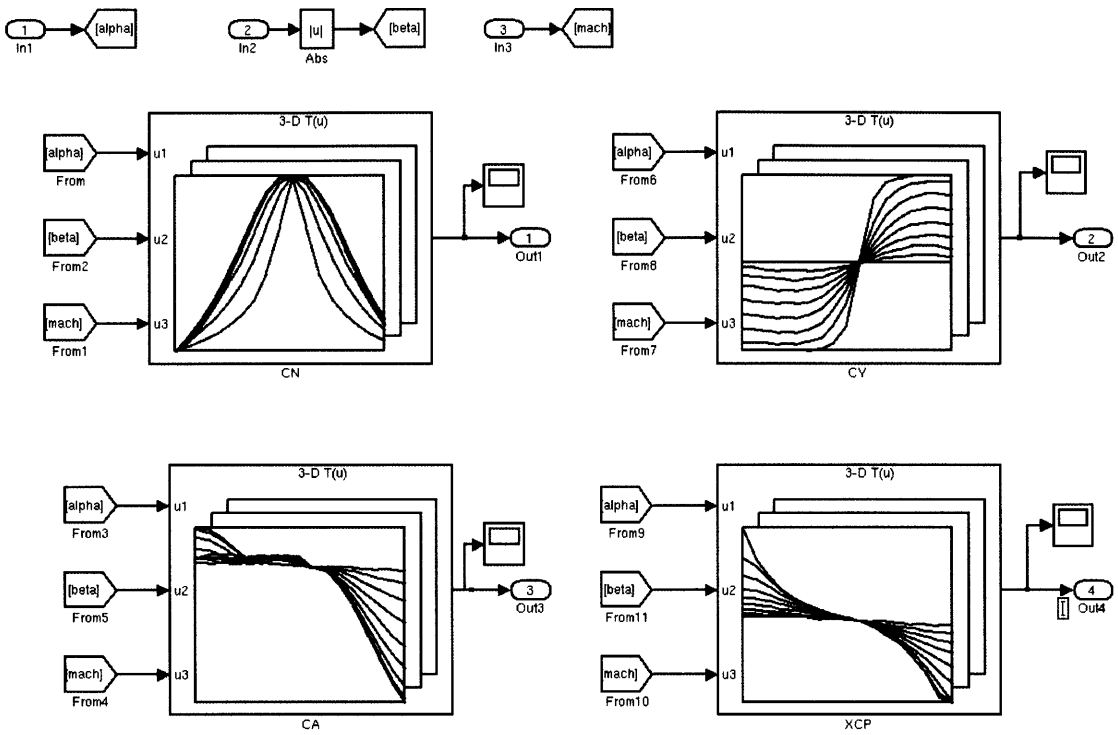

Figure 5.9 – Simulink Aerodynamics Block

Chapter 6: Evaluation of Vehicle Performance

This chapter quantifies the rocket's performance losses due to off-nominal ignition conditions and investigates a reference trajectory strategy to mitigate those losses. The first section explains the performance metric used as the point of comparison between different simulations. Next, the vehicle performance loss is determined for a variety of dispersed ignition conditions by running the Simulink model presented in Chapter 5 using a reference trajectory optimized for the "nominal" ignition condition. The performance losses due to dispersions in ignition conditions are determined for vehicles with different TVC actuator constraints in order to investigate the performance sensitivity to the actual actuator dynamics. Finally, alternate reference trajectories optimized for dispersed ignition conditions are used in the Simulink model to determine whether performance losses may be mitigated by selection of a reference trajectory better-suited to a given ignition state.

6.1 Performance Metrics

In the following sections, vehicle performance will be quantified using the 6-DOF Simulink model with various ignition conditions and reference trajectories. The goal of trajectory optimization is to maximize the total vehicle mass at the end of the trajectory. The end condition occurs when the vehicle attains the desired altitude, velocity, and flight path angle simultaneously. In each simulation, the vehicle achieves the end condition at a different time, and therefore, with a different total mass. However, the specific energy at the end condition is the same in each simulation. The specific energy is the sum of the specific kinetic and potential energies, which are given in Equations (6.1a)-(6.1b).

$$KE_{sp} = \frac{1}{2}\left|\vec{V}_{inertial}\right|^2 \tag{6.1a}$$

$$PE_{sp} = -\frac{GM_E}{R_E + Alt} - PE_0 \tag{6.1b}$$

$$PE_0 = -\frac{GM_E}{R_E} \tag{6.1c}$$

The vehicle mass at the end condition will be used to quantify performance. A smaller total mass at the end condition implies that the vehicle used more propellant to reach the same specific energy state. Using more propellant implies there is less available weight for the payload. The vehicle mass at the end condition for nominal ignition conditions (and a reference trajectory optimized for the nominal state), $m_{nominal}$, will be used as the point of comparison. The difference between $m_{nominal}$ and a dispersed case cutoff mass, $m_{dispersed}$, can be represented in terms of a loss in ΔV using Equation (6.2).

$$\Delta V = v_e \ln\left(\frac{m_{nominal}}{m_{dispersed}}\right) \tag{6.2}$$

This loss in ΔV corresponds to a difference in specific energy given by Equation (6.3)

$$\Delta Energy = \frac{1}{2}[(V_{nom} + \Delta V)^2 - V_{nom}^2] \tag{6.3}$$

The POST reference trajectories are 3-DOF optimized trajectories. The profiles define the optimal position and velocity in three dimensions, while the attitude is assumed aligned with the optimal thrust direction. The POST trajectory does not reflect how the GN&C system behaves. In a 6-DOF simulation, the vehicle's pitch profile will not exactly follow the reference profile. Therefore there will be a difference between the vehicle's state at the end of the trajectory in the 6-DOF simulation compared to that predicted by the reference trajectory. This discrepancy increases for less responsive TVC systems.

Since the goal is to compare the vehicle's mass at an identical end condition, corrections must be made to the vehicle's trajectory in order to make each simulation end at the same state. The simulation is first run with a very responsive TVC system, which allows the pitch profile to almost perfectly mirror the reference profile. The vehicle's altitude and flight path angle are recorded as a function of velocity. For all other simulation runs (with different ignition conditions, TVC constraints, or reference trajectories) the pitch rate command from guidance contains additional terms to null errors in altitude and flight path angle as a function of velocity relative to the "ideal" case. This way, the vehicle in every simulation reaches the energy condition cut off at a nearly identical altitude, velocity, and flight path angle. Residual errors in each velocity

component and the altitude are determined. The total residual error is calculated as the sum of the error terms in Equations (6.4a)—(6.4d).

$$E_{error\_vx} = \frac{1}{2}(v_{x_{dispersed}}^2 - v_{x_{nom}}^2) \tag{6.4a}$$

$$E_{error\_vy} = \frac{1}{2}(v_{y_{dispersed}}^2 - v_{y_{nom}}^2) \tag{6.4b}$$

$$E_{error\_vz} = \frac{1}{2}(v_{z_{dispersed}}^2 - v_{z_{nom}}^2) \tag{6.4c}$$

$$E_{error\_alt} = \frac{GM_E}{R_E + Alt_{dispersed}} - \frac{GM_E}{R_E + Alt_{nominal}} \tag{6.4d}$$

In order to ensure that the mass difference is a valid metric of comparison, the sum of the residual errors must be at least an order of magnitude less than the energy difference calculated in Equation (6.3).

6.2 Performance Quantification: Air Launch Light

This section quantifies performance losses due to off-nominal ignition conditions for the Air Launch Light vehicle. First, performance is determined in the case where the rocket follows a reference trajectory that is optimized for the nominal ignition condition. Next, the simulation is run with the same off-nominal condition with a reference trajectory that is optimized for that dispersed ignition state. These two performance

measurements are compared in order to determine if a significant performance gain may be achieved by selecting a better-suited reference trajectory. Four ignition states are considered, which are listed in Table 6.1. Furthermore, the effects of TVC actuator constraints on performance loss are investigated. Simulations for each dispersed case are run with three different sets of TVC actuator constraints listed in Table 6.2. An essentially unconstrained actuator, an angular acceleration limited actuator, and an angular velocity limited actuator are considered.

Table 6.1 – Ignition States Investigated for Air Launch Light

Ignition State Name	Pitch	Pitch Rate	Altitude	Speed
Nominal	40°	25°/s	50,000 ft.	Mach 0.5
Low Pitch / Pitch Rate	15°	15°/s	50,000 ft.	Mach 0.5
High Pitch / Pitch Rate	65°	35°/s	50,000 ft.	Mach 0.5
Low Altitude	40°	25°/s	48,000 ft.	Mach 0.5

Table 6.2 – TVC Actuator Constraints

TVC Actuator	Max Angle	Max Velocity	Max Acceleration
Fast	6°	20°/s	100 °/s^2
Acceleration Constrained	6°	20 °/s	5.7 °/s^2
Rate Constrained	6°	3°/s	100 °/s^2

6.2.1 Fast TVC Actuator

To begin, consider Air Launch Light equipped with a very responsive TVC actuator. The constraints on the TVC actuator are shown in the first row of Table 6.2. With these liberal constraints, the gimbaled rocket engine can respond very quickly to

disturbances. The 6-DOF Simulink model is first run with the nominal ignition condition with the reference trajectory optimized for the nominal condition. The reference trajectory calls for first stage engine cutoff at about 131 seconds after ignition. The vehicle's state (for the nominal ignition condition case) at 130.0 s is selected as the state against which the other simulations will be compared. The rocket's state at 130.0 s is described in Table 6.3 and the vehicle's pitch profile throughout the ascent trajectory is illustrated in Figure 6.1.

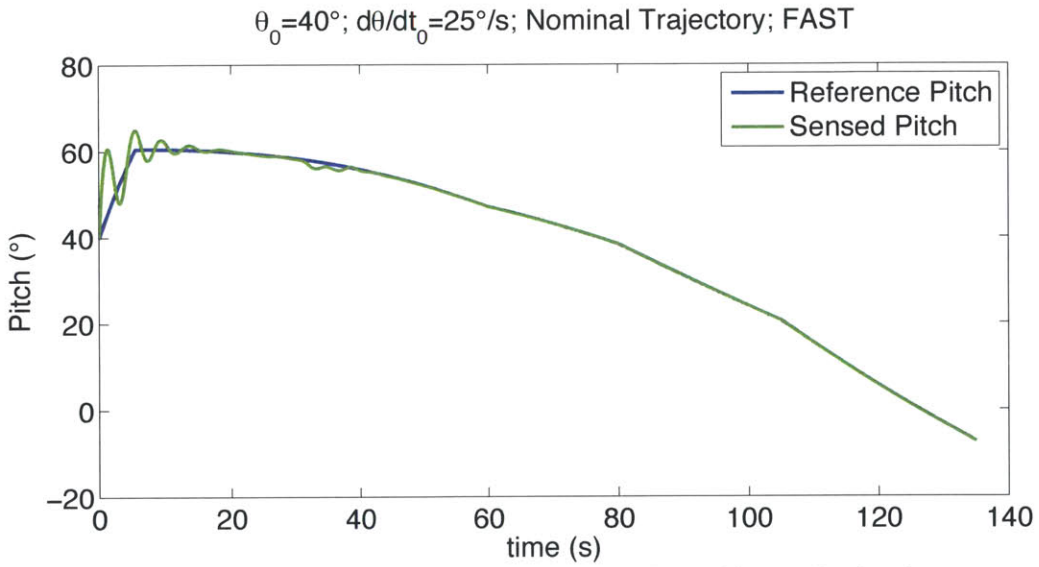

Figure 6.1 – Nominal ignition state pitch profile with nominal trajectory

Table 6.3 – Nominal Case Cutoff Condition

Quantity	Units	Value
Time	s	130.00
Mass	kg	2488.0
Specific Energy	MJ	6.7048
Altitude	km	82.930
Velocity	m/s	3435.9
Flight Path Angle	deg	13.357

The simulation was then run for the first off-nominal ignition state listed in Table 6.1. The "low pitch / pitch rate" case starts with an initial pitch of 15° and pitch rate of 15°/s. All other vehicle state variables are nominal at ignition. The simulation is first run with this dispersed ignition condition with the reference trajectory optimized for the nominal ignition condition. The resulting vehicle pitch profile is illustrated in Figure 6.2 (*top*). The vehicle's specific energy is measured throughout the ascent and the vehicle's state at the time it achieves the cutoff condition is recorded. The difference in vehicle state at the cutoff condition relative to that of the nominal case is shown in Table 6.4 (a). The table demonstrates that the vehicle reaches the cutoff altitude, velocity, and flight path angle 0.134 s later than the nominal ignition case. The off-nominal case therefore used 7 kg (15.5 lbs.) more propellant to achieve the same final state. Next, the simulation is run with a reference trajectory generated in POST that was optimized for the "low pitch / low pitch rate" ignition condition. The resulting pitch profile is shown in Figure 6.2 (*bottom*) and the vehicle state at cutoff is described in Table 6.4 (b). The vehicle reaches the end condition 0.151 s later, indicating about the same performance loss as the nominal trajectory. In both cases, however, the performance loss is very small.

Figures 6.3 (*top*) illustrates the pitch profile for the "high pitch / pitch rate" ignition case with the nominal trajectory, while Figure 6.3 (*bottom*) shows the pitch profile with a trajectory tailored for this dispersed ignition condition. The vehicle states for both cases at the end condition are stated in Tables 6.5 (a)—(b). Again, the results show that the performance loss is nearly the same (and very small) in both cases. The highly responsive TVC actuator is able to readily correct for disturbances. Therefore, there is little room for improvement, even with a better-suited trajectory.

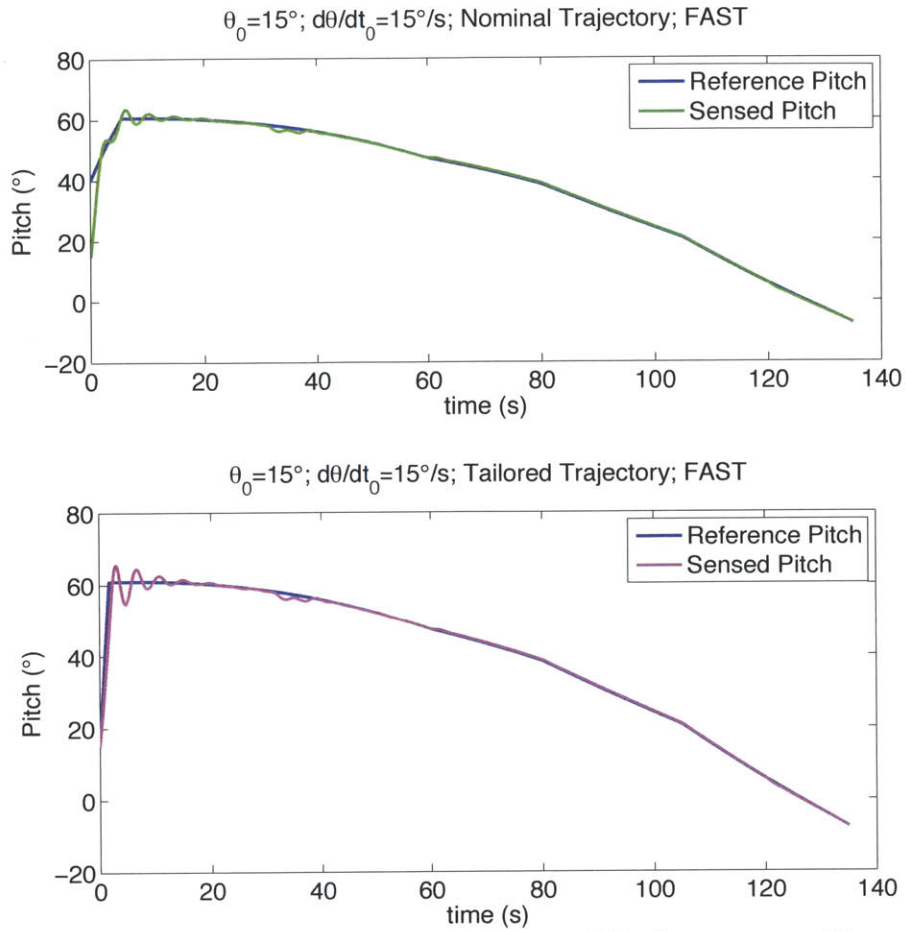

Figure 6.2—Reference and sensed pitch for low pitch/pitch rate case with nominal (*top*) and tailored trajectory (*bottom*) with fast TVC actuator

Table 6.4 (a)—Low Pitch/Pitch Rate Differentials; Nominal Trajectory

Quantity	**Units**	**Differential**
Time	s	+0.13416
Mass	kg	-7.0289
Altitude	m	-3.7753
Velocity	m/s	+0.010476
Flight Path Angle	deg	+0.013400

Table 6.4 (b)—Low Pitch/Pitch Rate Differentials; Tailored Trajectory

Quantity	**Units**	**Differential**
Time	s	+0.15099
Mass	kg	-7.9104
Altitude	m	-22.297
Velocity	m/s	+0.061953
Flight Path Angle	deg	+0.026067

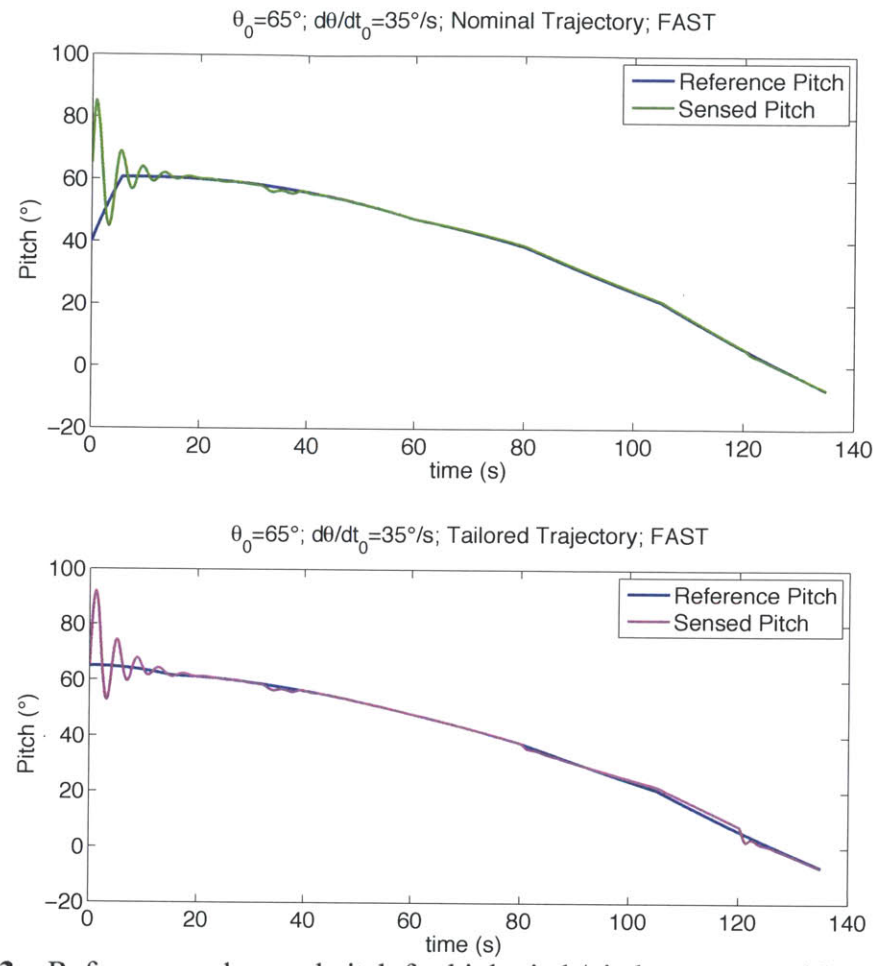

Figure 6.3—Reference and sensed pitch for high pitch/pitch rate case with nominal (*top*) and tailored trajectory (*bottom*) with a fast TVC actuator

Table 6.5 (a)—High Pitch/Pitch Rate Differentials; Nominal Trajectory

Quantity	**Units**	**Differential**
Time	s	+0.10586
Mass	kg	-5.5461
Altitude	m	-4.6145
Velocity	m/s	+0.012808
Flight Path Angle	deg	+0.0061397

Table 6.5 (b)—High Pitch/Pitch Rate Differentials; Tailored Trajectory

Quantity	**Units**	**Differential**
Time	s	+0.10799
Mass	kg	-5.6577
Altitude	m	-28.374
Velocity	m/s	+0.078837
Flight Path Angle	deg	+0.088217

6.2.2 Angular Acceleration Constrained TVC Actuator

Next, consider the air-launched rocket, but this time equipped with a TVC actuator that is highly constrained in its maximum angular acceleration. The actuator has the characteristics described in the second row of Table 6.1. The 6-DOF Simulink model is run for the nominal ignition condition with the reference trajectory optimized for the nominal condition. The rocket's state at 130.0 s is described in Table 6.6 and the vehicle's pitch profile throughout the ascent trajectory is illustrated in Figure 6.4. The vehicle's state under nominal conditions at 130.0 s after ignition is now used as the point of comparison for subsequent simulations with the acceleration-limited actuator. The pitch profile in Figure 6.4 illustrates more deviations from the reference profile compared with Figure 6.1 due to the TVC constraints.

The simulation is then run for each of the three dispersed cases in Table 6.1 with both the nominal trajectory and the trajectory tailored to the ignition condition. The pitch profiles for the low pitch / pitch rate case, high pitch / pitch rate case, and the low altitude case are presented in Figures 6.5, 6.6, and 6.7, respectively. The corresponding vehicle

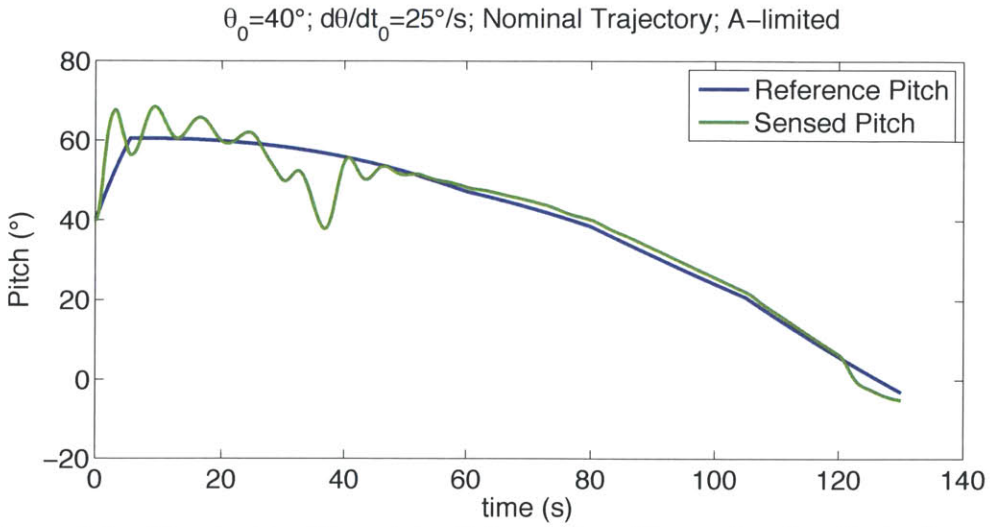

Figure 6.4 – Nominal ignition state pitch profile with acceleration-limited actuator

Table 6.6 – Nominal Case Cutoff Condition; Acceleration-limited TVC

Quantity	**Units**	**Value**
Time	s	130.00
Mass	lbs	2488.0
Specific Energy	MJ	6.6520
Altitude	km	82.601
Velocity	m/s	3421.4
Flight Path Angle	deg	13.441

states at the end condition are shown in Tables 6.7, 6.8, and 6.9. The results from the low pitch / pitch rate case show that the vehicle experiences a loss in performance of about 70 kg (154 lbs.) due to the off-nominal ignition condition when following the nominal trajectory. Furthermore, when run with the tailored trajectory, the performance loss is reduced to 13.8 kg (30.5 lbs.), a weight saving of about 56 kg (124 lbs.).

The high pitch / pitch rate case shows similar results. When following the nominal trajectory, the vehicle experiences a performance loss of about 115 kg. The tailored trajectory reduces the performance loss to 93 kg, a weight savings of 22 kg (49 lbs.). Finally, the simulation is run for the low initial altitude case. The results in Tables 6.9 (a) and (b) show that the performance loss is 21 kg with the nominal trajectory and 15 kg with the tailored trajectory. The low altitude case appears to result in lower performance loss than the cases with dispersed attitude and body rates. Therefore only a minor improvement is achieved with the tailored trajectory.

These results demonstrate that when a vehicle is equipped with an actuator incapable of quickly responding to off-nominal conditions, the vehicle suffers a notable performance loss due to dispersions in ignition conditions. Furthermore, using a reference trajectory that is optimized for the vehicle's true state at ignition reduces performance losses.

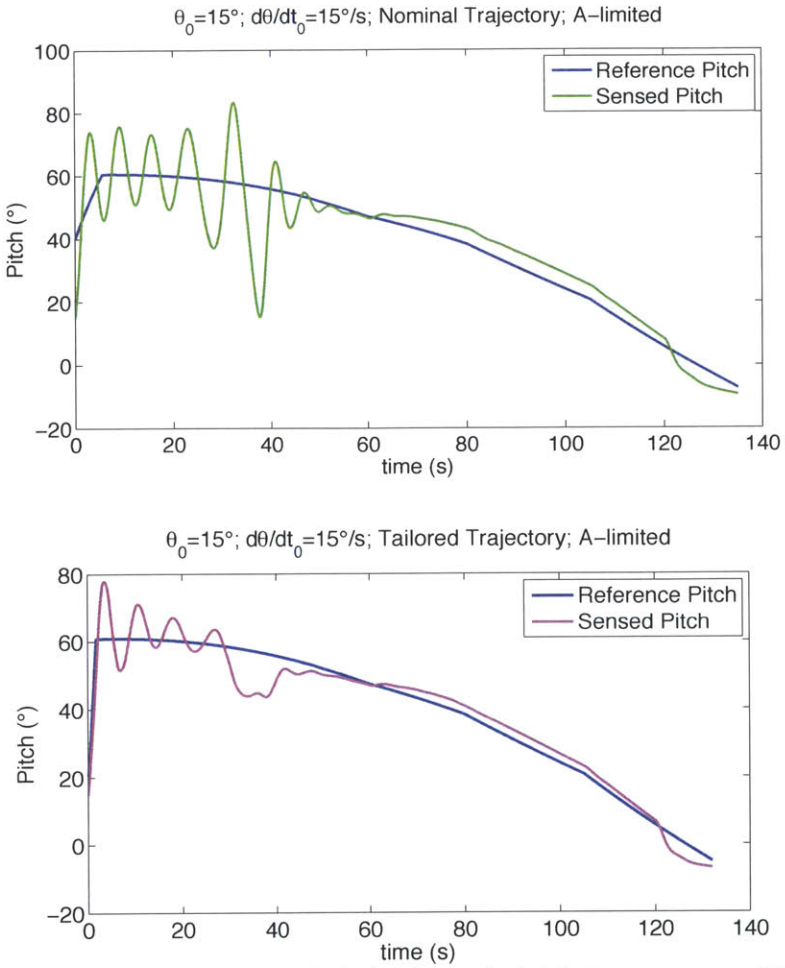

Figure 6.5—Reference and sensed pitch for low pitch/pitch rate case with nominal (*top*) and tailored trajectory (*bottom*) with acceleration-limited actuator

Table 6.7 (a)—Low Pitch/Pitch Rate Differentials; Nominal Trajectory; A-Limited

Quantity	**Units**	**Differential**
Time	s	+ 1.3372
Mass	kg	-70.056
Altitude	m	-78.178
Velocity	m/s	+0.21821
Flight Path Angle	deg	-0.0066316

Table 6.7 (b)—Low Pitch/Pitch Rate Differentials; Tailored Trajectory; A-Limited

Quantity	**Units**	**Differential**
Time	s	+ 0.26420
Mass	kg	-13.842
Altitude	m	-26.793
Velocity	m/s	+ 0.074804
Flight Path Angle	°	+ 0.032755

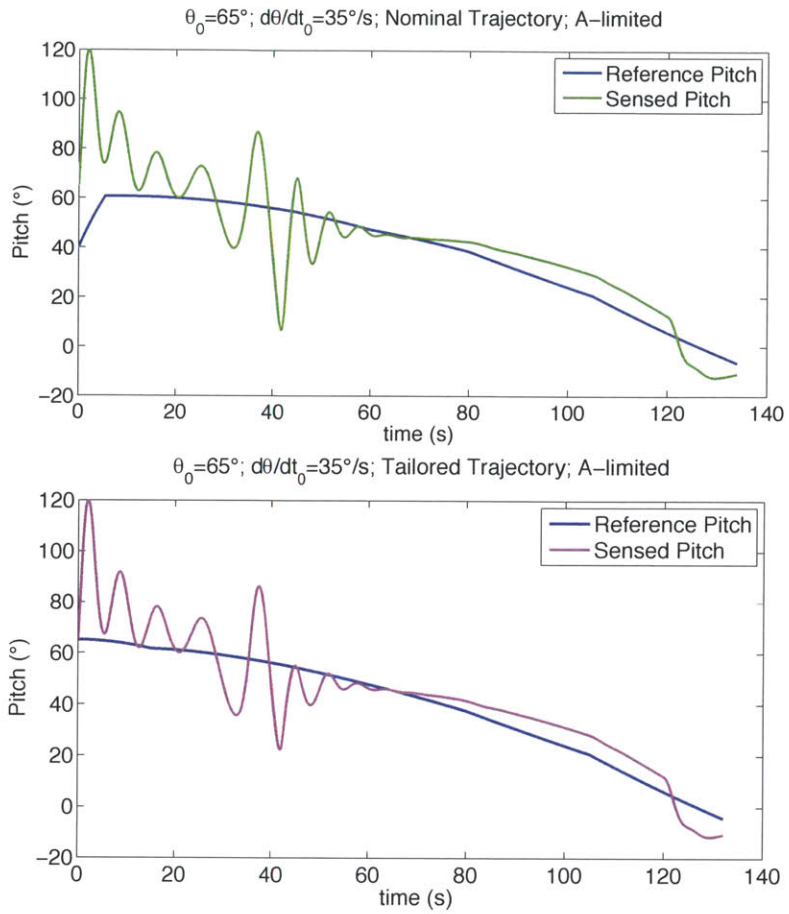

Figure 6.6—Reference and sensed pitch for high pitch/pitch rate case with nominal (*top*) and tailored trajectory (*bottom*) with acceleration-limited actuator

Table 6.8 (a)—High Pitch/Pitch Rate Differentials; Nominal Trajectory; A-Limited

Quantity	**Units**	**Differential**
Time	s	+ 2.1991
Mass	kg	-115.21
Altitude	m	-11.932
Velocity	m/s	+0.033339
Flight Path Angle	deg	-0.012769

Table 6.8 (b)—High Pitch/Pitch Rate Differentials; Tailored Trajectory; A-Limited

Quantity	**Units**	**Differential**
Time	s	+ 1.7788
Mass	kg	-93.190
Altitude	m	-35.789
Velocity	m/s	+ 0.099917
Flight Path Angle	deg	-0.020920

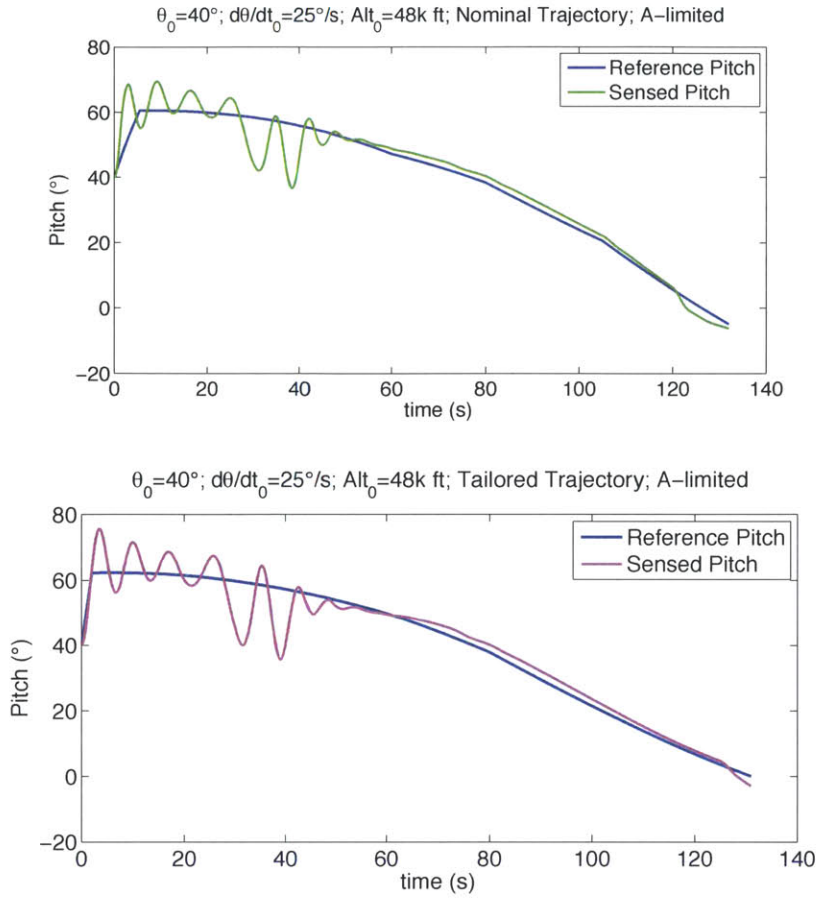

Figure 6.7—Reference and sensed pitch for low initial altitude case with nominal (*top*) and tailored trajectory (*bottom*) with acceleration-limited actuator

Table 6.9 (a)—Low Altitude Differentials; Nominal Trajectory; A-Limited

Quantity	**Units**	**Differential**
Time	s	+ 0.39883
Mass	kg	-20.895
Altitude	m	-11.210
Velocity	m/s	+ 0.031324
Flight Path Angle	deg	0.027508

Table 6.9 (b)—Low Altitude Differentials; Tailored Trajectory; A-Limited

Quantity	**Units**	**Differential**
Time	s	+ 0.28647
Mass	kg	-15.008
Altitude	m	-6.7124
Velocity	m/s	0.018762
Flight Path Angle	deg	+ 0.078834

6.2.3 Angular Velocity Constrained TVC Actuator

Next, consider the air-launched rocket when equipped with a TVC whose motion is constrained in angular velocity. The TVC constraints for this actuator are listed in the third row of Table 6.2. The simulation is run for the nominal ignition condition with the nominal reference trajectory and the velocity-constrained actuator. The rocket's state at 130.0 s is described in Table 6.10 and becomes the point of comparison for simulations runs with this actuator. Similar to the profiles with the acceleration-limited actuator, the pitch profile shown in Figure 6.8 for the velocity-constrained actuator shows more deviations from the reference profile compared to the fast actuator.

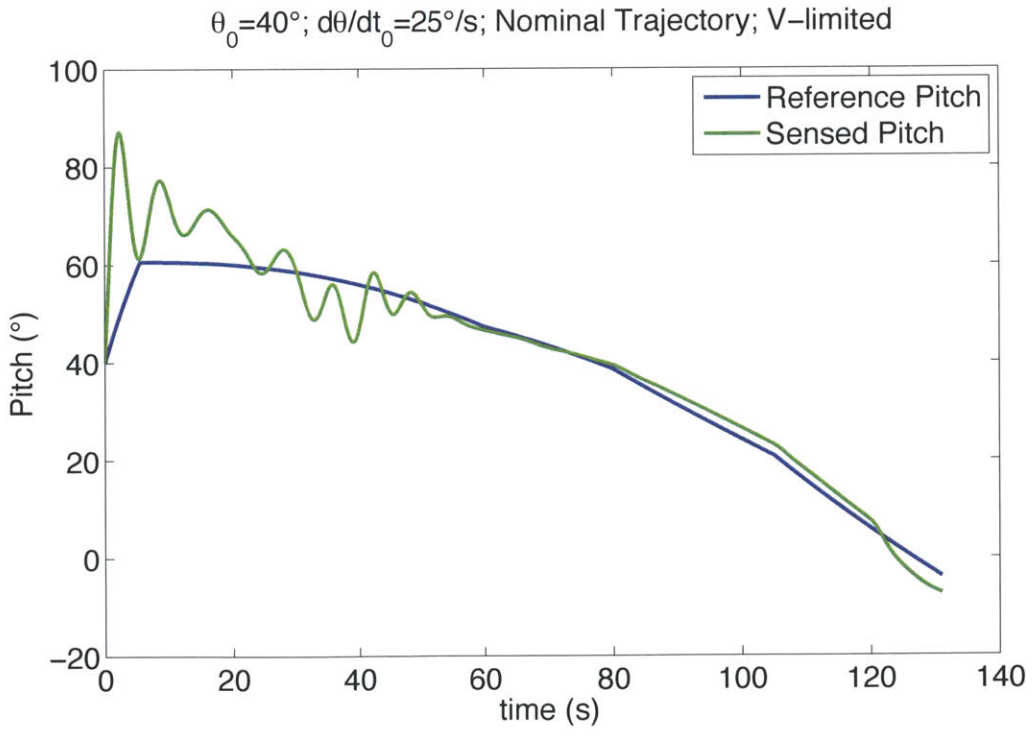

Figure 6.8—Nominal ignition state pitch profile for a velocity-limited actuator

Table 6.10 – Nominal Case Cutoff Condition; Velocity-limited TVC

Quantity	Units	Value
Time	s	130.00
Mass	kg	2488.0
Specific Energy	MJ	6.62944
Altitude	km	82.468
Velocity	m/s	3415.2
Flight Path Angle	deg	13.559

Now the three dispersed ignition cases are evaluated with the velocity limited actuator. The pitch profiles and vehicle states at the cutoff condition are presented in Figures 6.9 – 6.11 and Tables 6.11—6.13. A performance loss of 9 kg was measured for low pitch / pitch rate case for the nominal trajectory. This performance loss is reduced to only 0.14 kg when the rocket follows the tailored trajectory. The high pitch / pitch rate ignition condition produces a loss of 48 kg for the nominal trajectory and 22 kg for the tailored trajectory. Finally, the low altitude ignition case results in a 21 kg loss in performance when following the nominal trajectory and 8 kg when following the tailored trajectory.

The velocity-limited actuator performance losses due to off-nominal ignition conditions are smaller in magnitude than for the acceleration-limited actuator. An angular acceleration limit of $5.7°/s^2$ appears to be more constraining to the system than an angular velocity limit of 3 °/s. However, like the acceleration-limited case, the results from the simulations with the velocity-limited actuator indicate that use of a tailored trajectory for a specific ignition state provides a performance improvement over the nominal trajectory.

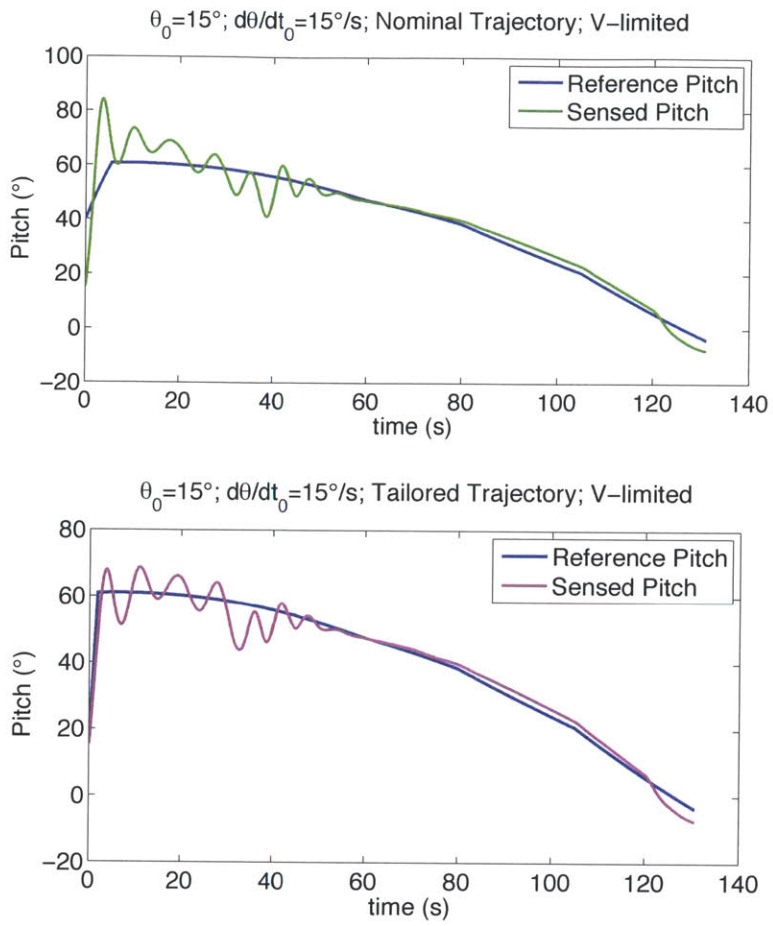

Figure 6.9—Reference and sensed pitch for low pitch/pitch rate case with nominal (*top*) and tailored trajectory (*bottom*) with velocity-limited actuator

Table 6.11 (a)—Low Pitch/Pitch Rate Differentials; Nominal Trajectory; V-Limited

Quantity	**Units**	**Differential**
Time	s	+ 0.17315
Mass	kg	-9.0713
Altitude	m	2.1696
Velocity	m/s	-0.0060498
Flight Path Angle	deg	0.0040160

Table 6.11 (b)—Low Pitch/Pitch Rate Differentials; Tailored Trajectory; V-Limited

Quantity	**Units**	**Differential**
Time	s	0.0026517
Mass	kg	-0.13893
Altitude	m	7.5027
Velocity	m/s	-0.020960
Flight Path Angle	deg	+ 0.016528

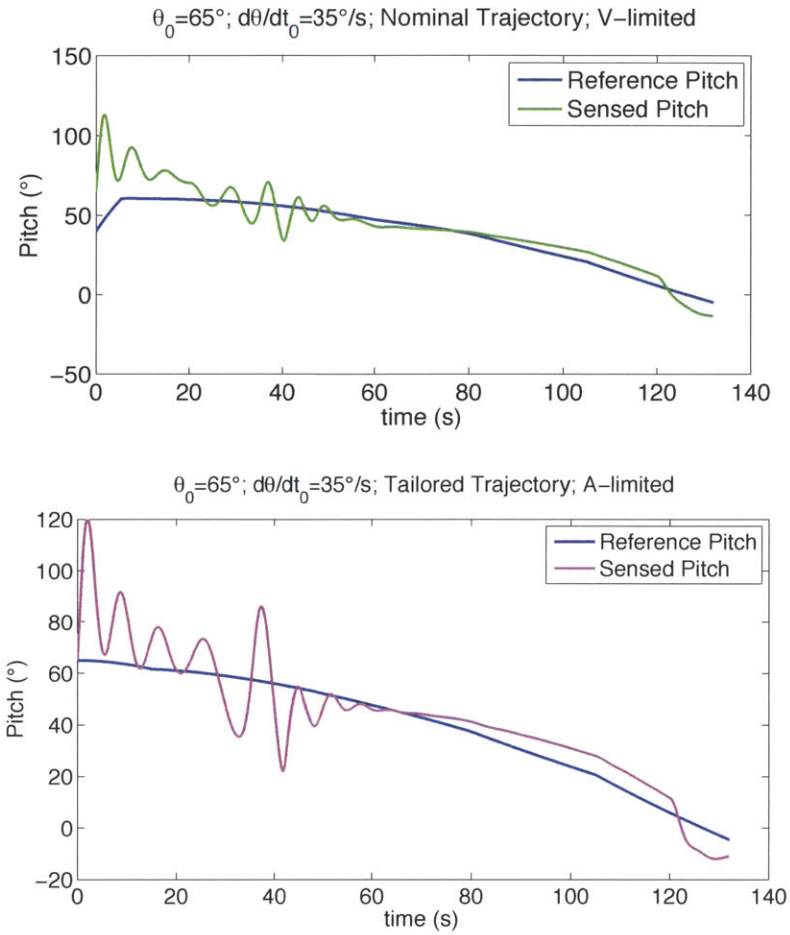

Figure 6.10—Reference and sensed pitch for high pitch/pitch rate case with nominal (*top*) and tailored trajectory (*bottom*) with velocity-limited actuator

Table 6.12 (a)—High Pitch/Pitch Rate Differentials; Nominal Trajectory; V-Limited

Quantity	**Units**	**Differential**
Time	s	+0.92251
Mass	kg	-48.3305
Altitude	m	32.355
Velocity	m/s	-0.090451
Flight Path Angle	deg	-0.029096

Table 6.12 (b)—High Pitch/Pitch Rate Differentials; Tailored Trajectory; V-Limited

Quantity	**Units**	**Differential**
Time	s	0.41686
Mass	kg	-21.839
Altitude	m	-10.310
Velocity	m/s	0.028846
Flight Path Angle	deg	+ 0.039170

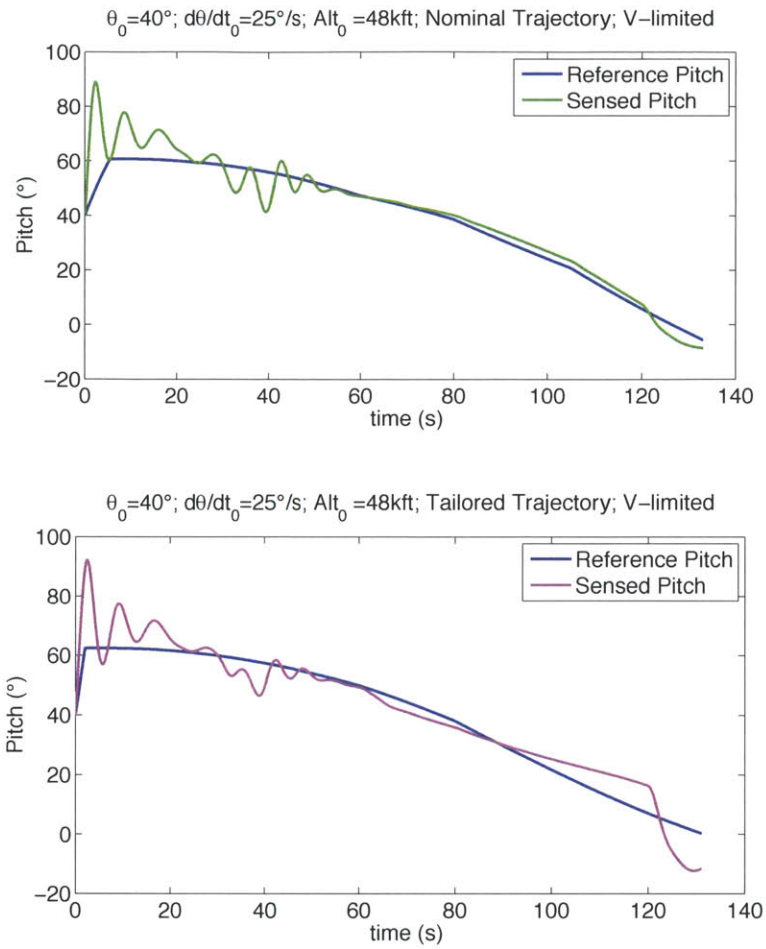

Figure 6.11—Reference and sensed pitch for low altitude case with nominal (*top*) and tailored trajectory (*bottom*) with velocity-limited actuator

Table 6.13 (a)—Low Altitude Differentials; Nominal Trajectory; V-Limited

Quantity	**Units**	**Differential**
Time	s	0.39795
Mass	kg	-20.848
Altitude	m	7.0092
Velocity	m/s	-0.019579
Flight Path Angle	deg	0.019880

Table 6.13 (b)—Low Altitude Differentials; Tailored Trajectory; V-Limited

Quantity	**Units**	**Differential**
Time	s	0.14928
Mass	kg	-7.8205
Altitude	m	-15.389
Velocity	m/s	0.043057
Flight Path Angle	deg	0.0579045

6.3 Performance Quantification: Air Launch Heavy

This section quantifies performance losses due to off-nominal ignition conditions for the larger Air Launch Heavy vehicle. The nominal and dispersed ignition states investigated are listed in Table 6.14. These states were selected based on the results of the Monte Carlo drop dynamics simulation presented in Chapter 4. For each dispersed state, the simulation is run with both the "nominal" and "tailored" reference trajectory. Once again, the performance for each case is quantified given different TVC actuator constraints, which are listed in Table 6.2.

Table 6.14 – Ignition States Investigated for Air Launch Heavy

Ignition State Name	Pitch	Pitch Rate	Altitude	Speed
Nominal	45°	30°/s	50,000 ft.	Mach 0.5
Low Pitch / Pitch Rate	20°	20°/s	50,000 ft.	Mach 0.5
High Pitch / Pitch Rate	70°	40°/s	50,000 ft.	Mach 0.5
Low Altitude	40°	25°/s	48,000 ft.	Mach 0.5

6.3.1 Fast TVC Actuator

The Simulink model of the first stage burn for Air Launch Heavy is first run with an essentially unconstrained TVC actuator. The vehicle state at the end of first stage burn given the nominal ignition condition is presented in Table 6.16. This vehicle state will be

used as the cutoff condition for subsequent simulations with the fast TVC actuator. Note that the cutoff time for Air Launch Heavy is 128.0 s after ignition. The pitch profile for the nominal case is illustrated in Figure 6.12. The simulation is then run for the dispersed ignition conditions. The performance is quantified in the same way as Section 6.2. The results from all three dispersed cases indicate there is a negligible performance loss due to dispersions when equipped with a very responsive TVC actuator. (The pitch profile plots and vehicle state tables were therefore excluded.) This result is the same as that seen for Air Launch Light with the fast actuator. The rocket's control system is able to quickly respond to the off-nominal conditions and easily correct the rocket back onto the desired trajectory. Therefore, there is little to no room for improvement, and it is not necessary to use a tailored reference trajectory.

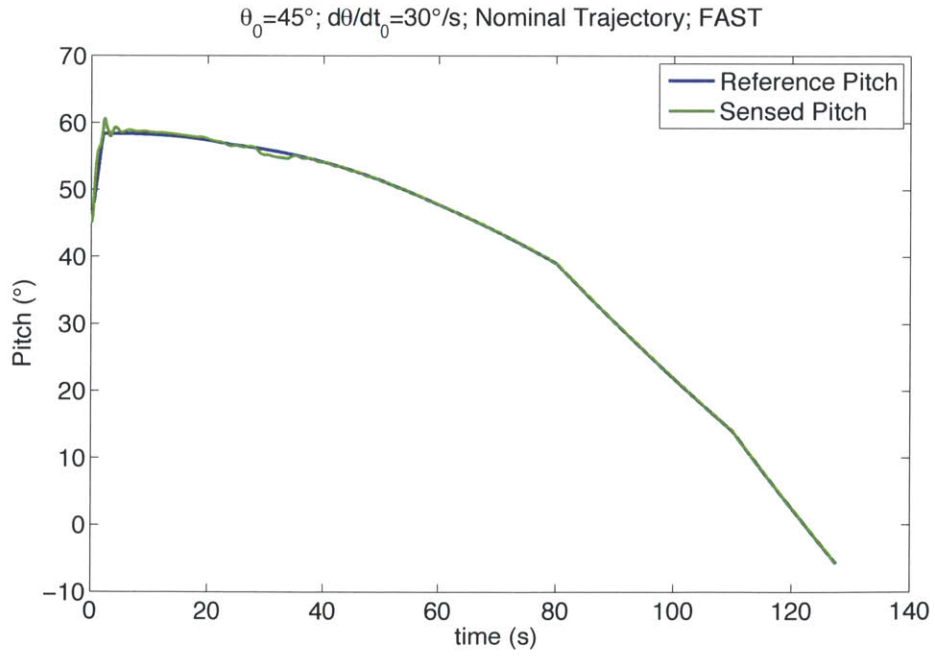

Figure 6.12—Nominal ignition state pitch profile for a fast actuator (Air Launch Heavy)

Table 6.16 – Nominal Case Cutoff Condition; Fast TVC; Air Launch Heavy

Quantity	Units	Value
Time	s	128.00
Mass	kg	5185.47
Specific Energy	MJ	6.49241450927
Altitude	km	81.0347853938
Velocity	m/s	3378.88044782
Flight Path Angle	deg	12.8640724

6.4.2 Angular Acceleration Constrained Actuator

Next, the simulations were run for each dispersed case with the acceleration-limited TVC actuator. The pitch profile and final vehicle state for the nominal case are presented in Figure 6.13 and Table 6.17. The pitch profiles for the low pitch / pitch rate ignition state with a nominal and tailored reference trajectory are shown in Figure 6.14. The difference between the vehicle state at the cutoff condition compared to that for the nominal case (Table 6.17) are presented in Table 6.18 The results indicate that the vehicle suffers a performance loss of about 30 kg relative to the nominal case when run with the nominal trajectory. On the contrary, it experiences a slight performance gain over the nominal case with the tailored trajectory, which means the rocket reaches the cutoff condition with more mass than the nominal case. Similarly, the high pitch / pitch rate case illustrates that the tailored trajectory results in a performance saving of about 45 kg over the nominal trajectory (Figure 6.15; Table 6.19). Finally, the low initial altitude

ignition condition case shows that the tailored trajectory produces a performance saving of about 43 kg over the nominal trajectory (Figure 6.16; Table 6.20).

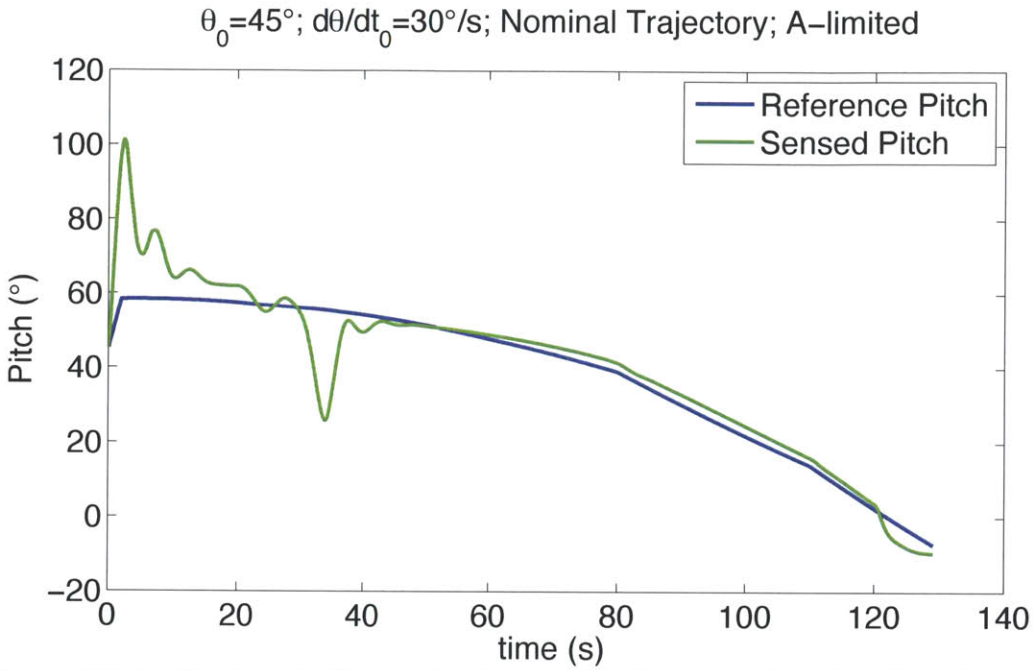

Figure 6.13—Nominal ignition state pitch profile for an acceleration-limited actuator (Air Launch Heavy)

Table 6.17 – Nominal Case Cutoff Condition; Acceleration-Limited TVC; Heavy

Quantity	Units	Value
Time	s	128.00
Mass	kg	5185.5
Specific Energy	MJ	6.3365
Altitude	km	80.315
Velocity	m/s	3334.5
Flight Path Angle	deg	13.279

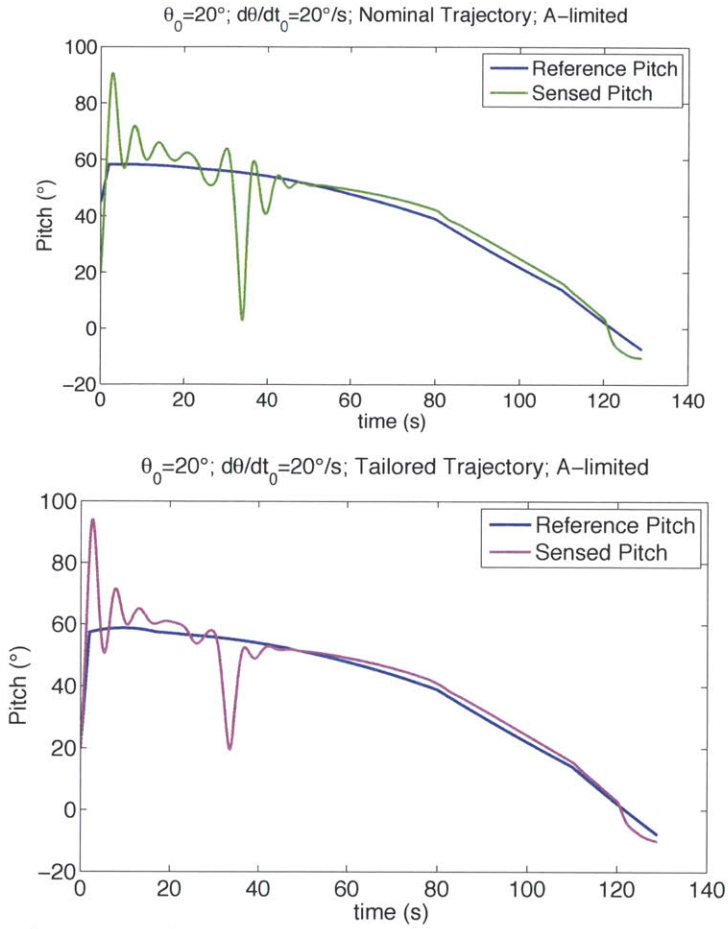

Figure 6.14—Reference and sensed pitch for low pitch/pitch rate case with nominal (*top*) and tailored trajectory (*bottom*) with acceleration-limited actuator (Heavy)

Table 6.18(a)–Low Pitch/Pitch Rate Differentials; Nominal Trajectory; A-Limit; Heavy

Quantity	**Units**	**Differential**
Time	s	+0. 28372
Mass	kg	-29.728
Altitude	m	26.004
Velocity	m/s	-0.074533
Flight Path Angle	deg	+ 0.027577

Table 6.18(b)–Low Pitch/Pitch Rate Differentials; Tailored Trajectory; A-Limit; Heavy

Quantity	**Units**	**Differential**
Time	s	-0.013624
Mass	kg	1.4275
Altitude	m	17.239
Velocity	m/s	-0.049430
Flight Path Angle	deg	+ 0.033879

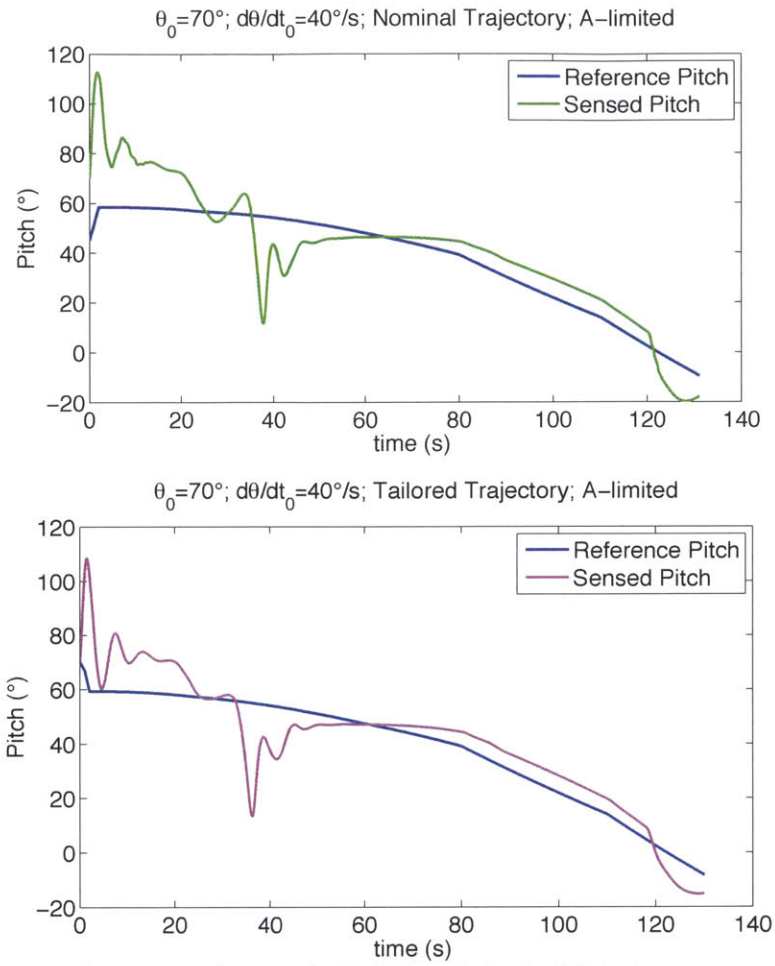

Figure 6.15—Reference and sensed pitch for high pitch/pitch rate case with nominal (*top*) and tailored trajectory (*bottom*) with acceleration-limited actuator (Heavy)

Table 6.19 (a)–High Pitch/Pitch Rate Differentials; Nominal Trajectory; A-limit; Heavy

Quantity	**Units**	**Differential**
Time	s	+1. 1418
Mass	kg	-119.6
Altitude	m	-44.243
Velocity	m/s	0.12679
Flight Path Angle	deg	0.0078000

Table 6.19(b)–High Pitch/Pitch Rate Differentials; Nominal Trajectory; A-limit; Heavy

Quantity	**Units**	**Differential**
Time	s	-0. 70842
Mass	kg	-74.228
Altitude	m	-3.0458
Velocity	m/s	0.0086913
Flight Path Angle	deg	+ 0.025121

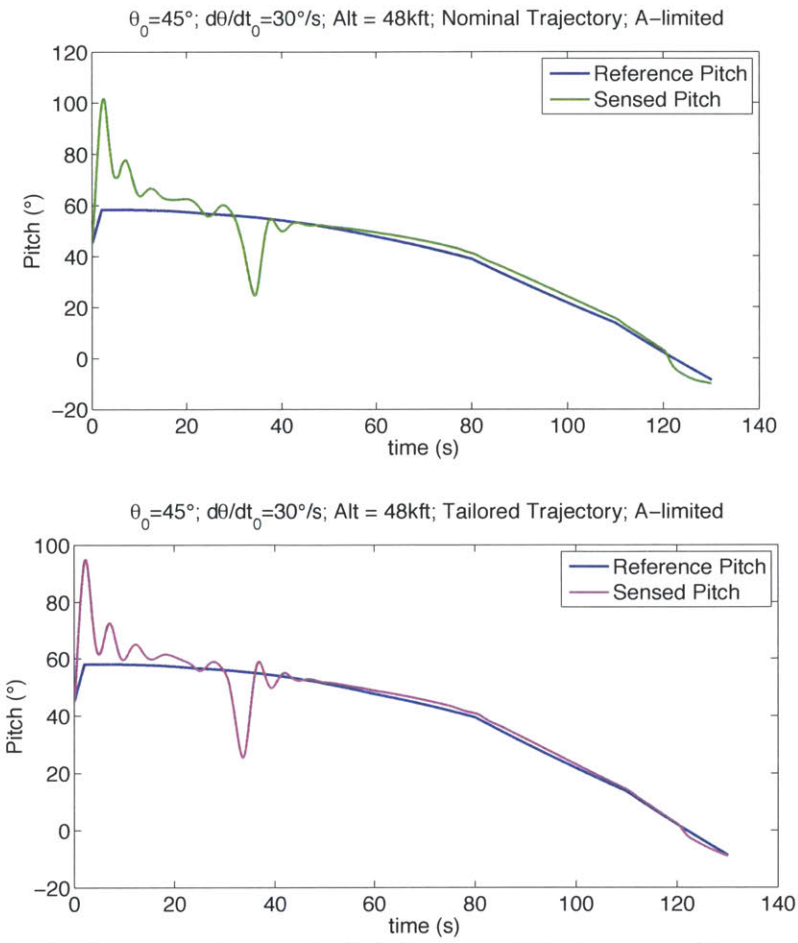

Figure 6.16—Reference and sensed pitch for low altitude case with nominal (*top*) and tailored trajectory (*bottom*) with acceleration-limited actuator (Heavy)

Table 6.20 (a)—Low Altitude Differentials; Nominal Trajectory; A-Limited; Heavy

Quantity	**Units**	**Differential**
Time	s	+0. 33289
Mass	kg	-34.880
Altitude	m	9.6715
Velocity	m/s	-0.027747
Flight Path Angle	deg	0.011098

Table 6.20 (b)—Low Altitude Differentials; Tailored Trajectory; A-Limited; Heavy

Quantity	**Units**	**Differential**
Time	s	-0 .080745
Mass	kg	+8.4604
Altitude	m	-15.083
Velocity	m/s	0.043240
Flight Path Angle	deg	0.013490

6.3.3 Angular Velocity Constrained Actuator

Finally, the vehicle performance is quantified for each dispersed case with the velocity-limited TVC actuator. The pitch profile and final vehicle state for the nominal case are presented in Figure 6.17 and Table 6.21. The pitch profiles for the low pitch / pitch rate ignition state given a nominal and tailored reference trajectory are shown in Figure 6.18 and the vehicle state differentials at cutoff are presented in Table 6.22. The results indicate that the vehicle can save 66 kg by using a tailored reference trajectory instead of the nominal trajectory. The high pitch / pitch rate case results are presented in Figure 6.19 and Table 6.23. Once again, the tailored trajectory produces a performance saving of about 84 kg compared to the nominal trajectory. Finally, the low initial altitude ignition condition case shows that the tailored trajectory produces a performance saving of 25 kg over the nominal trajectory (Figure 6.20; Table 6.24).

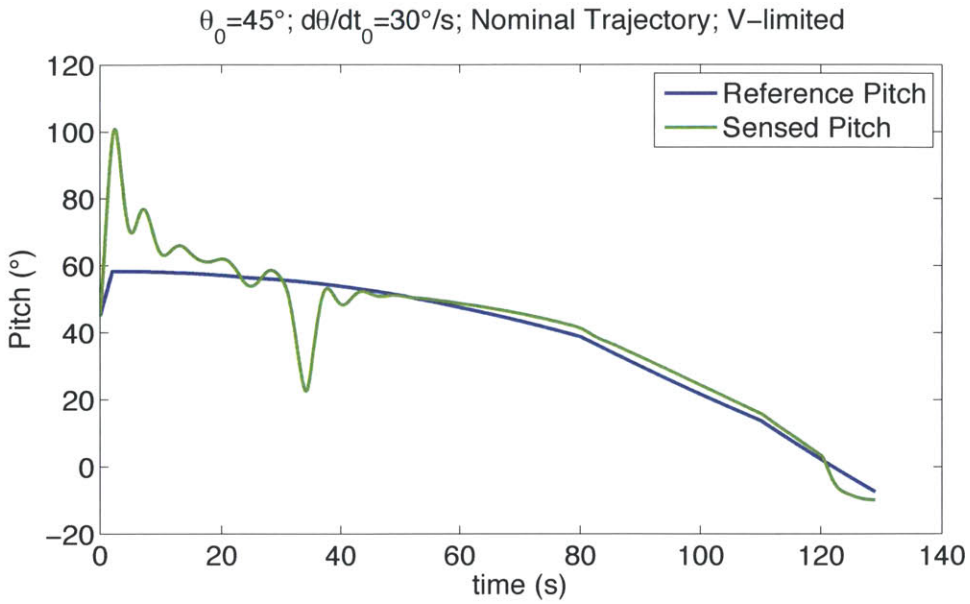

Figure 6.17—Nominal ignition state pitch profile for an angular velocity-constrained actuator (Heavy)

Table 6.21 – Nominal Case Cutoff Condition; Velocity-Limited TVC; Heavy

Quantity	Units	Value
Time	s	128.00
Mass	lb	5185.5
Specific Energy	MJ	6.3365
Altitude	km	80.320
Velocity	m/s	3331.3
Flight Path Angle	deg	13.294

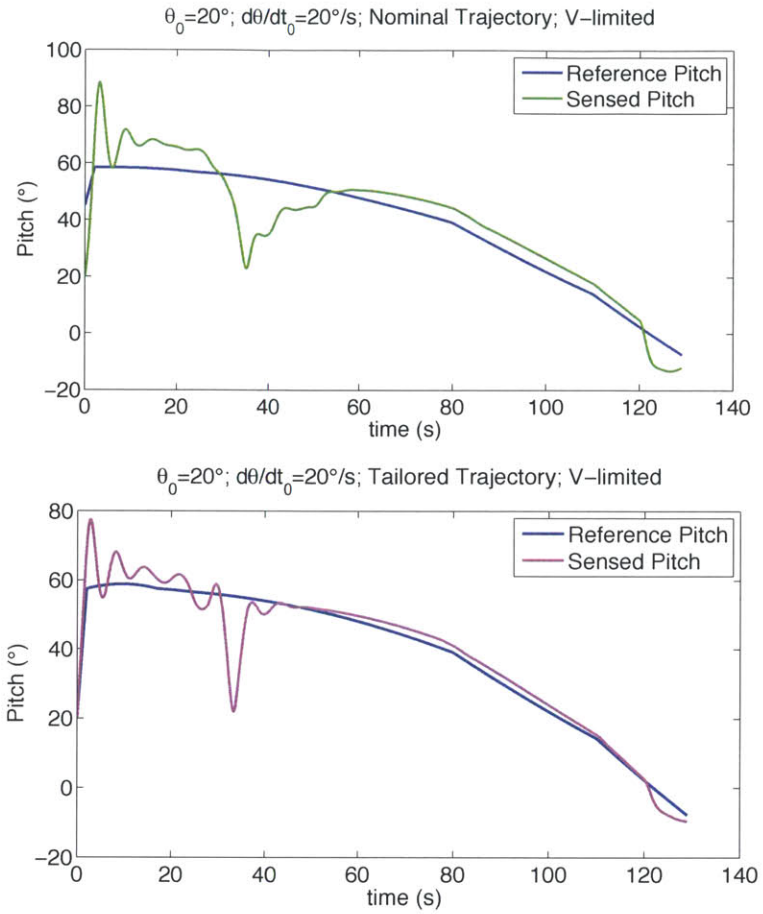

Figure 6.18—Reference and sensed pitch for low pitch/pitch rate case with nominal (*top*) and tailored trajectory (*bottom*) with velocity-limited actuator (Heavy)

Table 6.22(a)–Low Pitch/Pitch Rate Differentials; Nominal Trajectory; V-limited; Heavy

Quantity	**Units**	**Differential**
Time	s	+0 .49028
Mass	kg	-51.371
Altitude	m	-37.867
Velocity	m/s	0.10857
Flight Path Angle	deg	-0.022210

Table 6.22(b) –Low Pitch/Pitch Rate Differentials; Tailored Trajectory V-limited; Heavy

Quantity	**Units**	**Differential**
Time	s	-0.13956
Mass	kg	+14.624
Altitude	m	23.073
Velocity	m/s	-0.066174
Flight Path Angle	deg	0.0091318

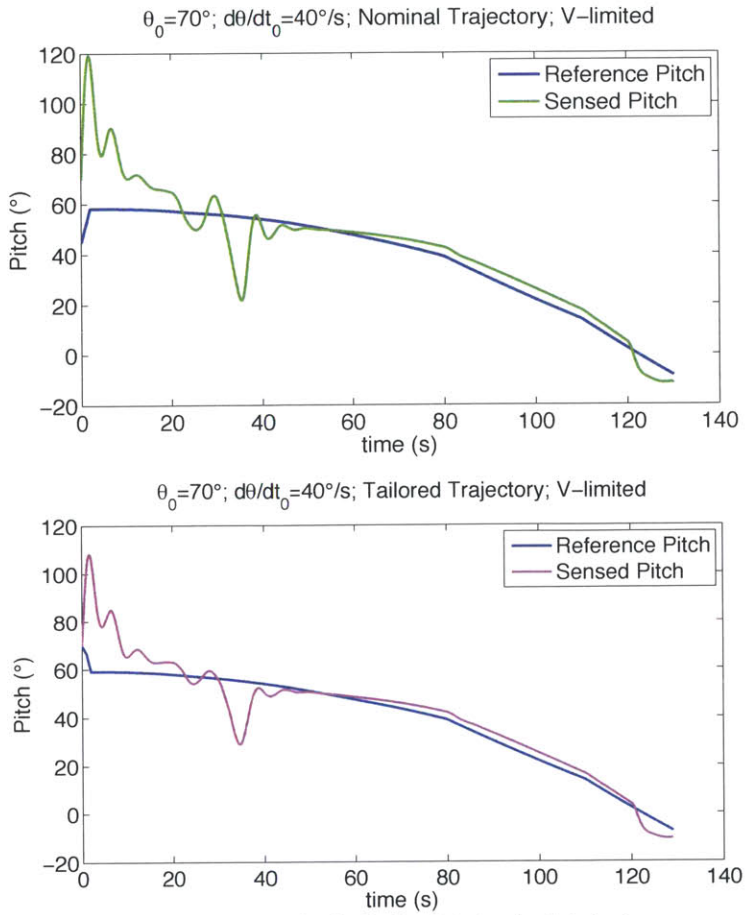

Figure 6.19—Reference and sensed pitch for high pitch/pitch rate case with nominal (*top*) and tailored trajectory (*bottom*) with velocity-limited actuator (Heavy)

Table 6.23(a)–High Pitch/Pitch Rate Differential; Nominal Trajectory; V-limited; Heavy

Quantity	**Units**	**Differential**
Time	s	+0 .61313
Mass	kg	-64.244
Altitude	m	-23.649
Velocity	m/s	0.067794
Flight Path Angle	deg	0.038553

Table 6.23 (b)–High Pitch/Pitch Rate Differential; Tailored Trajectory; V-limited; Heavy

Quantity	**Units**	**Differential**
Time	s	-0 .18742
Mass	kg	+19.638
Altitude	m	10.406
Velocity	m/s	-0.029890
Flight Path Angle	deg	-0.0056216

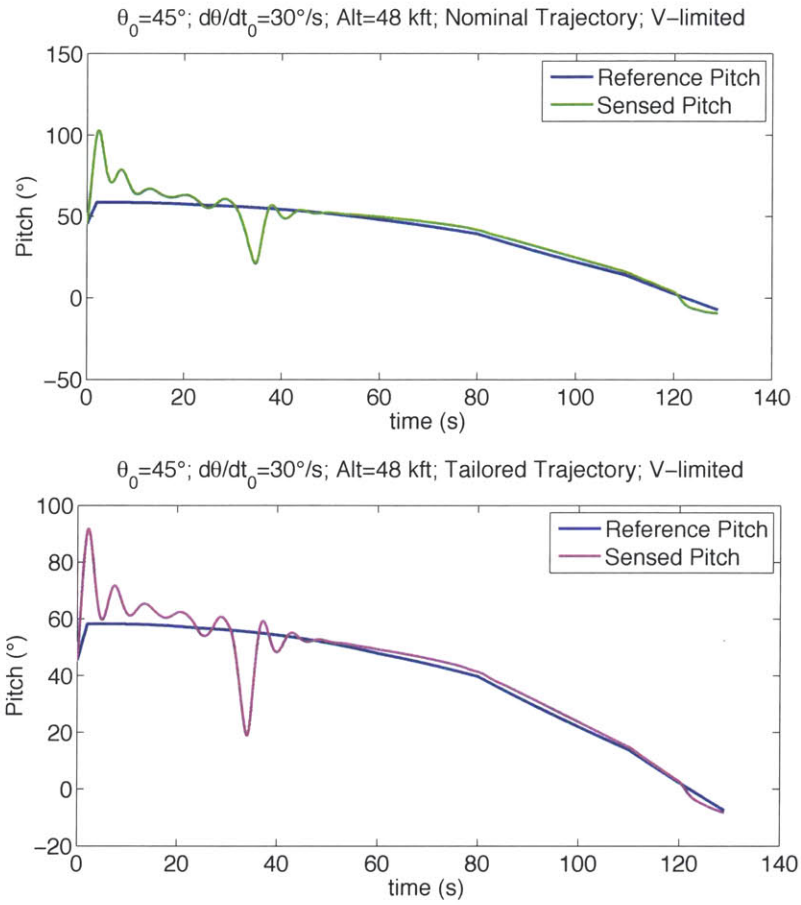

Figure 6.20—Reference and sensed pitch for low altitude case with nominal (*top*) and tailored trajectory (*bottom*) with velocity-limited actuator (Heavy)

Table 6.24 (a)—Low Altitude Differentials; Nominal Trajectory; V-limited; Heavy

Quantity	**Units**	**Differential**
Time	s	+0 .35816
Mass	kg	-37.530
Altitude	m	6.1706
Velocity	m/s	-0.017704
Flight Path Angle	deg	-0.012147

Table 6.24 (b)—Low Altitude Differentials; Tailored Trajectory; V-limited; Heavy

Quantity	**Units**	**Differential**
Time	s	+0.12076
Mass	kg	-12.653
Altitude	m	14.514
Velocity	m/s	-0.041626
Flight Path Angle	deg	-0.0071790

6.4 Conclusions

The goal of this chapter was to evaluate the potential performance losses that an air-launched rocket will experience due to expected dispersions in ignition conditions. Furthermore, the chapter examined a strategy for mitigating performance losses by selection of better-suited reference trajectories. A 6DOF Simulink model of the rocket system during the first stage burn was used to quantify performance given various ignition conditions, reference trajectories, and limits on the TVC actuator.

Simulations of both Air Launch Light and Air Launch Heavy equipped with a highly responsive TVC actuator revealed that performance losses due to off-nominal ignition conditions are small (on the order of 5 kg). This result can be expected because a highly responsive TVC system can readily compensate for disturbances. With such small performance differences, there is little room for improvement and therefore no need to use a tailored reference trajectory.

Next, performance losses due to dispersed ignition conditions were quantified for a rocket with a constrained TVC actuator. An actuator with a $5.7°/s^2$ angular acceleration limit and an actuator with a 3°/s velocity limit were examined for both rocket configurations. The performance losses for Air Launch Light under each dispersed case with both the nominal and tailored reference trajectories are shown in Tables 6.14 (acceleration-limited) and 6.15 (velocity-limited). Similarly, the performance losses for Air Launch Heavy are shown in Tables 6.16 and 6.17. In general, the tailored trajectories result in less performance loss than the nominal trajectory. The difference in performance loss between the nominal and tailored trajectory can be represented as a saving in Delta V

by Equation (6.2). Overall, the results demonstrate that for both the angular acceleration limited and velocity limited actuators, the rocket experiences significant performance loss. Furthermore, the performance loss is appreciably reduced using an optimized trajectory for each ignition condition.

It should be noted that the magnitude of vehicle performance losses are highly dependent on the vehicle configuration, aerodynamics, controller design, choice of gains, and the trajectory optimization method. The goal here was to choose a representative case to illustrate that air-launched rockets are vulnerable to losses due to dispersed ignition conditions and to demonstrate a potential strategy for loss mitigation. The analysis contained in this thesis reveals that a generic air-launched rocket is expected to experience significant dispersions in its ignition state. These dispersions will generate significant system performance losses for rockets with slower TVC actuators. Finally, the findings in this chapter demonstrate that when equipped with a constrained TVC system, selection of tailored trajectories produces notable performance gain, especially for cases with dispersed body attitude and rates at ignition.

Table 6.25 – Air Launch Light Performance Loss (Acceleration-limited)

Ignition State	**Performance Loss Nominal Trajectory (kg)**	**Performance Loss Tailored Trajectory (kg)**	**Difference (kg)**	**Delta V Improvement (m/s)**
Low Pitch / Pitch Rate	70.056	13.842	56.215	69.893
High Pitch / Pitch Rate	115.21	93.190	22.018	28.090
Low Altitude	20.895	15.008	5.8866	7.2475

Table 6.26 – Air Launch Light Performance Loss (Velocity-limited)

Ignition State	Performance Loss Nominal Trajectory (kg)	Performance Loss Tailored Trajectory (kg)	Difference (kg)	Delta V Improvement (m/s)
Low Pitch / Pitch Rate	9.0713	0.13893	8.9324	10.938
High Pitch / Pitch Rate	48.331	21.839	26.491	32.844
Low Altitude	20.848	7.8205	13.028	16.016

Table 6.27 – Air Launch Heavy Performance Loss (Acceleration-limited)

Ignition State	Nominal Trajectory Performance Loss (kg)	Tailored Trajectory Performance Loss (kg)	Difference (kg)	Delta V Improvement (m/s)
Low Pitch / Pitch Rate	29.728	-1.4275	31.155	18.322
High Pitch / Pitch Rate	119.64	74.228	45.408	27.137
Low Altitude	34.880	-8.4604	43.340	25.483

Table 6.28 – Air Launch Heavy Performance Loss (Velocity-limited)

Ignition State	Performance Loss Nominal Trajectory (kg)	Performance Loss Tailored Trajectory (kg)	Difference (kg)	Delta V Improvement (m/s)
Low Pitch / Pitch Rate	51.371	-14.624	65.995	38.842
High Pitch / Pitch Rate	64.244	-19.638	83.881	49.407
Low Altitude	37.530	12.653	24.877	14.660

6.5 Thesis Summary

The early 2000s has seen growing interest in air-launched systems for launching satellites into Low Earth Orbit. Although the Pegasus launch system is the only orbital air-launched rocket to date, new systems are expected to come online within the next decade. Air-launch provides many advantages over traditional ground launch, such as the ability to use higher expansion area ratio nozzles and eliminating the need for fixed ground infrastructure. However, air launch also presents unique challenges. This thesis investigated how uncertainties in an air-launched rocket's state at ignition affect the vehicle's performance. The goal of this study was to answer the three questions presented in Section 1.3. How each question was addressed in this thesis and the resulting conclusions are presented below.

1. **For a representative air-launched rocket configuration, what are the ranges of expected dispersions in vehicle velocity, attitude, and body rates at ignition?**

The first step in answering this question was to develop a generic vehicle configuration that may be used in an air-launched system. Chapter 2 presented two such vehicle configurations for a two-stage liquid propellant rocket. A two-stage rocket was selected for simplicity because only the first stage performance is of interest to this study. The two-stage configuration requires that the second stage be liquid propellant (or hybrid), because the second stage must be able to relight in order to perform a final circularization burn. Liquid propellant is also selected for the first stage for simplicity and

because liquid rockets can get higher specific impulse than solids. The body shape, mass properties, and propulsion system characteristics were estimated based on historical data from existing launch systems. Aerodynamic models for both vehicle geometries were obtained using USAF Missile DATCOM software and were presented in Chapter 3.

The next step was to determine the magnitude of dispersions in vehicle state expected at ignition. To accomplish this task, a 6-DOF simulation of the vehicle's behavior during the 4-second uncontrolled drop phase prior to ignition was developed in MATLAB. Chapter 4 derived the complete 6-DOF equations of motion that describe the rocket's behavior. The simulation can be run with various vehicle initial (release) state parameters and local lateral wind speeds. To begin, the simulation was run with a single dispersed release parameter or off-nominal wind speed. The results indicated that a dispersed pitch rate or yaw rate produced the largest dispersions in vehicle state parameters at ignition. The simulation was then run with each initial state parameter randomly selected from a Gaussian distribution. The results from 1000 Monte Carlo runs were used to create a statistical representation of the vehicle's ignition state. The mean value and standard deviation for each state parameter were presented in Chapter 4. The results indicated that both the heavy and light vehicles can expect dispersions in initial pitch and yaw with a standard deviation of ~10°. Furthermore, the expected dispersions in pitch rates have a standard deviation from ~6°/s, whereas the standard deviation for dispersions in yaw rate are about ~15°/s. The standard deviation for dispersions in yaw rate is larger than that for pitch rate due to the presence of significant side winds.

2. How much performance loss, in terms of payload mass to orbit, is incurred due to off-nominal ignition conditions when the rocket guidance follows a reference trajectory optimized for nominal ignition conditions?

In order to quantify vehicle performance, a 6-DOF simulation of the rocket's behavior during the first stage burn was constructed in Simulink. It is assumed that any performance loss incurred from dispersions early in the rocket's flight can be measured at the end of the first stage burn. During the powered portion of flight, the rocket's motion is monitored and controlled by an onboard GN&C system, which steers the rocket onto the desired ascent trajectory. The vehicle is maneuvered in pitch and yaw by thrust vector control (TVC), whereby the thrust direction is altered by gimbaling the rocket engine. Chapter 5 described how the GN&C system was modeled in Simulink. The model consists of four parts: the plant (vehicle), the controller, the TVC actuator, and vehicle state measurements. The plant is modeled by the full 6-DOF equations of motion derived in Chapter 4. The TVC actuator modeled in this study is electromechanical. Chapter 5 presented how the actuator was modeled in Simulink using transfer function, integrator, deadzone, and saturation blocks. The TVC law is a PID controller.

The vehicle's guidance law uses the onboard sensory measurements and a pre-programmed reference trajectory to command the TVC actuator. Reference trajectories were generated using the POST trajectory optimization tool. A single "nominal" reference trajectory, which was optimized for the nominal ignition condition, was generated. The simulation was run with a variety of ignition conditions using the same "nominal" trajectory. The vehicle's performance is quantified by measuring the final

system mass when the vehicle achieves the end condition. The end condition occurs when the vehicle attains a certain velocity, flight path angle, and altitude simultaneously. In each simulation, the rocket achieves this end condition at a different time, and therefore with a different total mass. The difference in mass at the end condition between a simulation with a nominal and dispersed ignition condition quantifies the performance loss due to the dispersion.

Three dispersed ignition condition cases were examined. One case had a low initial pitch orientation and pitch rate at ignition. The second case had a high initial pitch orientation and pitch rate at ignition. The last case was launched at an altitude 2,000 ft. below the nominal drop altitude. Performances losses due to dispersions were quantified for the rocket with various constraints on the TVC actuator. Simulations with a TVC actuator whose angular velocity and acceleration are essentially unconstrained indicated that dispersions in ignition conditions result in negligible performance loss. Next, performance losses were quantified for a rocket equipped with a TVC actuator whose motion is very constrained in angular acceleration. Each of the three dispersed ignition cases indicates that the rocket incurs a significant performance loss relative to the nominal case due to dispersions. Similarly, notable performance losses were incurred in each dispersed case for a TVC actuator whose motion was constrained in angular velocity.

3. Finally, can a method be developed to mitigate this performance loss by allowing the guidance system to select a trajectory better suited for the actual ignition condition?

Chapter 6 proved that significant performance loss may result from dispersed ignition conditions when the rocket guidance follows a reference trajectory optimized for the nominal ignition condition. These performance losses were observed when reasonable constraints were placed on the TVC actuator's motion. Next, the chapter investigated a reference trajectory strategy to mitigate these performance losses. Reference trajectories optimized for each of the three dispersed cases were generated in POST. The simulation was run for each of the dispersed cases using the reference trajectory "tailored" to its ignition condition. For each dispersed case with a constrained TVC actuator, the tailored reference trajectory resulted in less performance loss than the nominal trajectory. This result was observed for both the angular acceleration constrained and velocity constrained TVC actuators. Furthermore, for some of the Heavy rocket's dispersed cases, using the tailored trajectory resulted in a performance gain relative to the rocket's performance under the nominal ignition condition.

While the results of this study are highly dependent on the rocket's configuration and the characteristics of its GN&C system, three important conclusions can be drawn. First, a generic air-launched rocket will likely experience large dispersions in ignition conditions. Second, these dispersions can result in significant performance loss when the system is equipped with a realistic control system that cannot immediately correct for off-nominal conditions. Finally, a reference trajectory strategy that selects the best-suited trajectory for the actual ignition condition can successfully mitigate performance losses from dispersions. In the next decade, new air-launched Earth to orbit systems are

expected to come online. With the potential to produce significant vehicle weight savings, this reference trajectory strategy would certainly be of interest to developers of new air launch systems.

Appendix A. Missile DATCOM Input/Output

```
1       ***** THE USAF AUTOMATED MISSILE DATCOM * REV 03/11 *****

            AERODYNAMIC METHODS FOR MISSILE CONFIGURATIONS


   CONERR - INPUT ERROR CHECKING


   ERROR CODES - N* DENOTES THE NUMBER OF OCCURENCES OF EACH ERROR

   A - UNKNOWN VARIABLE NAME

   B - MISSING EQUAL SIGN FOLLOWING VARIABLE NAME

   C - NON-ARRAY VARIABLE HAS AN ARRAY ELEMENT DESIGNATION - (N)

   D - NON-ARRAY VARIABLE HAS MULTIPLE VALUES ASSIGNED

   E - ASSIGNED VALUES EXCEED ARRAY DIMENSION

   F - SYNTAX ERROR


   ************************* INPUT DATA CARDS *************************


  1 CASEID fineness1.31

  2  $FLTCON NALPHA=37.,NMACH=20.,MACH(1)=0.5,0.6,0.7,0.8,0.9,1.0,1.1,1.2,1.4,1.6,

  3   MACH(11) = 1.8,2.0,2.4,3.,4.,5.,6.,8.,10.,12.,

  4         ALT(1)=50000.,49463.,48978.,48286.,47836.,48129.,48639.,49413.,51532.,

  5   ALT(10)=54152.,57077.,60465.,68125.,80720.,102600.,126500.,151500.,

  6   ALT(18)=172400.,188500.,203700.,

  7         ALPHA(1)=0.,5.,10.,15.,20.,25.,30.,35.,40.,45.,50.,55.,60.,65.,70.,75.,

  8   ALPHA(17)=80.,85.,90.,95.,100.,105.,110.,115.,120.,125.,130.,135.,

  9   ALPHA(29)=140.,145.,150.,155.,160.,165.,170.,175.,180.,

 10         BETA=10.,
```

```
  11 ** BLANK CARD - IGNORED
$END       ** MISSING NAMELIST TERMINATION ADDED **
12  $AXIBOD NX=27.,X(1)=   0.,   0.0404,   0.1617,   0.3638,   0.6470,
13     1.0108,   1.4557,   1.9813,   2.5879,
14     3.2753, 3.2808,   13.1234,   13.1235,   18.0446,
15     33.4646,   36.7454,   36.7455,   37.4016,   37.9485,
16     38.4951, 39.0420,   39.5889,   40.1355,   40.6824,
17     41.2293,   41.7759,   42.3228,
  18 ** BLANK CARD - IGNORED
  19 ** BLANK CARD - IGNORED
20   R(1)=    0.,   0.1640,   0.3281,   0.4921,   0.6562,   0.8202,
21    0.9843,   1.1483,   1.3123,   1.4764, 1.4764,   1.4764,
22    1.4764,   2.4606,   2.4606,   1.9685,   0.4921,
23    0.4918,   1.0289,   1.4475, 1.7618,   1.9872,   2.1381,
24    2.2297,   2.2769,   2.2940,   2.2966,
  25 ** BLANK CARD - IGNORED
  26 ** BLANK CARD - IGNORED
  27 ** BLANK CARD - IGNORED
28  DEXIT=0.,$
29  $REFQ XCG=0.,LREF=5.,SREF=19.93055556,$
  30 ** BLANK CARD - IGNORED
31 DIM FT
32 HYPER
33 SPIN
34 PLOT
35 SAVE
36 NEXT CASE
```

```
   37 ** BLANK CARD - IGNORED

   38 ** BLANK CARD - IGNORED

   39 ** BLANK CARD - IGNORED
1        ***** THE USAF AUTOMATED MISSILE DATCOM * REV 03/11 *****    CASE   1

            AERODYNAMIC METHODS FOR MISSILE CONFIGURATIONS          PAGE   1

  CASE INPUTS

  FOLLOWING ARE THE CARDS INPUT FOR THIS CASE


CASEID fineness1.31

 $FLTCON NALPHA=37.,NMACH=20.,MACH(1)=0.5,0.6,0.7,0.8,0.9,1.0,1.1,1.2,1.4,1.6,

 MACH(11) = 1.8,2.0,2.4,3.,4.,5.,6.,8.,10.,12.,

      ALT(1)=50000.,49463.,48978.,48286.,47836.,48129.,48639.,49413.,51532.,

 ALT(10)=54152.,57077.,60465.,68125.,80720.,102600.,126500.,151500.,

 ALT(18)=172400.,188500.,203700.,

      ALPHA(1)=0.,5.,10.,15.,20.,25.,30.,35.,40.,45.,50.,55.,60.,65.,70.,75.,

 ALPHA(17)=80.,85.,90.,95.,100.,105.,110.,115.,120.,125.,130.,135.,

 ALPHA(29)=140.,145.,150.,155.,160.,165.,170.,175.,180.,

      BETA=10.,

 $END

 $AXIBOD NX=27.,X(1)=   0.,   0.0404,   0.1617,   0.3638,   0.6470,

    1.0108,   1.4557,   1.9813,   2.5879,

    3.2753, 3.2808,   13.1234,   13.1235,   18.0446,

   33.4646,   36.7454,   36.7455,   37.4016,   37.9485,

   38.4951, 39.0420,   39.5889,   40.1355,   40.6824,

   41.2293,   41.7759,   42.3228,

 R(1)=   0.,   0.1640,   0.3281,   0.4921,   0.6562,   0.8202,

  0.9843,   1.1483,   1.3123,   1.4764, 1.4764,   1.4764,
```

```
  1.4764,   2.4606,   2.4606,   1.9685,   0.4921,
  0.4918,   1.0289,   1.4475, 1.7618,   1.9872,   2.1381,
  2.2297,   2.2769,   2.2940,   2.2966,
 DEXIT=0.,$
 $REFQ XCG=0.,LREF=5.,SREF=19.93055556,$
DIM FT
HYPER
SPIN
PLOT
SAVE
NEXT CASE
   THE BOUNDARY LAYER IS ASSUMED TO BE TURBULENT
   THE INPUT UNITS ARE IN FEET, THE SCALE FACTOR IS   1.0000
   * WARNING * NON-ZERO BETA INPUT - NOLAT SET
1       ***** THE USAF AUTOMATED MISSILE DATCOM * REV 03/11 *****   CASE   1
           AERODYNAMIC METHODS FOR MISSILE CONFIGURATIONS         PAGE   2
                       fineness1.31
                 STATIC AERODYNAMICS FOR BODY ALONE


     ******* FLIGHT CONDITIONS AND REFERENCE QUANTITIES *******
    MACH NO  =      0.50             REYNOLDS NO = 5.905E+05 /FT
    ALTITUDE =    50000.0 FT       DYNAMIC PRESSURE =     42.63 LB/FT**2
    SIDESLIP =     10.00 DEG              ROLL =      0.00 DEG
    REF AREA =    19.931 FT**2       MOMENT CENTER =     0.000 FT
    REF LENGTH =     5.00 FT         LAT REF LENGTH =      5.00 FT


              ----- LONGITUDINAL -----     -- LATERAL DIRECTIONAL --
```

ALPHA	CN	CM	CA	CY	CLN	CLL
0.00	0.000	0.000	0.196	-0.419	1.175	0.000
5.00	0.216	-0.620	0.193	-0.434	1.249	0.000
10.00	0.470	-1.430	0.183	-0.470	1.430	0.000
15.00	0.779	-2.515	0.166	-0.513	1.655	0.000
20.00	1.144	-3.892	0.143	-0.554	1.886	0.000
25.00	1.580	-5.651	0.115	-0.598	2.137	0.000
30.00	2.088	-7.791	0.084	-0.638	2.379	0.000
35.00	2.650	-10.249	0.056	-0.667	2.581	0.000
40.00	3.256	-12.970	0.035	-0.684	2.726	0.000
45.00	3.887	-15.878	0.022	-0.685	2.800	0.000
50.00	4.525	-18.878	0.020	-0.669	2.793	0.000
55.00	5.183	-22.030	0.026	-0.640	2.720	0.000
60.00	5.841	-25.240	0.037	-0.595	2.570	0.000
65.00	6.441	-28.222	0.048	-0.530	2.321	0.000
70.00	6.953	-30.841	0.056	-0.446	1.979	0.000
75.00	7.356	-32.972	0.055	-0.348	1.558	0.000
80.00	7.627	-34.515	0.048	-0.237	1.073	0.000
85.00	7.755	-35.391	0.018	-0.120	0.546	0.000
90.00	7.730	-35.557	0.000	0.000	0.000	0.000
95.00	7.755	-34.984	-0.006	0.120	-0.540	0.000
100.00	7.627	-33.682	-0.024	0.237	-1.047	0.000
105.00	7.356	-31.713	-0.053	0.348	-1.498	0.000
110.00	6.953	-29.170	-0.093	0.446	-1.872	0.000
115.00	6.441	-26.173	-0.142	0.530	-2.152	0.000
120.00	5.841	-22.862	-0.199	0.595	-2.327	0.000

125.00	5.183	-19.387	-0.262	0.640	-2.394	0.000
130.00	4.525	-16.049	-0.329	0.669	-2.375	0.000
135.00	3.887	-12.950	-0.398	0.685	-2.283	0.000
140.00	3.256	-10.039	-0.467	0.684	-2.110	0.000
145.00	2.650	-7.412	-0.534	0.667	-1.866	0.000
150.00	2.088	-5.144	-0.597	0.638	-1.571	0.000
155.00	1.580	-3.286	-0.654	0.598	-1.243	0.000
160.00	1.144	-1.893	-0.703	0.554	-0.917	0.000
165.00	0.779	-0.952	-0.743	0.513	-0.626	0.000
170.00	0.470	-0.359	-0.772	0.470	-0.359	0.000
175.00	0.216	-0.077	-0.790	0.434	-0.155	0.000
180.00	0.000	0.000	-0.796	-0.419	0.075	0.000

ALPHA	CL	CD	CL/CD	X-C.P.
0.00	0.000	0.196	0.000	-2.804
5.00	0.198	0.211	0.938	-2.876
10.00	0.431	0.262	1.646	-3.041
15.00	0.710	0.362	1.959	-3.227
20.00	1.026	0.526	1.951	-3.403
25.00	1.384	0.772	1.792	-3.576
30.00	1.766	1.117	1.581	-3.732
35.00	2.139	1.566	1.365	-3.867
40.00	2.472	2.119	1.166	-3.984
45.00	2.733	2.764	0.989	-4.084
50.00	2.893	3.479	0.832	-4.172
55.00	2.951	4.260	0.693	-4.251

60.00	2.889	5.077	0.569	-4.321
65.00	2.678	5.858	0.457	-4.382
70.00	2.326	6.553	0.355	-4.435
75.00	1.851	7.119	0.260	-4.483
80.00	1.277	7.520	0.170	-4.525
85.00	0.658	7.727	0.085	-4.564
90.00	0.000	7.730	0.000	-4.600
95.00	-0.670	7.726	-0.087	-4.511
100.00	-1.301	7.516	-0.173	-4.416
105.00	-1.852	7.119	-0.260	-4.311
110.00	-2.291	6.566	-0.349	-4.195
115.00	-2.593	5.897	-0.440	-4.064
120.00	-2.748	5.158	-0.533	-3.914
125.00	-2.758	4.396	-0.627	-3.741
130.00	-2.657	3.678	-0.722	-3.547
135.00	-2.467	3.030	-0.814	-3.331
140.00	-2.194	2.451	-0.895	-3.083
145.00	-1.865	1.958	-0.952	-2.796
150.00	-1.509	1.561	-0.967	-2.464
155.00	-1.156	1.261	-0.917	-2.079
160.00	-0.834	1.052	-0.793	-1.655
165.00	-0.561	0.919	-0.610	-1.221
170.00	-0.329	0.842	-0.391	-0.763
175.00	-0.146	0.806	-0.181	-0.358
180.00	0.000	0.796	0.000	-0.179

X-C.P. MEAS. FROM MOMENT CENTER IN REF. LENGTHS, NEG. AFT OF MOMENT CENTER

1 ***** THE USAF AUTOMATED MISSILE DATCOM * REV 03/11 ***** CASE 1

AERODYNAMIC METHODS FOR MISSILE CONFIGURATIONS PAGE 3

fineness1.31

STATIC AERODYNAMICS FOR BODY ALONE

******* FLIGHT CONDITIONS AND REFERENCE QUANTITIES *******

MACH NO = 0.50 REYNOLDS NO = 5.905E+05 /FT

ALTITUDE = 50000.0 FT DYNAMIC PRESSURE = 42.63 LB/FT**2

SIDESLIP = 10.00 DEG ROLL = 0.00 DEG

REF AREA = 19.931 FT**2 MOMENT CENTER = 0.000 FT

REF LENGTH = 5.00 FT LAT REF LENGTH = 5.00 FT

---------- DERIVATIVES (PER DEGREE) ----------

ALPHA	CNA	CMA	CYB	CLNB	CLLB
0.00	0.0392	-0.1050			
5.00	0.0470	-0.1430			
10.00	0.0564	-0.1894			
15.00	0.0673	-0.2460			
20.00	0.0801	-0.3132			
25.00	0.0944	-0.3894			
30.00	0.1070	-0.4594			
35.00	0.1168	-0.5177			
40.00	0.1237	-0.5627			
45.00	0.1269	-0.5907			
50.00	0.1295	-0.6151			
55.00	0.1316	-0.6362			
60.00	0.1258	-0.6190			

65.00	0.1112	-0.5594
70.00	0.0915	-0.4741
75.00	0.0674	-0.3663
80.00	0.0399	-0.2409
85.00	0.0103	-0.1037
90.00	0.0000	0.0405
95.00	-0.0103	0.1865
100.00	-0.0399	0.3258
105.00	-0.0674	0.4500
110.00	-0.0915	0.5531
115.00	-0.1112	0.6303
120.00	-0.1258	0.6784
125.00	-0.1316	0.6812
130.00	-0.1295	0.6435
135.00	-0.1269	0.6008
140.00	-0.1237	0.5535
145.00	-0.1168	0.4890
150.00	-0.1070	0.4120
155.00	-0.0944	0.3245
160.00	-0.0801	0.2330
165.00	-0.0673	0.1532
170.00	-0.0564	0.0874
175.00	-0.0470	0.0359
180.00	-0.0392	-0.0051

Appendix B. POST Input File

```
l$search
c*************************************************************************
c  problem
c    maximize weight
c    subject to
c             gdalt - 303805 = 0
c             veli  - 25853 = 0
c             gammai -  0  = 0
c*************************************************************************
c listin = 1,
 maxitr  =    50,
 srchm   =     4,
 opt     =     1,
 optvar  = 'weight',
 optph   =   80,
 wopt    =  1.0e-3,
 coneps  =  89.98,
c
 nindv   =     14,
 indvr   =  6hpitpc2, 6hpitpc3, 6hpitpc2, 6hpitpc3,
 indph   =      10,     10,     20,     20,
 u       =    SUB_GUESS_ph1_pdot, SUB_GUESS_ph1_pddot, SUB_GUESS_ph2_pdot,
SUB_GUESS_ph2_pddot,
 indvr(5) =  6hpitpc2, 6hpitpc3,
 indph(5) =    30,     30,
 u(5)    =    SUB_GUESS_ph3_pdot, SUB_GUESS_ph3_pddot,
 indvr(7) = 6hpitpc2, 6hpitpc3, 6hpitpc2, 6hpitpc3,
 indph(7) =     40,    40,   50,  50,
 u(7)    =  SUB_GUESS_ph4_pdot, SUB_GUESS_ph4_pddot, SUB_GUESS_ph5_pdot,
SUB_GUESS_ph5_pddot,
 indvr(11) =  6hpitpc2, 6hpitpc3,
 indph(11) =  60, 60,
 u(11)    = SUB_GUESS_ph6_pdot, SUB_GUESS_ph6_pddot,
 indvr(13) =  6hpitpc2, 6hpitpc3,
 indph(13) =  70, 70,
 u(13)    = SUB_GUESS_ph7_pdot, SUB_GUESS_ph7_pddot,
c
c Final Position and Vel
 ndepv   =     4,
 depvr   =  'gdalt', 'veli', 'gammai',
 depval  =  SUB_TARG_gdalt, SUB_TARG_veli, SUB_TARG_gammi,
 deptl   =  1000, 0.1, 0.001,
 depph   =  80, 80, 80,
 depvr(4) =  'xmax1',
 depval(4)=  6000,
 depph(4) =  80 ,
```

```
 idepvr(4) = 1,
c
 $
l$gendat
 prnc=0,   / 0=> Binary profile file time interval is DT
 prnca=0,  / 0=> ASCII profile file time interval is DT
 prnt(97)='alphadt','betadt','bankdt','alphidt','betaidt','bankidt','pitrdt',
        'rolrdt','yawrdt','pitidt','rolidt','yawidt',
        'alphi','betai','banki','pitmom','yawmom','dragw','mass',
 npc(12)=2,
 title  = 0h* ALASA Baseline*,
 event   =       10,
c
 npc(2)  =       1, 1, 1,
 npc(8)  =       1,
 npc(9)  =       1,
 npc(15) =       1,
 npc(16) =       1,       / 1=> Spherical earth
 npc(21) =       0,
 iwdf(1) = 2,
c
 iguid(1) =      1,
 iguid(4) =      0,
c
 maxtim  =  4000.0,
 altmax  =500000000.0,
 altmin  =-1e3,
 fesn    =     100,
 dt      =    1.0,
 pinc    =    5.0,
 time    =    0.0,
 timeo   =    SUB_INIT_timeo,
 azl     =    SUB_INIT_azl,
 xi      =   SUB_INIT_x, SUB_INIT_y, SUB_INIT_z,
 vxi     =   SUB_INIT_vx, SUB_INIT_vy, SUB_INIT_vz,
 piti    =    -20.0,
 pitpc(2)   = SUB_GUESS_ph1_pdot, SUB_GUESS_ph1_pddot,
 neng    =       1,
 wgtsg   =  SUB_SYS_wgtsg1,
 wpropi  =  SUB_SYS_wprop1,
 wpld    =  SUB_SYS_wpld,
 ispv    =  SUB_SYS_isp1,
 gxp     =  0.0,
 gyp     =     0.0,
 gzp     =   0.0,
 sref    =  19.93,
 lref    =    5.0,
c
 monx(1) = 'qaltot',
 $
l$tblmlt  $
```

```
l$tab
 table    = 6htvc1t ,1,'time',4,1,1,1,
 0, 0.0, 0.01 , 71930.0, 0.6, 71930.0, 142, 71930.0,
 $
l$tab
  table    = 6hcat   ,2,6halpha ,6hmach  ,37,5,1,1,1,1,1,1,1,1,
 0.5,
 0, 0.2760, 5, 0.2730, 10, 0.2610, 15, 0.2380, 20,
 0.2030, 25, 0.1600, 30, 0.1120, 35, 0.0650, 40, 0.0280,
 45, 0.0060, 50, 0.0010, 55, 0.0110, 60, 0.0290, 65,
 0.0510, 70, 0.0670, 75, 0.0710, 80, 0.0670, 85, 0.0250,
 90, 0, 95, -0.0090, 100, -0.0360, 105, -0.0790, 110,
 -0.1380, 115, -0.2110, 120, -0.2950, 125, -0.3890, 130,
 -0.4880, 135, -0.5910, 140, -0.6940, 145, -0.7930, 150,
 -0.8860, 155, -0.9710, 160, -1.0440, 165, -1.1030, 170,
 -1.1460, 175, -1.1730, 180, -1.1820,
 0.6,
 0, 0.2720, 5, 0.2700, 10, 0.2580, 15, 0.2350, 20,
 0.2010, 25, 0.1550, 30, 0.1040, 35, 0.0550, 40, 0.0150,
 45, -0.0120, 50, -0.0220, 55, -0.0130, 60, 0.0110, 65,
 0.0390, 70, 0.0600, 75, 0.0670, 80, 0.0670, 85, 0.0250,
 90, 0, 95, -0.0090, 100, -0.0360, 105, -0.0790, 110,
 -0.1380, 115, -0.2110, 120, -0.2950, 125, -0.3890, 130,
 -0.4880, 135, -0.5910, 140, -0.6940, 145, -0.7930, 150,
 -0.8860, 155, -0.9710, 160, -1.0440, 165, -1.1030, 170,
 -1.1460, 175, -1.1730, 180, -1.1820,
 0.7,
 0, 0.2710, 5, 0.2680, 10, 0.2570, 15, 0.2340, 20,
 0.1980, 25, 0.1510, 30, 0.0980, 35, 0.0450, 40, -0.0030,
 45, -0.0350, 50, -0.0410, 55, -0.0280, 60, 0, 65,
 0.0330, 70, 0.0570, 75, 0.0660, 80, 0.0690, 85, 0.0250,
 90, 0, 95, -0.0100, 100, -0.0380, 105, -0.0840, 110,
 -0.1460, 115, -0.2230, 120, -0.3130, 125, -0.4110, 130,
 -0.5170, 135, -0.6250, 140, -0.7340, 145, -0.8390, 150,
 -0.9380, 155, -1.0270, 160, -1.1040, 165, -1.1670, 170,
 -1.2130, 175, -1.2410, 180, -1.2510,
 0.8,
 0, 0.4820, 5, 0.4800, 10, 0.4720, 15, 0.4580, 20,
 0.4380, 25, 0.4140, 30, 0.3850, 35, 0.3530, 40, 0.3180,
 45, 0.2810, 50, 0.2430, 55, 0.2040, 60, 0.1670, 65,
 0.1310, 70, 0.0980, 75, 0.0670, 80, 0.0410, 85, 0.0180,
 90, 0, 95, -0.0020, 100, -0.0100, 105, -0.0210, 110,
 -0.0370, 115, -0.0570, 120, -0.0790, 125, -0.1040, 130,
 -0.1310, 135, -0.1590, 140, -0.1860, 145, -0.2130, 150,
 -0.2380, 155, -0.2610, 160, -0.2800, 165, -0.2960, 170,
 -0.3080, 175, -0.3150, 180, -0.3170,
 0.9,
 0, 1.2600, 5, 1.2520, 10, 1.2260, 15, 1.1840, 20,
 1.1250, 25, 1.0530, 30, 0.9690, 35, 0.8750, 40, 0.7750,
 45, 0.6700, 50, 0.5650, 55, 0.4610, 60, 0.3620, 65,
 0.2710, 70, 0.1890, 75, 0.1200, 80, 0.0640, 85, 0.0240,
```

```
90, 0, 95, -0.0080, 100, -0.0330, 105, -0.0730, 110,
-0.1280, 115, -0.1950, 120, -0.2730, 125, -0.3590, 130,
-0.4510, 135, -0.5460, 140, -0.6410, 145, -0.7330, 150,
-0.8200, 155, -0.8980, 160, -0.9650, 165, -1.0190, 170,
-1.0600, 175, -1.0840, 180, -1.0930,
$
l$tab
 table    = 6hcnat   ,2,6halpha ,6hmach  ,37,5,1,1,1,1,1,1,1,1,
0.5,
0, 0, 5, 0.2400, 10, 0.5820, 15, 1.0250, 20,
1.5640, 25, 2.2040, 30, 2.9780, 35, 3.8480,
40, 4.7950, 45, 5.7910, 50, 6.8050, 55, 7.8430,
60, 8.9040, 65, 9.8770, 70, 10.7170, 75, 11.3840,
80, 11.8440, 85, 12.0760, 90, 12.0640, 95, 12.0760,
100, 11.8440, 105, 11.3840, 110, 10.7170, 115,
9.8770, 120, 8.9040, 125, 7.8430, 130, 6.8050, 135,
5.7910, 140, 4.7950, 145, 3.8480, 150, 2.9780, 155,
2.2040, 160, 1.5640, 165, 1.0250, 170, 0.5820, 175,
0.2400, 180, 0,
0.6,
0, 0, 5, 0.2400, 10, 0.5850, 15, 1.0350, 20,
1.5900, 25, 2.2990, 30, 3.1340, 35, 4.0840, 40,
5.1270, 45, 6.3130, 50, 7.5970, 55, 8.8910, 60,
10.0450, 65, 11.0580, 70, 11.9240, 75, 12.6090,
80, 13.0800, 85, 13.3160, 90, 13.3060, 95, 13.3160,
100, 13.0800, 105, 12.6090, 110, 11.9240, 115,
11.0580, 120, 10.0450, 125, 8.8910, 130, 7.5970,
135, 6.3130, 140, 5.1270, 145, 4.0840, 150, 3.1340,
155, 2.2990, 160, 1.5900, 165, 1.0350, 170, 0.5850,
175, 0.2400, 180, 0,
0.7,
0, 0, 5, 0.2410, 10, 0.5880, 15, 1.0440, 20,
1.6400, 25, 2.3930, 30, 3.2910, 35, 4.3240, 40, 5.5950,
45, 6.9870, 50, 8.3130, 55, 9.6120, 60, 10.7940, 65,
11.6310, 70, 12.3210, 75, 12.8450, 80, 13.1890, 85, 13.3440,
90, 13.3060, 95, 13.3440, 100, 13.1890, 105, 12.8450, 110,
12.3210, 115, 11.6310, 120, 10.7940, 125, 9.6120, 130, 8.3130,
135, 6.9870, 140, 5.5950, 145, 4.3240, 150, 3.2910, 155,
2.3930, 160, 1.6400, 165, 1.0440, 170, 0.5880, 175, 0.2410,
180, 0,
0.8,
0, 0, 5, 0.2410, 10, 0.5910, 15, 1.0570, 20,
1.6900, 25, 2.4880, 30, 3.4480, 35, 4.6840, 40, 6.0630,
45, 7.4430, 50, 8.7780, 55, 9.8340, 60, 10.7940, 65,
11.6310, 70, 12.3210, 75, 12.8450, 80, 13.1890, 85, 13.3440,
90, 13.3060, 95, 13.3440, 100, 13.1890, 105, 12.8450, 110,
12.3210, 115, 11.6310, 120, 10.7940, 125, 9.8340, 130, 8.7780,
135, 7.4430, 140, 6.0630, 145, 4.6840, 150, 3.4480, 155,
2.4880, 160, 1.6900, 165, 1.0570, 170, 0.5910, 175, 0.2410,
180, 0,
0.9,
```

```
 0, 0, 5, 0.2420, 10, 0.5950, 15, 1.0810, 20,
 1.7450, 25, 2.5900, 30, 3.6980, 35, 5.0260, 40, 6.4160,
 45, 7.6860, 50, 8.8120, 55, 9.8730, 60, 10.8380, 65, 11.5760,
 70, 12.0490, 75, 12.3810, 80, 12.5750, 85, 12.6340,
 90, 12.5630, 95, 12.6340, 100, 12.5750, 105, 12.3810, 110,
 12.0490, 115, 11.5760, 120, 10.8380, 125, 9.8730, 130, 8.8120,
 135, 7.6860, 140, 6.4160, 145, 5.0260, 150, 3.6980, 155,
 2.5900, 160, 1.7450, 165, 1.0810, 170, 0.5950, 175, 0.2420,
 180, 0,
 endphs  =      1,
 $
l$gendat
 event   =      20, critr   = 6htime  ,  value   = SUB_GUESS_ph1_duration,
 iguid(4) =     0,
 pitpc(2)   = SUB_GUESS_ph2_pdot, SUB_GUESS_ph2_pddot,
 endphs  =      1,
 $
l$gendat
 event   =      30, critr   = 6htime  ,  value   = 20.0,
 pitpc(3)  =    0,
 pitpc(2)   = SUB_GUESS_ph3_pdot, SUB_GUESS_ph3_pddot,
 endphs  =      1,
 $
l$gendat
 event   =      40, critr   = 6htime  ,  value   = 24.0,
 pitpc(2)   = SUB_GUESS_ph4_pdot, SUB_GUESS_ph4_pddot,
 $
l$tblmlt  $
l$tab
  table   = 6hcat   ,2,6halpha ,6hmach  ,14,16,1,1,1,1,1,1,1,1,
  0.9,
  0, 1.2600, 5, 1.2520, 10, 1.2260, 15, 1.1840,
  20, 1.1250, 25, 1.0530, 30, 0.9690, 35, 0.8750,
  40, 0.7750, 45, 0.6700, 50, 0.5650, 55, 0.4610,
  60, 0.3620, 65, 0.2710,
  1,
  0, 2.2800, 5, 2.2650, 10, 2.2160, 15,
  2.1370, 20, 2.0290, 25, 1.8950, 30, 1.7400,
  35, 1.5670, 40, 1.3820, 45, 1.1910, 50,
  0.9980, 55, 0.8090, 60, 0.6300, 65, 0.4650,
  1.1,
  0, 3.0510, 5, 3.0290, 10, 2.9640, 15,
  2.8560, 20, 2.7100, 25, 2.5300, 30, 2.3200,
  35, 2.0870, 40, 1.8380, 45, 1.5800, 50,
  1.3200, 55, 1.0670, 60, 0.8270, 65, 0.6070,
  1.2,
  0, 3.1690, 5, 3.1470, 10, 3.0780, 15,
  2.9670, 20, 2.8140, 25, 2.6260, 30, 2.4070,
  35, 2.1650, 40, 1.9050, 45, 1.6370, 50,
  1.3670, 55, 1.1040, 60, 0.8540, 65, 0.6260,
  1.4,
```

0, 0.6780, 5, 0.6850, 10, 0.7070, 15,
0.7370, 20, 0.7710, 25, 0.8060, 30, 0.8380,
35, 0.8060, 40, 0.8050, 45, 0.7910, 50,
0.7630, 55, 0.7200, 60, 0.6640, 65, 0.5950,
1.6,
0, 0.6790, 5, 0.6870, 10, 0.7090, 15,
0.7420, 20, 0.7780, 25, 0.8160, 30, 0.8520,
35, 0.8200, 40, 0.8200, 45, 0.8070, 50,
0.7800, 55, 0.7380, 60, 0.6820, 65, 0.6120,
1.8,
0, 0.6740, 5, 0.6820, 10, 0.7060, 15,
0.7400, 20, 0.7790, 25, 0.8180, 30, 0.8570,
35, 0.8250, 40, 0.8270, 45, 0.8160, 50,
0.7890, 55, 0.7480, 60, 0.6920, 65, 0.6220,
2,
0, 0.6650, 5, 0.6740, 10, 0.6990, 15,
0.7340, 20, 0.7750, 25, 0.8160, 30, 0.8570,
35, 0.8260, 40, 0.8290, 45, 0.8190, 50,
0.7940, 55, 0.7530, 60, 0.6970, 65, 0.6270,
2.4,
0, 0.6480, 5, 0.6570, 10, 0.6830, 15,
0.7210, 20, 0.7630, 25, 0.8080, 30, 0.8510,
35, 0.8210, 40, 0.8270, 45, 0.8190, 50,
0.7960, 55, 0.7560, 60, 0.7020, 65, 0.6320,
3,
0, 0.6250, 5, 0.6340, 10, 0.6610, 15,
0.7010, 20, 0.7460, 25, 0.7930, 30, 0.8390,
35, 0.8110, 40, 0.8190, 45, 0.8130, 50,
0.7920, 55, 0.7540, 60, 0.7010, 65, 0.6330,
4,
0, 0.5990, 5, 0.6080, 10, 0.6370, 15,
0.6780, 20, 0.7250, 25, 0.7740, 30, 0.8230,
35, 0.7960, 40, 0.8070, 45, 0.8030, 50,
0.7840, 55, 0.7480, 60, 0.6970, 65, 0.6310,
5,
0, 0.5790, 5, 0.5890, 10, 0.6180, 15,
0.6600, 20, 0.7080, 25, 0.7590, 30, 0.8090,
35, 0.7830, 40, 0.7940, 45, 0.7920, 50,
0.7740, 55, 0.7400, 60, 0.6900, 65, 0.6250,
6,
0, 0.5760, 5, 0.5860, 10, 0.6150, 15,
0.6570, 20, 0.7050, 25, 0.7560, 30, 0.8070,
35, 0.7800, 40, 0.7920, 45, 0.7900, 50,
0.7730, 55, 0.7390, 60, 0.6890, 65, 0.6240,
8,
0, 0.5640, 5, 0.5740, 10, 0.6040, 15,
0.6460, 20, 0.6950, 25, 0.7470, 30, 0.7990,
35, 0.7730, 40, 0.7850, 45, 0.7840, 50,
0.7670, 55, 0.7340, 60, 0.6850, 65, 0.6210,
10,
0, 0.5600, 5, 0.5710, 10, 0.6000, 15,

```
 0.6430, 20, 0.6920, 25, 0.7440, 30, 0.7960,
 35, 0.7700, 40, 0.7830, 45, 0.7820, 50,
 0.7660, 55, 0.7330, 60, 0.6840, 65, 0.6200,
 12,
 0, 0.5620, 5, 0.5730, 10, 0.6020, 15,
 0.6450, 20, 0.6940, 25, 0.7460, 30, 0.7970,
 35, 0.7710, 40, 0.7840, 45, 0.7830, 50,
 0.7660, 55, 0.7330, 60, 0.6840, 65, 0.6200,
$
l$tab
 table   = 6hcnat   ,2,6halpha ,6hmach  ,14,16,1,1,1,1,1,1,1,1,
0.9,
0, 0, 5, 0.2420, 10, 0.5950, 15,
1.0810, 20, 1.7450, 25, 2.5900, 30, 3.6980,
35, 5.0260, 40, 6.4160, 45, 7.6860, 50,
8.8120, 55, 9.8730, 60, 10.8380, 65, 11.5760,
1,
0, 0, 5, 0.2530, 10, 0.6450, 15,
1.2210, 20, 2.0280, 25, 3.1110, 30, 4.5740,
35, 6.1630, 40, 7.6870, 45, 9.0900, 50,
10.4600, 55, 11.6330, 60, 12.4640, 65, 13.1560,
1.1,
0, 0, 5, 0.2630, 10, 0.6870, 15,
1.3450, 20, 2.2810, 25, 3.6240, 30, 5.2900,
35, 7.0220, 40, 8.6020, 45, 10.1960, 50,
11.4820, 55, 12.4970, 60, 13.4860, 65, 14.3120,
1.2,
0, 0, 5, 0.2650, 10, 0.6990, 15,
1.3910, 20, 2.3930, 25, 3.8690, 30, 5.5930,
35, 7.1380, 40, 8.7480, 45, 10.1000, 50,
11.2220, 55, 12.3080, 60, 13.3530, 65, 14.2850,
1.4,
0, 0, 5, 0.3280, 10, 0.7720, 15,
1.3470, 20, 2.0570, 25, 2.8880, 30, 3.8170,
35, 4.8180, 40, 5.8630, 45, 6.9200, 50,
7.9580, 55, 8.9470, 60, 9.8570, 65, 10.6590,
1.6,
0, 0, 5, 0.3440, 10, 0.8090, 15,
1.4110, 20, 2.1560, 25, 3.0270, 30, 4,
35, 5.0490, 40, 6.1440, 45, 7.2520, 50,
8.3400, 55, 9.3770, 60, 10.3300, 65, 11.1710,
1.8,
0, 0, 5, 0.3560, 10, 0.8360, 15,
1.4590, 20, 2.2290, 25, 3.1290, 30, 4.1350,
35, 5.2190, 40, 6.3510, 45, 7.4960, 50,
8.6210, 55, 9.6920, 60, 10.6770, 65, 11.5470,
2,
0, 0, 5, 0.3640, 10, 0.8560, 15,
1.4940, 20, 2.2830, 25, 3.2050, 30, 4.2360,
35, 5.3460, 40, 6.5050, 45, 7.6780, 50,
8.8310, 55, 9.9280, 60, 10.9370, 65, 11.8280,
```

```
 2.4,
 0, 0, 5, 0.3760, 10, 0.8840, 15,
 1.5420, 20, 2.3560, 25, 3.3080, 30, 4.3720,
 35, 5.5180, 40, 6.7140, 45, 7.9250, 50,
 9.1140, 55, 10.2470, 60, 11.2880, 65, 12.2080,
 3,
 0, 0, 5, 0.3860, 10, 0.9070, 15,
 1.5830, 20, 2.4180, 25, 3.3950, 30, 4.4870,
 35, 5.6640, 40, 6.8910, 45, 8.1340, 50,
 9.3550, 55, 10.5170, 60, 11.5870, 65, 12.5300,
 4,
 0, 0, 5, 0.3940, 10, 0.9260, 15,
 1.6150, 20, 2.4680, 25, 3.4650, 30, 4.5790,
 35, 5.7800, 40, 7.0330, 45, 8.3010, 50,
 9.5470, 55, 10.7340, 60, 11.8250, 65, 12.7880,
 5,
 0, 0, 5, 0.3980, 10, 0.9350, 15,
 1.6310, 20, 2.4910, 25, 3.4980, 30, 4.6230,
 35, 5.8350, 40, 7.1000, 45, 8.3800, 50,
 9.6380, 55, 10.8350, 60, 11.9370, 65, 12.9090,
 6,
 0, 0, 5, 0.4000, 10, 0.9390, 15,
 1.6390, 20, 2.5040, 25, 3.5160, 30, 4.6460,
 35, 5.8650, 40, 7.1360, 45, 8.4230, 50,
 9.6870, 55, 10.8910, 60, 11.9980, 65, 12.9750,
 8,
 0, 0, 5, 0.4020, 10, 0.9440, 15,
 1.6480, 20, 2.5170, 25, 3.5330, 30, 4.6700,
 35, 5.8950, 40, 7.1730, 45, 8.4660, 50,
 9.7370, 55, 10.9470, 60, 12.0590, 65, 13.0410,
 10,
 0, 0, 5, 0.4030, 10, 0.9460, 15,
 1.6510, 20, 2.5230, 25, 3.5420, 30, 4.6810,
 35, 5.9090, 40, 7.1900, 45, 8.4860, 50,
 9.7600, 55, 10.9720, 60, 12.0880, 65, 13.0720,
 12,
 0, 0, 5, 0.4030, 10, 0.9480, 15,
 1.6540, 20, 2.5260, 25, 3.5460, 30, 4.6870,
 35, 5.9160, 40, 7.1990, 45, 8.4970, 50,
 9.7720, 55, 10.9870, 60, 12.1030, 65, 13.0890,
 endphs  =       1,
 $
l$gendat
 event   =      50, critr   = 6htime  ,  value   = 60.0,
 pitpc(2)   = SUB_GUESS_ph5_pdot, SUB_GUESS_ph5_pddot,
 endphs  =       1,
 $
l$gendat
 event   =      60, critr   = 6htime  ,  value   = 80.0,
 pitpc(2)   = SUB_GUESS_ph5_pdot, SUB_GUESS_ph5_pddot,
 endphs  =       1,
```

```
 $
l$gendat
 event   =      70, critr   = 6htime  ,  value   = 110.0,
 pitpc(2)   = SUB_GUESS_ph5_pdot, SUB_GUESS_ph5_pddot,
 endphs  =       1,
 $
l$gendat
 event   =      80, critr   = 'veli' ,  value   = SUB_TARG_veli,
 endphs  =       1,

 endprb  =       1,
 endjob  =       1,
 $
```

References

AFRL-RB-WP-TR-2011-3071, *Missile DATCOM User's Manual – 2011 Revision*, Air Force Research Laboratory, Air Vehicles Directorate, Wright-Patterson Air Force Base, OH.

Chin, S. S., Missile Configuration Design, New York: McGraw-Hill, 1961.

Coppinger, R. 2012. "Virgin Galactic Unveils LauncherOne Rocket for Private Satellite Launches," 11 July. *Space.com* Web. Retrieved 9 May 2013.

DePasquale, D. Charania, A. C., Kanayama, H., Matsuda, S., 2010. "Analysis of the Earth-to-Orbit Launch Market for Nano and Microsatellites", *AIAA SPACE 2010 Conference & Exposition*, AIAA 2010-8602.

de Selding, P. B., 2012. "Vega Builders See Opportunity in Rising Russian Rocket Prices." July 20. *Space News*. Retrieved 9 May 2013.

Dnepr Space Launch System User's Guide. 2001. Retrieved from http://snebulos.mit.edu/projects/crm/DNEPR/Dnepr_User_Guide.pdf

Falcon 1 Launch Vehicle Payload User's Guide. 2008. Revision 7. Space Exploration Technologies. Retrieved from http://www.spacex.com/Falcon1UsersGuide.pdf

Francis, R. J., 1999. *A Systems Study of Very Small Launch Vehicles*, Thesis: Massachusetts Institute of Technology.

Hall, R., Holland, S., and Blevins, J. 2011. "Aerodynamic Characterization of a Modern Launch Vehicle", 49th AIAA Aerospace Sciences Meeting, DOI: 10.2514/6.2011-10. AIAA 2011-10.

Isakowitz, S. 2004. International Reference Guide to Space Launch Systems. Fourth Edition, American Institute of Aeronautics and Astronautics.

Johnson, C., Bies, M., & McManus, M., 1994. "Determination of Drop Transient Forcing Functions for the Pegasus Launch Vehicle," AIAA-94-1703.

Justus, C. G., Leslie, F. W., NASA/TM—2008—215581. *The NASA MSFC Earth Global Reference Atmospheric Model—2007 Version*. Marshall Space Flight Center, Huntsville, AL. November 2008.

Kranzusch, K., 2007 Space Shuttle Solid Rocket Booster Control Limitations due to Failure of an Hydraulic Power Unit" Georgia Institute of Technology.

Leone, D., 2012. "Demise of GEMS May Cost Orbital 150 Jobs, Doom Pegasus" 15 July. *Space News* Web. 9 May 2013.

Leone, D. 2012. "Stratolaunch Charts Course for a Tough Market" 16 January. *Space News* Web. Retrieved 9 May 2013.

Linehan, D. 2008. SpaceShipOne: An Illustrated History, Zenith Press. Minneapolis, MN.

Logan, W. V. et al., "Engine Thrust Effects on Air-Launched Rocket Aerodynamic Characteristics at High Angle of Attack", 42nd AIAA/ASME/SAE/ASEE Joint Propulsion Conference & Exhibit, AIAA 2006-4963, 2006.

McNamara, S., Restrepo, C., Medina, E., Whitley, R., Madsen, J., & Proud, R., 2011. "Gain Scheduling for the Orion Launch Abort Vehicle Controller." *AIAA Guidance and Conrol Conference*. AIAA 2011-6259.

Messier, D., 2012. "Russia Likely to End Dnepr Launch Program" 27 May. *Parabolic Arc*. Retrieved 9 May 2013.

Nielsen, J. N., Missile Aerodynamics, New York: McGraw-Hill, 1960.

Noffz, G. K., Curry, R., Haering, E., Kolodziej, P., "Aerothermal Test Results from the First Flight of the Pegasus Air-Launched Space Booster", NASA Technical Memorandum, October 1991.

Nugent, R., Munakata, R., Chin, A., Coelho, R., & Puig-Sauri, J., 2008. The CubeSat: "The Picosatellite Standard for Research and Education." *AIAA SPACE 2008 Conference*. AIAA-2008-7734.

O'neill, I., "SpaceX: The Falcon is Dead, Long Live the Falcon?" 30 Sep. 2011. *Discovery News*. Retrieved on 9 May 2013.

Penchuk, A. and Croopnick, S., "Digital Autopilot for Thrust Vector Control of the Shuttle Orbital Maneuvering System", AIAA Journal of Guidance, Vol. 6, No. 6, 1983, pp. 436.

Pinson, R., Schmitt, T., & Hanson, J., 2008. "Development of a Smooth Trajectory Maneuver Method to Accommodate the Ares I Flight Control Constraints" AIAA Guidance, Navigation and Control Conference, AIAA 2008-6292.

Sarigul-Klijn, N., Noel, C., & Sarigul-Klijn, M., 2004. "Air Launching Earth-to-Orbit Vehicles: Delta V Gains from Launch Conditions and Vehicle Aerodynamics", *42nd AIAA Aerospace Sciences Meeting*, AIAA 2004-872.

Rovner, D. 1991. GN&C for Pegasus Air-Launched Space Booster: Design and First Flight Results. SAE Technical Paper Series 911105.

Sarigul-Klijn, M., Sarigul-Klijn, N., Hudson, G., Holder, L., Liesman, G., Shell, D., & Webber, C., 2006. "Gravity Air Launching of Earth-to-Orbit Space Vehicles", *AIAA SPACE 2006*, AIAA 2006-7256.

Sarigul-Klijn, M., Sarigul-Klijn, N., Hudson, G., McKinney, B., Voss, J., Chapman, P., Morgan, B., et al. 2008. "Selection of a Carrier Aircraft and a Launch Method for Air Launching Space Vehicles", *AIAA SPACE 2008 Conference*, AIAA 2008-7835.

Sikharulidze, Y., Karpov, A., Ivanov, R., 2005. "A Concept of Guidance for an Air-Launch Vehicle with Compensation of Initial Downrange and Launch Time Errors at Direct Insertion into a Rendezvous Point in the Orbit", *Cosmic Research*, Vol. 43, No. 5, pp. 342-360.

Tewari, A., Automatic Control of Atmospheric and Space Flight Vehicles: Design and Analysis with MATLAB and Simulink. New York: Springer, 2011.

Whitehead, J. C., 2006. "Air Launch Trajectories to Earth Orbit", *42nd AIAA/ASME/ SAE/ASEE Joint Propulsion Conference & Exhibit*, AIAA 2006-4785.